HYDRAULIC FRACTURE HEIGHT: MODELING AND EVALUATION USING MICROSEISMIC CLOSURE WINDOW

A Dissertation

by

SONGXIA LIU

Submitted to the Office of Graduate and Professional Studies of
Texas A&M University
in partial fulfillment of the requirements for the degree of

DOCTOR OF PHILOSOPHY

Chair of Committee,	Peter P. Valkó
Committee Members,	Walter B. Ayers
	Nobuo Morita
	Richard Gibson
Head of Department,	Alfred D. Hill

December 2017

Major Subject: Petroleum Engineering

ABSTRACT

Hydraulic fracturing stimulation has become a standard practice to enhance productivity of oil and gas wells in unconventional reservoirs (such as shale, tight sand, coal beds, etc.) previously considered difficult to access. Microseismic (MS) monitoring is routinely used during hydraulic fracturing currently, as a diagnostic technique to assess the created fracture geometry.

Despite the technical and economic successes, hydraulic fracturing suffers two uncertainties. First, hydraulic fracture height prediction by equilibrium-height method, significantly affecting fracture treatment design and other issues, is rarely done rigorously, owing to the complexity of the algebra and the reservoir geology. The secondary, unrealistic solution pairs of height tips exist but are not addressed by previous height models. Second, fracture dimensions and stimulated reservoir volume (SRV) implied by MS events are still controversial, because adjacent fracture stimulation stages of horizontal wells severely overlap each other, thus leading to over estimation of future production. In this work, we addressed the first problem by developing a Multilayer Fracture Equilibrium-Height Model (MFEH); the second problem by extracting shut-in period MS data (Closure Window) to describe effective SRV.

First, we developed the MFEH model that can rigorously calculate the stress intensity factor (SIF) at two fracture tips and solve the equilibrium height problem in multilayer formation, no matter where the perforations are placed. The MFEH model eliminates those unrealistic secondary solutions by seeking the tip solution pair from the positions nearest the initial fracture. In addition, we introduced a rigorous concept of net pressure base to calculate “apparent” net pressure, by setting fracture toughness of initial fracture tip locations to zero and then calculating the minimum treating pressure to grow the initial fracture.

By comparing the MFEH model with previous models, we found the three-layer models are not reliable due to errors in the equations; the modified MW model is correct in the equation to calculate SIF but didn't address the secondary solution problem; MShale and FracPro have little difference from the MFEH model if layers are normally stressed, although MShale is more reliable than FracPro, but they yield large discrepancy when there are abnormally high or low stress in the adjacent layers of the perforated interval. By studying the tip growth sensitivity to in-situ stress, fracture toughness, and fluid density, we found tip jump is caused by low in-situ stress; tip stability is imposed by large fracture toughness and/or large in-situ stress.

Second, we developed an Excel-VBA program to divide the MS events for each fracture stage into three windows: Pad, Proppant, and Closure Windows. The Closure Window includes only MS events during the shut-in period (from the end of slurry pumping), where leakoff and fracture closing are the dominant phenomena. Then we developed a Mathematica program to calculate SRV volume and area. We applied the Closure Window method to 5 shale wells. The overlap of MS events of stages is reduced in Closure Window. Closure Window shifts apart from other two windows, and shifts away from previous stage. Historic production is better matched with reduced fracture geometry. The SRV area ratio of Closure/Entire window is 0.7, and SRV volume ratio of Closure/Entire window is 0.75.

Finally, to improve fracture treatment design, and predict productivity, we did an integrated study of two Fayetteville fractured horizontal wells using a fracture simulator and a reservoir simulator, integrating geology data, reservoir properties from well logs and well test, perforation and well survey data, fracture pump schedules, and MS monitoring data, as well as parameters from literature. Fracture geometry and production are history-matched. Some preliminary means to improve fracture effectiveness are proposed.

ACKNOWLEDGEMENTS

First and foremost, I praise God my dear Heavenly Father for creating me, and bestowing on me the precious wisdom and unique personality that no one else in the world can give; for bringing me to the lovely Texas A&M University in U.S. to get PhD degree which I had never dreamed of; for watching over me through all trials and binding up my wounds and broken heart; for purifying my character by the refining fire of hardships; for not giving me up and still reviving me and drawing me closer to Him even when I turned away from Him in my weakness; for the powerful inspiration on my research ideas and guiding me to the direction (e.g. Microseismic Closure Window and many other projects), which I could not have come up with in a couple of months without God; for providing me the financial support with all kinds of resources, and emotional support by putting all the precious people around me; for leading me to the final point of my PhD degree of dissertation and defense. To God be the glory forever and ever!

I am very grateful to Southwest Energy Company for their financial support, and providing the microseismic and fracture stimulation data; I am greatly thankful to Steven McKetta for his reaching out and making this collaboration a reality. Without Steve and Southwest, I would not have been published the papers and finished my dissertation without financial burden. I also would like to thank Marathon for their fracture data of several Eagle Ford shale wells on which we did research and published papers.

I want to express my deep gratitude to my PhD degree supervisor, Dr. Peter Valko. He is very just, accepting me as his PhD student without bias when I was helpless. I deeply appreciate his patience on me during these years, guiding me through the research with his ingenious

perspective, and giving me the freedom and a relaxing environment to do research without over-demanding, so that I could become an independent, mature researcher as I am now. I thank him greatly for the financial support that sustained my PhD program, especially during this downturn of the oil industry. I really admire his quick and clear mind, upright character, his healthy and simple lifestyle, and focus and devotion to the research, which I will try to follow in my future career.

I would like to extend my sincerest appreciation to Dr. Walter Ayers, my great mentor, fatherly advisor, and best friend. He proofread all my papers, trained me to present conference papers and other research projects. His humbleness, tremendous love and compassion for students, simplicity, extraordinary patience, devotion, punctuality, and discipline, all set an example of what a loving, lovely and knowledgeable teacher should be like.

I want to express my sincere respect, admiration, and gratitude to my other two committee members, Dr. Richard Gibson and Dr. Nobuo Morita. They are very knowledgeable in their areas, and deep-thinking. I thank them for their patient teaching in class, answering all my questions, the encouragement on me, the time and effort reviewing my proposal, dissertation, conference presentation slides, and for the insightful comments.

I also thank the journals of SPE Production and Operation and SPE Reservoir Evaluation & Engineering, and their reviewers, who perfected my papers with detailed, insightful comments. I learned a lot from this peer-review process.

I must take time to thank my church family in College Station: my spiritual mother - Esther Robert; my spiritual grandma - MaryAnn, Joyce, Noida; my beloved Pastor Travis; my sisters in Christ - Elissa, Shevonne, Shirley Ann, Kristine, Nancy, Rosemary, Ginger; my brothers in Christ - Dare, Kevin, Inzune Hwang, John Dixon, Dale, Eric, Oscar; my spiritual

grandpa – Duane, Luid, and so on. I am greatly thankful for their unfailing love, constant prayers, and thoughtful help and support, and tolerance for me. They have watched me grow through the years here in U.S.

Finally, I would like to express the deep appreciation to my parents for raising me up, tolerating my rebellions and immaturity in the past, supporting me to get education, and giving me the freedom to choose my path. A profound gratitude to my brother - not only in the blood sense but also in Christ, for his unfailing love, company, emotional and spiritual support, interceding prayers, and the happiness he gave me.

CONTRIBUTORS AND FUNDING SOURCES

This work was supervised by a dissertation committee consisting of Professor Peter P. Valkó [advisor] and Professors Walter B. Ayers and Nobuo Morita of the Department of Petroleum Engineering and Professor Richard Gibson of the Department of Geology and Geophysics.

All work for the dissertation was completed independently by the student.

Graduate study was supported by a research fellowship from Southwestern Energy Company, and the Graduate Teaching Assistant fellowship from Department of Petroleum Engineering, Texas A&M University.

NOMENCLATURE

b_i	Intercept of the internal (net) pressure, psi
c	Fracture half-length, ft
d_{ref}	Reference depth, here specified at the middle of perforation interval, ft
d_{mid}	Depth at the middle of the fracture, ft
diffu, diffd	Difference between stress intensity factor and fracture toughness, psi$\sqrt{\text{in.}}$
IntTopToX(x)	Normalized integration form of K_{I+} in terms of z
h	Thickness of perforated interval, also as initial fracture height, ft
h_i	Thickness of the i-th layer, ft
Δh_u, Δh_d	Upper and lower height growth outside perforated interval, ft
K_I, K_{I-}, K_{I+}	SIF of either tip, upper, and lower tip, psi$\sqrt{\text{in.}}$
K_{ICi}	Fracture toughness of i-th layer, psi$\sqrt{\text{in.}}$
m	Hydrostatic gradient, $m=\rho g$, psi/ft
P_{net}	Net pressure, psi
P_{mid}	Pressure at the middle of the fracture, psi
P_{ref}	Pressure at the reference depth, psi
tipu, tipd	Upper and lower tip depths, ft
x	Depth coordinate, with zero point selected as the center of the crack, ft
$x_{1,i}$, $x_{2,i}$	Relative depths (in range of -1 to 1) of the top and bottom of the i-th layer
ρ	Density of fluid, lbm/ft^3
σ_i	In-situ stress of the i-th layer, psi

TABLE OF CONTENTS

Page

LIST OF FIGURES

Page

LIST OF TABLES

Page

1. INTRODUCTION AND LITERATURE REVIEW

1.1 Hydraulic Fracturing

In conventional hydrocarbon reservoirs, oil and gas deposit in a sponge-like trap in rock, which makes extraction easy. However, shale oil and gas occur in extremely tight rock that must be broken so the fluids trapped within can flow. A well is drilled vertically to the depth of a shale deposit and then horizontally for many meters. A slurry of water, chemicals, and sand is pumped under very high pressure through the well bore and forced into the rock at designed intervals. Thus the rock is fractured, with the sand keeping the fractures open. Hydraulic fracturing greatly increases both the rate and total amount of oil or gas that can be extracted. (https://str.llnl.gov/july-2014/ryerson)

Oil and gas produced from unconventional (low-permeability) reservoirs, especially shales and tight sands, has become a major hydrocarbon resource in North America for the past two decades (EIA 2016). **Fig. 1** shows US dry natural gas and crude oil production from different reservoir sources from 1990-2015, projected to 2040. Gas production from shale and tight sand accounts for around 2/3 of the total US dry gas production, tight oil accounts for around 1/2 of the total US crude oil production, and they will continue to increase. This "shale revolution" is a product of the combination of improved technology for hydraulic fracturing and for horizontal well drilling, which enable oil and gas to be produced from tight reservoirs at economical rates and volumes.

Hydraulic fracturing is the process of pumping high-pressure fluid and proppant into a wellbore to break down the subsurface rocks and create fractures in the hydrocarbon-bearing formation, which allows the oil and gas to flow at economic rates. We inject pad fluid first to

create fractures that are wide enough to accept a propping agent; then we pump proppant-laden (usually sand, or ceramic beads) slurry as the fractures continue to grow; then we flow back the fluid leaving proppant behind to keep the fractures open once the pressure inside the fractures drops.

(a)Dry Natural Gas, TCF/year **(b)Crude Oil, Mbbls/day**

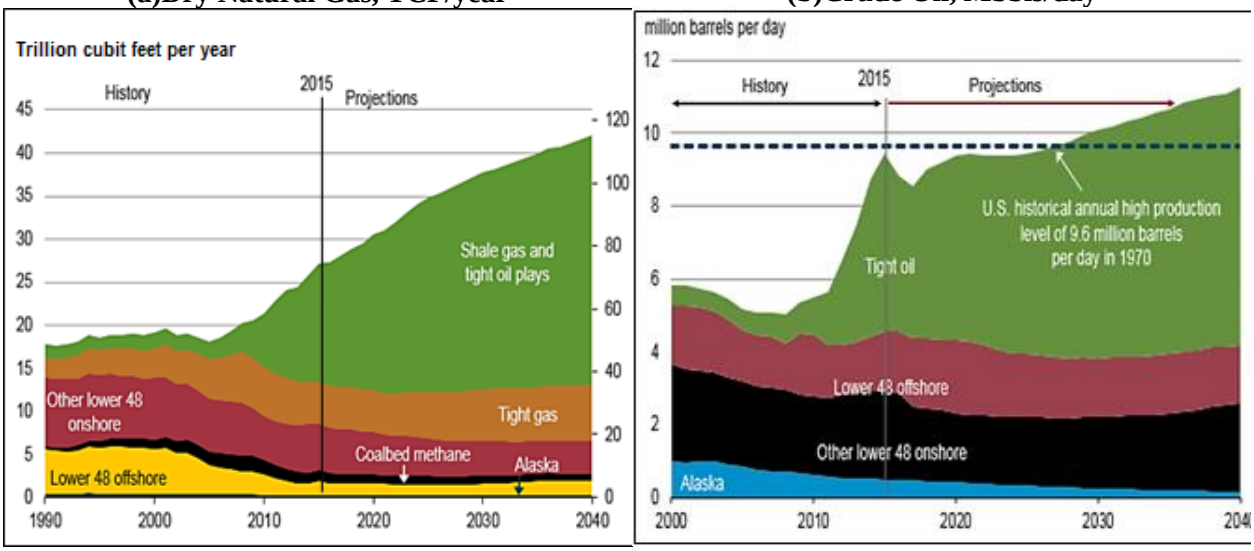

Fig. 1 U.S. (a) dry natural gas and (b) crude oil production by source. (From U.S. Energy Information Administration (EIA), Annual Energy Outlook 2016: http://www.eia.gov/forecasts/aeo/pdf/0383(2016).pdf)

The first hydraulic fracturing treatment was implemented in 1947 in a low-productivity gas well in Kansas, by Pan American Petroleum Corp, to compare the results of acidizing and fracturing. Clark (1949) introduced the concept of "hydraulic fracturing" or "hydrafrac" to petroleum industry (Clark 1949). He described the steps of the process, requirements for fluid, proppant, pump, and confining of fractures within desired formation. Also he reported a shallow-well field experiment confirming the effectiveness of fracturing, and field results showing increase of production and pressure profile with distinct breakdown pressure, and economic

feasibility. Hazards to personnel were also briefly discussed. Following these tests in the 1940's hydraulic fracturing was rarely used until the oil and gas industry became aware of the huge volumes of gas-saturated sandstones with permeability too low for economic recovery by conventional methods.

Modern fracturing matured in the 1980s and 1990s through several joint industry–US Department of Energy projects, in the Rocky Mountain, Gulf Coast and Appalachian basins, and elsewhere. Hydraulic fracturing of shale grew rapidly in the late 1990s, when energy companies (starting with Mitchell Energy) learned how to best stimulate the Barnett Shale in north Texas. Today, hydraulic fracture stimulation has become a standard practice to enhance productivity of oil and gas wells in unconventional reservoirs.

1.2 Fracture Height Modeling and Evaluation

1.2.1 Fracture Height Containment and Diagnostics

One of the most important questions encountered in hydraulic fracturing is the overall geometry of induced fractures, especially fracture height; in other words, whether fractures will propagate into overlying and underlying layers. Hydraulic fracture height prediction is an important task, because the results significantly affect fracture treatment design as well as environmental, safety and economic considerations.

Fracture diagnostics methods include the following (Holditch 2006):

- Direct far-field technology: tiltmeter and microseismic monitoring;
- Direct near-wellbore technology: tracer, temperature, production, borehole image, and downhole video logs;

- Indirect fracture modeling technology: fracture modeling of net pressure, pressure-transient-test analysis, and production-data analysis; and
- Net pressure analysis: interpret 4 modes of net-pressure behavior, log(Pn) vs log(Δt), in the field or after the treatment.

Among the above methods, only direct far-field monitoring and indirect fracture modeling can determine fracture size and direction.

1.2.2 Factors affecting Fracture Height

Many factors influence fracture height evolution in multilayer formations, including: layer interface (or composite layering effect) and its shear strength, natural fractures/faults, in-situ stress, fracture toughness, Young's modulus, Poisson ratio, tensile strength, fluid leak-off into formations, fracturing fluid density, fluid viscous friction inside fracture, sealing of fracture tip by fluid-loss-control components, treating pressure (or pump rate), interaction of multiple transverse hydraulic fractures, etc. Studies have been done in theory, lab experiments, field data, mineback field tests, and numerical modeling (Daneshy 1978; Simonson et al. 1978; van Eekelen 1982; Warpinski et al. 1982; Warpinski et al. 1982; Biot et al. 1983; Ahmed 1984; Mendelsohn 1984; Teufel and Clark 1984; Morita et al. 1988; Thiercelin et al. 1989; Warpinski 1991; Valko and Economides 1993; Barree and Mukherjee 1996; Smith et al. 2001; Gu and Siebrits 2008; Dozier 2009; Green et al. 2009; Jeffrey and Bunger 2009; Ramurthy et al. 2009; Zuluaga et al. 2010; Weng et al. 2011; Fisher and Warpinski 2012; Hurt and Germanovich 2012; O'Brien et al. 2012; Yang et al. 2012a; Geilikman et al. 2013; Kresse and Weng 2013; Abbas et al. 2014; Chuprakov and Prioul 2015; Khanna and Kotousov 2016).

Among the many factors affecting fracture height mentioned above, the five most influential ones are as follows: *in-situ stress*; *weak layer interfaces* (and its shear strength); *fracture toughness*; *mechanical properties* (Young's modulus, shear modulus, Poisson ratio, and tensile strength); and *fluid leakoff*. Their effects are briefly discussed below. In this work, we will look at only the factors that affect the equilibrium-height migration: in-situ stress, σ; fracture toughness, K_{IC}; and fluid density, ρ.

1) In-situ stress has been recognized as the most important factor to contain fracture height. The higher in-situ horizontal stress, or confining stress in the lab, the less fracture height (van Eekelen 1982; Warpinski et al. 1982; Warpinski et al. 1982).

2) The weaker the layer interface (less interfacial shear strength, less normal stress against the interface, or less surface roughness / friction coefficient) is, the more likely the fracture height to be contained (Daneshy 1978; Simonson et al. 1978; Biot et al. 1983; Teufel and Clark 1984).

3) Higher fracture toughness will contain height growth (Thiercelin et al. 1989; Garagash and Detournay 2005; Garagash 2006; Zhang et al. 2010). The fracture toughness only control the fracture when the fracture is small; the fluid-loss-control material will increase the fracture pseudo-toughness significantly (Morita et al. 1988).

4) Elastic modulus is a second-order, indirect factor for height growth by affecting fracture width, net pressure, and horizontal stress profile in layers: rock of high Young's modulus will have narrow width and high pressure drop, thus shorter height; stiffer bounding layer will decrease the stress intensity factor of the approaching fracture before penetration into it, thus halting it; high shear modulus of outer layers induces compressional horizontal stress in the middle, target layer, thus higher breakdown

pressure, but tensile stress in the stiffer bounding layer will increase and may cause fracture jump into it; increase of tensile strength will contain or hinder fracture growth (Simonson et al. 1978; van Eekelen 1982; Teufel and Clark 1984; Morita et al. 1988; Smith et al. 2001; Gu and Siebrits 2008).

5) High leak-off will reduce pressure in the fracture and thus stop fracture growth (Ahmed 1984; Barree and Mukherjee 1996; Hurt and Germanovich 2012; Kresse and Weng 2013). Therefore, it is also a secondary, indirect factor.

1.2.3 Equilibrium-Height Modeling

While many factors can contribute to additional height containment, the consensus is that the so called "equilibrium-height belonging to a certain treating pressure" calculates fracture height for non-naturally fractured, layered formations, and provides an upper limit of fracture height for all reservoir conditions. Equilibrium-height is the fracture height when the integration of weighted net pressure inside the fracture along the height, i.e. stress intensity factor (Eq. 1), K_I, is equal to the fracture toughness, K_{IC}, at the upper and lower tips. If the calculated K_I at either tip is smaller than the associated K_{IC}, the tip will not grow; if the calculated K_I at either tip is higher than the associated K_{IC}, the tip will grow (Valkó and Economides 1995). The basic equilibrium-height model assumes that the vertical propagation is quasi-static with respect to the net pressure evolution. This is a straightforward assumption in the so-called fracture-tougness dominated propagation regime, but might be not valid in the so-called viscosity-dominated propagation regime. In the toughness-dominated fracture propagation regime, nearly all energy is dissipated by fracture tip propagation (rock deformation), while in viscosity-dominated regime, energy is mainly dissipated by viscous fluid flow friction inside fractures (Detournay 2004;

Bunger et al. 2007; Kovalyshen and Detournay 2013; Bao et al. 2015). The stress intensity factors are defined as

$$K_{I+} = \sqrt{\frac{1}{\pi c}} \int_{-c}^{c} P_{net}(x) \sqrt{\frac{c+x}{c-x}}\, dx$$

$$K_{I-} = \sqrt{\frac{1}{\pi c}} \int_{-c}^{c} P_{net}(x) \sqrt{\frac{c-x}{c+x}}\, dx \quad \ldots\ldots\ldots\ldots\ldots\ldots\ldots\ldots \quad \ldots\ldots\ldots\ldots\ldots\ldots\ldots\ldots\ldots\ldots\ldots\ldots (1)$$

Where c is fracture half height, Pnet(x) is net pressure at a depth x, and the origin for the variable x is placed in the center of the vertical crack.

Complexity of the Integration for SIF

Solutions for the "equilibrium-height" problem have been known since the 1970s, and several models have been developed for calculating hydraulic fracture height (Simonson et al. 1978; Ahmed 1984; Newberry et al. 1985; Meyer 1986; Fung et al. 1987; Morita et al. 1988; Meyer et al. 1990; Economides and Nolte 2000; Economides et al. 2012). However, because of the complexity of the algebra involved, the equations used in these early models were overly simplified and gave unreliable results **(Table 1)**.

We summarized 5 models in Table 1 (Simonson et al. 1978) (Ahmed 1984; Newberry et al. 1985; Fung et al. 1987; Mack and Warpinski 2000; Economides et al. 2012) (Weng et al. 2011). Simonson's model (1978) is for symmetric 3-layer formation with the same overlying and underlying rock properties; the second model (Ahmed 1984; Newberry et al. 1985; Economides et al. 2012) is for asymmetric 3-layer formation with different overlying and underlying rock properties. They both have typos. The last three models are for asymmetric, multilayer formations. They belong to the same family. Fung's model (1987) assumes constant inner net pressure along the height; Mack and Warpinski's model considers hydrostatic pressure change

along the height, but has typos. Lastly, Weng's model (Weng et al. 2011) corrected the typo/error in Mack and Warpinski model, and accurately solves the equilibrium-height problem, although the paper just gives the analytical expressions of stress intensity factors, without clear demonstration of the physical meaning and derivation. However to give credit and honor to the original work of Mack and Warpinski, we will call both the Weng's model and Mack and Warpinski's model together as modified Mack and Warpinski's model (MW). The notation of Equ. 9 in Table 1 for modified MW model is given in **Fig. 2**: h_f is the total frac height, h_{cp} is the distance between the lower tip and a reference depth in the perforation interval, h_i is the distance between the lower tip and the i-th layer top, p_{cp} is the pressure at h_{cp}, the first layer is the layer in which the lower tip resides and the n-th layer is where the upper tip resides and σ_i is the in-situ stress in the i-th layer.

Some models assume perforations are placed in the lowest-stressed layer, therefore inaccurately solve the height when otherwise. Cohen et al. (2015) presented the inaccurate height growth in conventional P3D model which assumes perforation is placed in a high stress layer (Cohen et al. 2015); then, they proposed a stacked height growth model based on previous work of Mack and Warpinski (2000) and Weng et al. (2011). Cohen et al. (2015) split elements into vertically connected stacked elements and stacked fractures, so that fracture can have multiple fronts/tips propagating in several low-stressed zones (Cohen et al. 2015; Cohen et al. 2017).

Model	Assumptions	Fracture Height Equations	Errors and Correct Form
Simonson et al. (1978)	Symmetric 3-layer formations; with same upper and lower in-situ stress $\sigma_u = \sigma_d = \sigma_b$; constant treating pressure	$p_{net} = p - p_o = \frac{K_{IC}}{\sqrt{\pi L}}\left(\frac{1}{\sqrt{(1+\epsilon)}} - 1\right) + 2\frac{(\sigma_b - \sigma_a)}{\pi}\mathrm{ArcCos}\left[\frac{1}{1+\epsilon}\right]$ (Eq. 7)	$\frac{1}{1+\epsilon} = \cos\left[\frac{\left(K_{IC} - (p-\sigma_a)\sqrt{\pi L(1+\epsilon)}\right)}{2(\sigma_b - \sigma_a)\sqrt{L(1+\epsilon)}}\right]$ (Eq. 5) Right form: $\frac{1}{1+\epsilon} = \cos[\sqrt{\pi}\frac{(K_{IC}-(p-\sigma_a)\sqrt{\pi L(1+\epsilon)})}{2(\sigma_b-\sigma_a)\sqrt{L(1+\epsilon)}}]$ $\sqrt{\pi}$ is missiong in the original equation.
Ahmed (1984), Newberry et al. (1985), and Economides et al. (2012)	Asymmetric 3-layer formations, i.e., KICu ≠ KICd, σd ≠ σu, hu ≠hd	$\Delta p_f = \frac{C_1}{\sqrt{h_u}}\left[K_{IC}\left(1 - \sqrt{\frac{h_u}{h}}\right) + C_2(\sigma_u - \sigma)\sqrt{h_u}\cos^{-1}\left(\frac{h}{h_u}\right)\right] + C_3\rho(h_u - 0.5h)$ $\Delta p_f = \frac{C_1}{\sqrt{h_d}}\left[K_{IC}\left(1 - \sqrt{\frac{h_d}{h}}\right) + C_2(\sigma_d - \sigma)\sqrt{h_d}\cos^{-1}\left(\frac{h}{h_d}\right)\right] - C_3\rho(h_d - 0.5h)$	1) Starting from Simonson et al. (1978) Eq. 7, they made some replacements h=L, h_u=h_d=l, 2h_u-h=h_u, 2h_d-h=h_d. The correct replacement: h=2L, h_u=h_d=L+l, 1/(1+ε)=L/l. 2) They substituted σ_b with σ_d (σ_c) for downward, and with σ_u (σ_b) for upward, without considering that both σ_d and σ_u are involved in the integration of K_I in either direction. 3) C1=0.163, C2=3.91, C3=0.0069 Right values: C1=0.2303, C2=2.764, C3=0.0069 4) In Economides et al. (2012), p.623, unit of K_{IC} is"psi/$\sqrt{\text{inch}}$"; the $\cos^{-1}$ term is evaluated in "degree". Unit of K_{IC} should be psi$\sqrt{\text{inch}}$, $\cos^{-1}$ term should be evaluated in radian. 5) No reason or derivation process for $C_3\rho(h_{d/u} - 0.5h)$, the last term to consider hydrostatic pressure in the above two equations.
Fung et al. (1987)	Asymmetric multilayer formations; Constant inner pressure along the fracture height	$F_{\sigma m} = \sqrt{\frac{h/2}{\pi}}\left\{(p-\sigma_n)\pi + \sum_{i=1}^{n}(\sigma_{i+1} - \sigma_i)[2\sin^{-1}\sqrt{\frac{2h_i}{i}} - (-1)^m\sqrt{1 - (\frac{2h_i - h}{h})^2}]\right\}$ (Eq. 3) $F_{\sigma m}$ is SIF; m=1 for lower tip; m=2 for upper tip. SIF definition (Eqs. 1, 2) $F_{\sigma 1} = \sqrt{\frac{2}{\pi h}}\int_{-h/2}^{h/2}[p - \sigma(y)]\sqrt{\frac{1-y}{1+y}}dy$ $F_{\sigma 2} = \sqrt{\frac{2}{\pi h}}\int_{-h/2}^{h/2}[p - \sigma(y)]\sqrt{\frac{1+y}{1-y}}dy$	"1" under the square root of Equs. 1 and 2 should be "h/2". $F_{\sigma 1} = \sqrt{\frac{2}{\pi h}}\int_{-h/2}^{h/2}[p - \sigma(y)]\sqrt{\frac{1-y}{1+y}}dy$ $F_{\sigma 2} = \sqrt{\frac{2}{\pi h}}\int_{-h/2}^{h/2}[p - \sigma(y)]\sqrt{\frac{1+y}{1-y}}dy$

Table 1. Summary of current equilibrium-fracture-height models.
Equation numbers here are from references for readers to easily find.

Model	Assumptions	Fracture Height Equations	Errors and Correct Form
Mack and Warpinski (2000)	Asymmetric multilayer formations; SI units	$K_{Iu} = \sqrt{\frac{\pi h_f}{2}}\left(p_{cp} - \sigma_n + \rho g\left(h_{cp} - \frac{3}{4}h_f\right)\right) + \sqrt{\frac{2}{\pi h_f}}\sum_{i=1}^{n-1}(\sigma_{i+1} - \sigma_i)\left[\frac{h_f}{2}\cos^{-1}\left(\frac{h_f - 2h_i}{h_f}\right) - \sqrt{h_i - (h_f - h_i)}\right]$ $K_{Id} = \sqrt{\frac{\pi h_f}{2}}\left(p_{cp} - \sigma_n + \rho g\left(h_{cp} - \frac{1}{4}h_f\right)\right) + \sqrt{\frac{2}{\pi h_f}}\sum_{i=1}^{n-1}(\sigma_{i+1} - \sigma_i)\left[\frac{h_f}{2}\cos^{-1}\left(\frac{h_f - 2h_i}{h_f}\right) - \sqrt{h_i - (h_f - h_i)}\right]$ (Eqs. 6-46 and 6-47)	The last term $\sqrt{h_i - (h_f - h_i)}$ will yield complex number when $2h_i < h_f$. It should be $\sqrt{h_i(h_f - h_i)}$ which is correct in Weng et al (2011) model.
Weng et al (2011)	Asymmetric multilayer formations; SI units; Based on Mack and Warpinski (2000)	$K_{Iu} = \sqrt{\frac{\pi h_f}{2}}\left(\rho g\left(h_{cp} - \frac{3h_f}{4}\right) + p_{cp} - \sigma_n\right) + \sqrt{\frac{2}{\pi h_f}}\sum_{i=1}^{n-1}(\sigma_{i+1} - \sigma_i)\left[\frac{h_f}{2}\cos^{-1}\left(\frac{h_f - 2h_i}{h_f}\right) - \sqrt{h_i(h_f - h_i)}\right]$ $K_{Id} = \sqrt{\frac{\pi h_f}{2}}\left(\rho g\left(h_{cp} - \frac{h_f}{4}\right) + p_{cp} - \sigma_n\right) + \sqrt{\frac{2}{\pi h_f}}\sum_{i=1}^{n-1}(\sigma_{i+1} - \sigma_i)\left[\frac{h_f}{2}\cos^{-1}\left(\frac{h_f - 2h_i}{h_f}\right) + \sqrt{h_i(h_f - h_i)}\right]$ (Eq. 9)	They have different algebra formulas from our model, but obtain the same results as our model. However, they didn't give the detailed procedure to solve fracture height tip locations, nor did they address the secondary height solution problem.

Table 1. Continued.

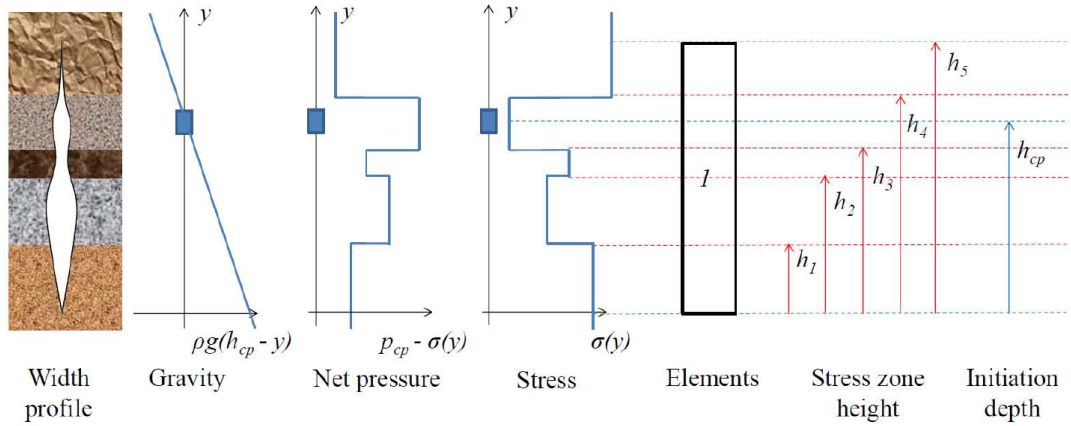

Fig. 2. Notation for the Modified MW model. Reprinted from Cohen et al. (2017).

Secondary Solutions

The equilibrium-height model rarely has one unique solution; more often, multiple solutions exist, although usually only one has physical meaning (Valko and Economides 1993; Valkó and Economides 1995; Liu and Valko 2015). See **Fig. 3** for the appearance of the second solution pair (dash lines) for a simple 3-layer case. It is unrealistic because after 6650 psi, the upper tip suddenly retreats, and the lower tip suddenly crosses a stable region and goes to a much deeper depth and then retreats. None of the current models addressed this issue. We need to eliminate the unrealistic secondary solutions in the height model.

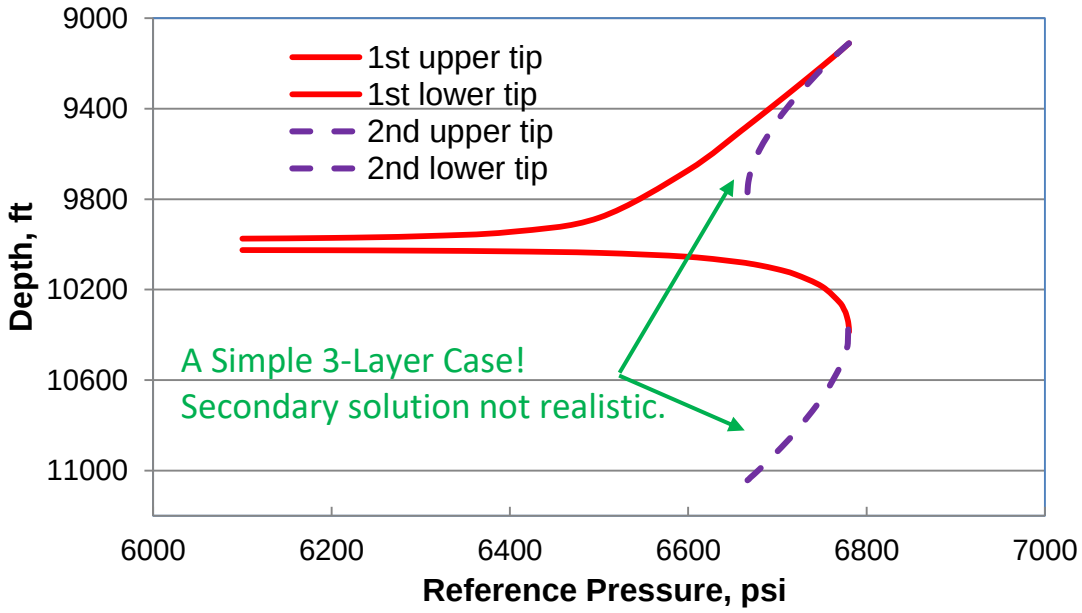

Fig. 3. Secondary solution pair (purple dash lines) appears in a simple 3-layer case.

Equivalent P3D Net Pressure Concept

In the detailed height calculation net pressure is varying vertically. Many fracture simulators are of P3D type, where vertical fracture propagation is loosely coupled with the 2D

lateral propagation model through the equivalent net pressure which is aggregated as one quantity at a lateral location. We use net pressure to calculate width, height, design the fracture treatment, and perform onsite and post-frac analyses in P3D models. However, definition of reported/apparent net pressure varies in various models.

Although net pressure inside a fracture is different at each x depth in each layer ($P_{net}(x) = \rho g x + P_{mid} - \sigma_i$), we usually talk about "apparent" net pressure at a reference depth $P_{net}(@\, d_{ref}) = P_{ref} - P_{base}$, where P_{base} is the net pressure base at d_{ref}, beyond which the fracture will grow. This is what is usually called σ_{min}, "closure pressure", "minimum in-situ stress" or "minimum horizontal stress". When reference net pressure P_{net} in the fracture is positive, the fracture is open; when P_{net} is negative, the fracture is closed. The common practice for selecting the base value is: minimum in-situ stress σ_{min} at the middle of perforated intervals, or σ_{min} at reference depth, or thickness-weighted in-situ stress (Kim 2010).

However, according to rigorous fracture mechanics definition, an initial fracture covering perforated zone will only grow when stress intensity factor overcomes the in-situ fracture toughness, rather than reference treating pressure overcoming minimum in-situ horizontal stress. It's a criterion of integrated energy rather than a stress. The discrepancy of P_{base}will be more obvious in vertical wells when several different intervals are perforated. Since we always perforate a well to somehow create initial fractures before injecting fluid, P_{base} should be defined as the minimum reference treating pressure at which the initial line crack (covering the perforated zone) will lose stability/Equilibrium, if the fracture toughness of the two adjacent layers containing the tips are artificially set to zero (Yang et al. 2012a, 2012b). Such a definition of P_{base} satisfies two requirements: 1) in the simple 1+2 layer case it gives back the usual definition of net pressure base (in-situ stress in the middle layer or center of perforation) and 2) it

will make sure that the initial fracture covering the perforated interval will not propagate under any negative net pressure. We noticed that definitions used in commercial software usually do not satisfy the second requirement. In other words, the initial fracture covering the perforated interval may grow under *negative net pressure*, or Pbase is larger than minimum treating pressure for the initial fracture to grow out of perforated interval. In this case, fracture width wf calculated from will be meaningless.

1.3 Fracture Evaluation by Microseismic Monitoring

1.3.1 Microseismic Monitoring in Hydraulic Fracturing

What is Microseismic Monitoring? And how is it applied in hydraulic fracturing? Here are some definitions from the main microseismic service companies:

"Microseismic Monitoring is like putting a stethoscope to the surface of the earth and listening to the sounds the rocks make as they are being fractured. Those sounds are then further used to create an actual image of how and where the rocks fracture." (MicroSeismic, Inc.: http://www.microseismic.com/technical-resources/frequently-asked-questions/microseismic-monitoring)

"Microseismic monitoring is the passive observation of very small-scale earthquakes which occur in the ground as a result of human activities or industrial processes such as mining, hydraulic fracturing, enhanced oil recovery, geothermal operations or underground gas storage." "These micro-earthquakes are too small to be felt on the surface, but they can be detected by sensitive equipment such as geophones and accelerometers." "Microseismic events are caused when human activities such as mining or oil and gas production change the stress distribution or the volume of a rock mass. When the rock attempts to redistribute the stress within the rock

mass, it will suddenly slip or shear along pre-existing zones of weakness such as along faults or fracture networks. This small failure results in the release of energy in the form of seismic waves and is known as a microseismic event." (ESG: https://www.esgsolutions.com/technical-resources/microseismic-knowledgebase/microseismic-monitoring-101)

MS monitoring has become the most common diagnostic technique to monitor and determine where fractures are going in hydraulic fracturing. It uses the downhole, near-surface or surface geophones to listen to the small sounds from rocks. It provides the only 3-D view of the fracture network or reservoir drainage region.

MS data hold a wealth of information including: fracture geometry (length, height, width, azimuth, asymmetry, fracture network complexity), SRV, stage effectiveness, natural fractures (NF) and faults, reservoir properties, influence of the treatment on reservoirs, rock mechanics, distance in depth between fracture and aquifer, and MS events magnitude (Warpinski 2009; King and Leonard 2011; Fisher and Warpinski 2012; Gale et al. 2014). MS monitoring has become routine in hydraulic fracturing (Chitrala et al. 2011).

1.3.2 Source Mechanisms of MS Events

MS events can be triggered by any underground movements, resulting from many sources: hydraulically induced fractures, reactivation of NF or previously created hydraulic fractures (HF) (Warpinski 2009; Gale et al. 2014), leakoff induced secondary fractures, stratigraphic boundaries, and operational noise (Shuck et al. 2015). Both stress perturbation and fluid leakoff can cause MS events due to shear and tensile failures (Warpinski and Teufel 1987; Seth Busetti 2014). MS events can be detected by downhole geophone strings, even if their

moment magnitude (Mw) is very small; the minimum magnitude of MS that geophones can detect is usually less than 0, or Mw <0, for hydraulic fracturing (Davies et al. 2013).

Both pressure perturbation and fluid leakoff can cause MS events by shear and tensile failure, therefore, not all detected MS locations connect to the fracture network or contribute to fluid flow (Rassenfoss 2015). In addition, the largest shear stress and resultant shear failure are near the main HF (Warpinski et al. 2004; Palmer et al. 2007), and the microseismic events are mainly in immediate proximity to HF, according to various hydraulic fracture experiments (Athavale and Miskimins 2008; Chitrala et al. 2011).

1.3.3 Some Problems with Application of MS Data

To physically see the exact fracture geometry from MS data is impossible, and an SRV derived from MS data is very uncertain (Warpinski 2009; Rassenfoss 2015). Our Closure Window idea was triggered by the following three facts, which reflect common problems that persist with application of MS data.

First, our study showed that the MS clouds of adjacent fracture stimulation stages of horizontal wells severely overlap each other, which should not occur unless significant volumes of the fluid went to the previous fractures. The overlap masks the real SRV of the current fracturing stage.

Second, when using the MS data to history match the fracture geometry and production, we found a) the large fracture dimensions read from the entire MS window of a stage are very difficult to match with given frac job data, e.g. slurry rate, slurry volume, injection time; b) using SRV obtained from the entire MS window usually leads to production rate estimation that is higher than real production, and c) using SRV obtained from the entire MS window requires

forcing unrealistic estimates for other parameters (fracture geometry, number of producing fractures) during a detailed history matching of actual production history. These observations are consistent with those of Palmer et al. (2013, 2014), who also found that complex fracture networks determined either from simulation or read directly from MS clouds, are larger than "true effective" fracture networks/SRV. For example the SRV after a well is turned on is approximately 10% smaller than the "MS volume" (Palmer et al. 2013), therefore, microseismic evaluation forecasts higher production than actually reported (Palmer et al. 2014).

Third, our question became: how can we identify the "true effective" fracture geometry and associated SRV of each stage? We compared the timing of MS monitoring and the frac job records and found that, for a Fayetteville fracture stimulated horizontal well, MS monitoring lasted until 1hr after they stopped pumping the slurry and shut in the well. We found that there were many MS events during the shut-in period.

The common notion is that there is little seismicity after the shut-in of a well, since there is no fluid injection and leakoff is slow and hence the "slow or small volume injections may not create any microseisms" (Warpinski 2009). Therefore, people don't usually measure MS data during the period of shut-in and before flow-back. However, our observations indicate that this period could contain significant information about the fracture geometry and SRV, and it may be a valuable source of information.

Based on the above observation, we investigated MS data by classifying various time windows, one of them being the "Closure Window" corresponding to the shut in period of the well after the pumping was stopped.

2. STATEMENT OF PROBLEMS

Summarizing the background of fracture stimulation issues identified several primary research problems, stated below.

First, because of the complexity of the algebra involved, even the simplest "equilibrium-height model" is rarely solved correctly, and the suggested procedures are oversimplified and give unreliable results. The current models also require perforations to be placed in the low-stressed layer. We identified the following 2 secondary research problems.

a) The equilibrium-height model rarely has one unique solution; more often, multiple solutions exist, although usually only one has physical meaning. Current models haven't dealt with this problem.

b) Many fracture simulators are of P3D type, where vertical fracture propagation is loosely coupled with the 2D lateral propagation model through net pressure. However, definition of reported/apparent net pressure varies in various models and commercial software.

Second, MS clouds of adjacent fracture stimulation stages of horizontal wells severely overlap each other, which makes it hard to identify the true effective fracture geometry of each stage. Complex fracture networks determined from MS clouds data recorded during pad injection and proppant-laden fluid injection are larger than "true effective" fracture networks, thus yield larger SRV, and lead to over-estimation of future production (or require unrealistic values for other parameters, when history matching actual production.)

3. OBJECTIVES

The primary objectives of this work are:

1) Develop a multilayer fracture equilibrium-height model (MFEH) that can rigorously solve the equilibrium fracture height problem, in a non-fractured reservoir and without formation interface barriers, no matter where the perforations are placed; and can avoid unrealistic secondary solutions. Develop a new concept of net pressure base to calculate “apparent” net pressure in a fracture model based on rigorous fracture mechanics. Compare the MFEH model with other models and commercial software, to check their validity, since the equilibrium height provides the upper limit (maximum hf). Finally, investigate the effects of fracture toughness, in-situ stress, fluid density, and their interactive effects. Create fracture-height map for a given problem that can be used to check the realism of an actual set of results from a commercial fracture simulator.

2) Find a new method - Closure Window method - to interpret MS data, and obtain the true effective fracture geometry and SRV, leading to more accurate prediction of future production. Creating the new method several sub-problems should be solved: Develop an Excel-VBA program to divide the MS events of each fracture stage into three windows: the Pad Window, the Proppant Window, and the Closure Window, based on the fracture stimulation record. The Closure Window includes only MS events during the shut-in period. Separate and interpret the unique information in the Closure Window and get deeper insight into the fracturing process. Finally, develop an algorithm to calculate area and volume of effective SRV from Closure Window MS data.

4. A RIGOROUS MULTILAYER FRACTURE-EQUILIBRIUM-HEIGHT (MFEH) MODEL*

4.1 Summary

Fracture height is a critical input parameter for 2D hydraulic fracturing design models, and also an important output result of 3D models. While many factors may influence fracture height evolution in multilayer formations, the consensus is that the so called "equilibrium-height belonging to a certain treating pressure" predicts fracture height for non-naturally fractured media with perfect layer interfaces, and therefore provides an upper limit for all other reservoir conditions However, because of the complexity of the algebra involved, published height models are overly simplified and do not provide reliable results. Current models do not address the problem of secondary, unrealistic solutions.

We revisited the equilibrium-height problem, started from the definition of fracture stress intensity factor (SIF), considered variation of layered formation properties and effects of hydrostatic pressure, and developed a mathematically rigorous model- Multilayer Fracture-Equilibrium-Height Model (MFEH) using the programming environment "Mathematica". The detailed derivation of SIF and workflow of MFEH model are provided. A new, rigorous definition of net pressure and net pressure base is proposed used in the model. The secondary solutions are eliminated by the MFEH model.

The model is compared with existing models and software, under the same ideal geology condition. Generally, MShale calculated smaller height, and FracPro larger height, than the MFEH model. Most of the difference is attributable to the different interpretation of the "net

*Part of this chapter is reprinted with permission from "A Rigorous Hydraulic-Fracture Equilibrium-Height Model for Multilayer Formations" by Songxia Liu and Peter P. Valkó, 2017. SPE Production & Operations, SPE 173335-PA, Preprint. Copyright 2017 by Society of Petroleum Engineers.

pressure". In the normally stressed case, the results from both commercial software are acceptable, although MShale is more reliable. The discrepancy is much larger when there is abnormally high or low stress in the adjacent layers of the perforated interval. Second and even third and fourth solutions for a 3-layer problem were found and proved unrealistic; however they can be avoided in our MFEH model. The full-height map with very large top and bottom formation thicknesses shows the ultimate trend of height growth map, i.e., when the fracture tip will grow to infinity, and suggests the maximum pressure to be used. The effects of formation rock and fluid properties on the fracture height growth were investigated. Tip jump is caused by low in-situ stress; tip stability is imposed by large fracture toughness and/or large in-situ stress. If the fluid density is ignored, the result regarding to which tip will grow into infinity could be totally different. Other fracture-containment mechanisms are discussed in other papers (Gu and Siebrits 2008; Dozier 2009; Green et al. 2009; Jeffrey and Bunger 2009; Ramurthy et al. 2009; Zuluaga et al. 2010; Weng et al. 2011; Fisher and Warpinski 2012; O'Brien et al. 2012), and are not in our scope of equilibrium-height study. In order to assess the potential effects of reservoir parameter uncertainties on height map, two 3-layer pseudo problems were constructed based on a multilayer-formation to create an outer and inner height envelope.

The improved multilayer fracture-equilibrium-height model (MFEH) fully characterizes height evolution amid various formation and fluid properties (fracture toughness, in-situ stress, thickness, fluid density, etc.), and rigorously and rapidly solves the equilibrium-height. The equilibrium-height can be used to (1) provide input data for 2D model, (2) improve 3D model governing equations, (3) determine the net pressure needed to achieve a certain height growth, and (4) suggest the maximum net pressure assuring no fracture invasion into aquifers. This

model may be incorporated into current hydraulic fracture propagation simulators to yield more accurate and cost-effective hydraulic fracturing designs.

4.2 Derivation of the Multilayer Fracture-Equilibrium-Height Model (MFEH)

4.2.1 Stress Intensity Factor at Upper and Lower Fracture Tips

Using the computer algebra software, Mathematica, we modeled hydraulic fracture in a multilayer formation **(Fig. 4).** We started with the definition of SIF at lower and upper tips K_{I+} and K_{I-}, i.e., the integration of weighted net pressure along fracture height, taking hydrostatic fluid pressure into account (Eqs. 1 and 2). Please note that all pressures in this paper are inside the fracture; here we don't consider BHTP inside wellbore, perforation friction, tortuosity, etc.

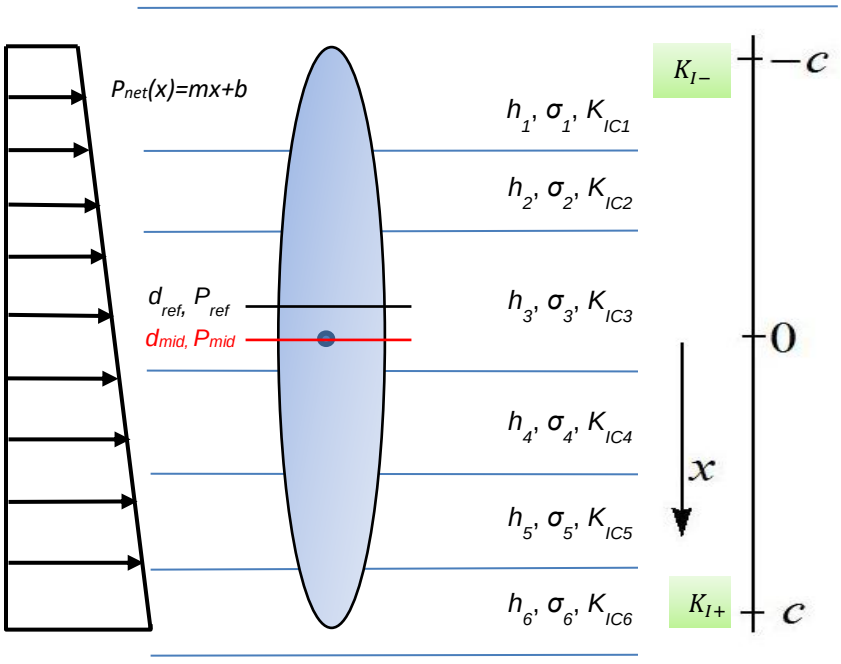

Fig. 4. Hydraulic fracture in a multilayer formation with hydrostatic fluid pressure inside.

$$K_{I+} = \sqrt{\frac{1}{\pi c}} \int_{-c}^{c} P_{net}(x) \sqrt{\frac{c+x}{c-x}} dx$$

$$K_{I-} = \sqrt{\frac{1}{\pi c}} \int_{-c}^{c} P_{net}(x) \sqrt{\frac{c-x}{c+x}} dx \quad \ldots\ldots (1)$$

where fracture half height $c = (tipd - tipu)/2$, *tipu* and *tipd* are the upper and lower tip locations (depths).

Net Pressure for location *x* at each layer *i* , $P_{net}(x)$, is defined as the pressure in the fracture minus the in-situ stress, as below:

$$P_{net}(x) = \rho g x + P_{mid} - \sigma_i = \rho g x + \left[P_{ref} + \rho g\ (\mathrm{d_{mid}} - \mathrm{d_{ref}})\right] - \sigma_i = mx + \mathrm{b_i} \quad \ldots\ldots (2)$$

where $m = \rho g$, $\mathrm{b_i} = P_{ref} + \rho \mathrm{g}(\mathrm{d_{mid}} - \mathrm{d_{ref}}) - \sigma_i$; ρ is fracture fluid density; $P_{mid} = P_{ref} + \rho g\ (\mathrm{d_{mid}} - \mathrm{d_{ref}})$, is the pressure at the middle of a fracture; $\mathrm{d_{mid}} = (tipd + tipu)/2$, is depth at the middle of a fracture and also the origin of x, $\mathrm{d_{ref}}$ is the depth of reference fracture pressure (P_{ref}), e.g. the injection point at bottomhole, or vertical depth of perforation cluster/stage in a horizontal well; σ_i is the in-situ stress of the i-th layer. Then

$$K_{I+} = \sqrt{\frac{1}{\pi c}} \int_{-c}^{c} P_{net}(x) \sqrt{\frac{c+x}{c-x}}\, \mathrm{d}x = \sqrt{\frac{1}{\pi c}} \int_{-c}^{c} (mx + \mathrm{b_i}) \sqrt{\frac{c+x}{c-x}}\, \mathrm{d}x$$

$$K_{I-} = \sqrt{\frac{1}{\pi c}} \int_{-c}^{c} P_{net}(x) \sqrt{\frac{c-x}{c+x}}\, \mathrm{d}x = \sqrt{\frac{1}{\pi c}} \int_{-c}^{c} (-my + \mathrm{b_i}) \sqrt{\frac{c+y}{c-y}}\, \mathrm{d}y \quad \ldots\ldots (3)$$

where *y*=-*x*, -*c* becomes the bottom of a fracture.

The integration of K_{I+} from fracture top (–*c*) to location x, $IntTopToX(x)$ is

$$IntTopToX(m, \mathrm{b_i}, x) = \sqrt{\frac{1}{\pi c}} \int_{-c}^{x} (mx + \mathrm{b_i}) \sqrt{\frac{c+x}{c-x}}\, dx$$

$$= \frac{2c\sqrt{c-x}(2\mathrm{b_i} + mc)\sin^{-1}\left(\sqrt{\frac{c+x}{2c}}\right) - (c-x)\sqrt{c+x}\left(2\mathrm{b_i} + m(2c+x)\right)}{2\sqrt{\pi c(c-x)}} \ldots\ldots\ldots\ldots\ldots\ldots (4)$$

$$IntTopToX(m, \mathrm{b_i}, -c) = 0 \quad \ldots\ldots\ldots\ldots\ldots\ldots\ldots\ldots\ldots\ldots\ldots\ldots\ldots\ldots\ldots\ldots\ldots\ldots\ldots\ldots\ldots\ldots\ldots\ldots\ldots (5)$$

$$IntTopToX(m, \mathrm{b_i}, c) = \lim_{x \to c}[IntTopToX(x)] = \frac{1}{2}(2b_i + mc)\sqrt{\pi c} \ldots\ldots\ldots\ldots\ldots\ldots\ldots\ldots\ldots\ldots\ldots\ldots (6)$$

The SIF $K_{I+,i}$ at the bottom of *i*-th layer, caused only by fracture pressure and in-situ stress of *i*-th layer, is

$$K_{I+,i} = IntTopTo\,X\left(m, \mathrm{b_i}, x_{2,i}\right) - IntTopTo\,X\left(m, \mathrm{b_i}, x_{1,i}\right) \ldots\ldots\ldots\ldots\ldots\ldots\ldots\ldots\ldots\ldots\ldots\ldots\ldots\ldots (7)$$

The total SIF at lower fracture tip, K_{I+}, caused by all layers, is

$$K_{I+} = \sum_{i=1}^{n} K_{I+,i} = \sum_{i=1}^{n}\left(IntTopTo\,X\left(m, \mathrm{b_i}, x_{2,i}\right) - IntTopTo\,X\left(m, \mathrm{b_i}, x_{1,i}\right)\right) \ldots\ldots (8)$$

where $x_{1,i}$ and $x_{2,i}$ are the top and bottom depths of the *i*-th layer, $x \in (-c, c)$; for each layer *i*, σ_i is the same for calculating $IntTopToX(x_{2,i})$ and $IntTopToX(x_{1,i})$.

For the SIF at upper fracture tip, K_{I-}, to be able to use the same function $IntTopToX$, we opposite the $x \in (-c, c)$ coordinate, so $-c$ becomes the bottom of the fracture; then replace m by $-m$ (because gravity g is to negative direction under the new coordinate); and $x_{2,i}$ by $-x_{1,i}$, $x_{1,i}$ by $-x_{2,i}$. Therefore,

$$K_{I-} = \sum_{i=1}^{n} K_{I-,i} = \sum_{i=1}^{n}(IntTopToX(-m, \mathrm{b_i}, -x_{1,i}) - IntTopToX(-m, \mathrm{b_i}, -x_{2,i})) \ldots (9)$$

Given fracture tip locations (*tipu* and *tipd*), fluid density (ρ), layer properties (σ_i, K_{ICi}, depth $x_{1,i}, x_{2,i}$, thickness hi, perforation zones, etc), and a reference depth-pressure pair (d_{ref}, P_{ref}), a Mathematica subroutine "*calcKIdiffs*" calculates SIFs, K_{I+} and K_{I-}, and then the differences between K_{I+} / K_{I-} and fracture toughness (K_{ICi}) in the layers where the fracture tips are located:

$$diffu = K_{I-} - K_{ICi}$$

$$diffd = K_{I+} - K_{ICi} \quad \ldots\ldots\ldots\ldots\ldots\ldots (10)$$

The fracture tip will be stable, if its corresponding difference is non-positive ($diffu \leq 0$ and/or $diffd \leq 0$); one or both tips will grow if the associated difference(s) is positive ($diffu > 0$ and $diffd > 0$). This can calculate the scenario that one tip is stable and the other grows. That is the criterion of equilibrium height. Then, we solve the two nonlinear equations *diffu*=0 and *diffd*=0 for the equilibrium tip locations *tipu* and *tipd*.

4.2.2 MFEH Model Description

We have developed the Fracture-Equilibrium- Height Model for up to 6-layer problem in the previous work (Liu and Valko 2015). Now we generalize it to any number of formation layers, no matter how many perforation intervals are made and whether they are placed in high- or low-stressed layers. Here is the workflow of MFEH model, comprised of 5 subroutines: *calcKIdiffs*, *prefufun*, *prefdfun*, *maketabs*, and *usetabs*.

***calcKIdiffs* Subroutine**

We calculate *diffu*/ *diffd*, the two differences between K_{I+} / K_{I-} and fracture toughness (K_{ICi}) in the layers where the fracture tips are located, using Equ. 10, for given layer data (depth, thickness, stresses, fracture toughness), reference depth and treating pressure at this depth, upper

and lower tip depths. The layer data is a matrix. The i-th row is the i-th layer's top depth, thickness, minimum horizontal stress, fracture toughness, and a Boolean variable indicating if the layer is perforated.

prefufun, prefdfun **Subroutines**

prefufun, *prefdfun* subroutines are used to find, for a given tips combination of *tipu* and *tipd*, the minimum pressure at d_{ref} for upper or lower tip to start to grow (*diffu* ≥0, *diffd* ≥0), respectively, using *calcKIdiffs* subroutine.

maketabs **Subroutine**

maketabs subroutine is to discretize all layers into small height elements, and make two lists- *tiputab/ tipdtab* representing upper/lower tip locations, ordered from the nearest to farthest distance away from perforated intervals, then make a maxtix *tdutab* representing all upper-lower tip pairs. For all upper-lower tip pairs, calculate two pressure matrixes *pfutab/ pfdtab* when upper/ lower tip starts to lose stability, using *prefufun*/ *prefdfun* subroutines. In matrix form: *pfutab(i, j), pfdtab(i, j), i* representing lower-tip location index in *tipdtab*, *j* representing upper-tip location index in *tiputab*.

usetabs **Subroutine**

usetabs subroutine finds the upper and lower equilibrium tip location, *tipuint/tipdint* for a prescribed reference pressure, using previously created lists and matrixes (*tiputab/tipdtab, pfutab/pfdtab*). For a given pressure, *prefint*, we start from the smallest upper-tip location index *j*=1 in *tiputab*, and fix this *j*, to search the first lower-tip position index *i* in *tipdtab* that keeps lower-tip stable (*pfdtab* (*i*, *j*) ≥ *prefint*); any lower tip before the i-th will be unstable and grow, because given pressure will be larger than the unstable pressure (*pfdtab* (*i*, *j*) ≤ *prefint*). Then check whether this (*i*, *j*) location index also makes upper-tip stable (*pfutab* (*i*, *j*) ≥ *prefint*); if yes,

this (*i*, *j*) is the location index in *tdutab(i, j)* corresponding to upper-lower tip pair solution (*tipuint*, *tipdint*); if not, this *j* position is too small under this *prefint* pressure for upper-tip to be stable or in equilibrium, so we need to go to the next upper-tip location index *j* in *tiputab*, and repeat the searching of *i* index, until we find a *j* index to make $pfutab(i, j) \geq prefint$. Now we find the equilibrium tip location index (*i*, *j*) and corresponding depths *tipuint*, *tipdint* for this pressure *prefint*. Finally, we interpolate the tip locations compared to previous upper-lower tip pairs to get the right solution (*tipuint*, *tipdint*). This way we can make sure height map evolves along the primary solution path, and avoid secondary solutions. Because we always start from the smallest upper tip and find the smallest corresponding lower tip locations, and interpolate the solutions based on previous, smaller tip locations. **Fig. 5** is the workflow of MFEH model:

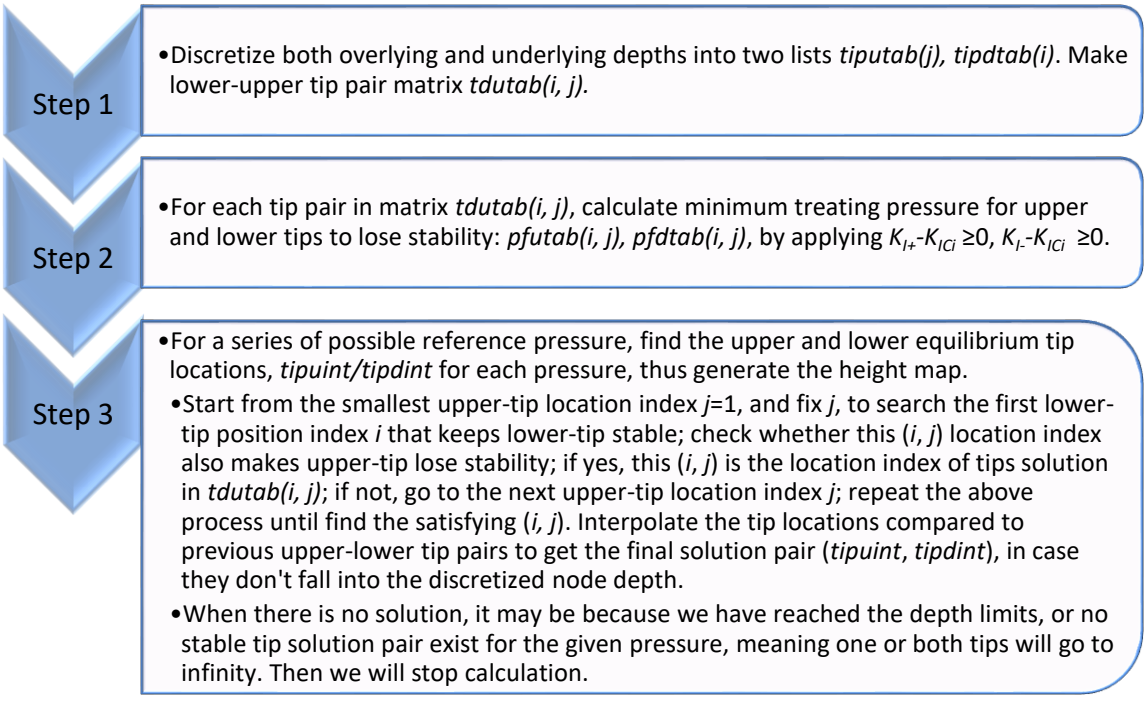

Fig. 5. The workflow of MFEH model.

4.2.3 A New Net Pressure Base Definition

As stated in Section 1.2.3, the net pressure base P_{base} is used to calculate apparent P_{net}, which is further used in the calculation of fracture width in the P3D model. So we need to find out a rigorous definition to calculate P_{base}. According to rigorous fracture mechanics definition, an initial fracture covering perforated zone will start to grow under a certain pressure, P_{base}, when stress intensity factor overcomes the in-situ fracture toughness, rather than reference treating pressure overcoming minimum in-situ horizontal stress. It's a criterion of integrated energy rather than a stress (think about Eqs. 1 and 10). The discrepancy of net pressure base will be more obvious in vertical wells when several different intervals are perforated. Here, we developed a new, rigorous method to calculate P_{base}: the minimum reference pressure at which the initial line crack (covering the perforated zone) will lose stability/equilibrium, or grow out of perforation zone, when the fracture toughness of the two layers containing the tips are artificially set to zero (Yang et al. 2012a, 2012b). Such a definition of P_{base} satisfies two requirements: 1) in the simple 1+2 layer case it gives back the usual definition of net pressure base, minimum in-situ stress σ_{min} at the middle layer; and 2) it will make sure that the initial fracture covering the perforated interval will not propagate under any negative net pressure. We noticed that definitions used in commercial software usually do not satisfy the second requirement, i.e., fracture may grow under negative net pressure.

For the base case in Table 3, we set layer 3 and 4 as perforated interval. The minimum in-situ stress σ_{min} is 5700 and 7350 psi, respectively. We calculated the minimum P_{ref} for the initial fracture to grow (when KI≥KIC), and the P_{base} from different methods mentioned above in section 4.2.3. Then we compared apparent P_{net} of different methods, in **Table 2**. We see that

for thickness-weighted σ_{min} as the base pressure, P_{net} is -205 psi, a negative value, when the initial fracture starts to grow!

Pressure, psi	Our Method	Thickness-Weighted σ_{min}	σ_{min} at Perforation Center
Pref_min	5809	5809	5809
Pbase	5777	6014	5700
Apparent Pnet	32	-205	109

Table 2. P_{base} and apparent P_{net} from different methods.

4.3 Height Map for Base Case

Based on the formation data described by Warpinski et al. (1994) (Warpinski et al. 1994), we set up our base case data as in **Table 3**, and set the reference depth at 9,255 ft and specific gravity of fracturing fluid as 1.1. We calculated the equilibrium-height map, i.e., fracture upper and lower tip locations vs. reference treating pressure **(Fig. 6a)**. Some results are listed in **Table 4**. The lower tip drops abruptly from the 4th layer through the 6th layer around 6550 psi, because the 5th layer has much lower in-situ stress 5,800 psi, compared to 7,350 psi and 8,200 psi in the neighboring layers. This height map can be used as a maximum limit for the height at wellbore calculated in 3-D model design, under a specific treating pressure.

No. of Layer	Top Depth, ft	Thickness h_i, ft	In-Situ Stress σ_i, psi	Fracture Toughness K_{ICi}, psi$\sqrt{\text{in.}}$	Perforation
1	8990	90	7150	2000	False
2	9080	90	7150	2000	False
3	9170	170	5700	2000	True
4	9340	40	7350	2000	False
5	9380	75	5800	2000	False
6	9455	195	8200	2000	False

Fracturing fluid density *SG*	1.1
Reference depth , d_{ref}, ft	9255

Table 3. Input data for the base case study.

	Base case	Full map case
Why the calculation stopped	Upper boundary was reached	Lower tip lost stability
Maximum pressure, psi	6,898	7,583
Maximum height, ft	511.4	-
tipu at end, ft	8,990	7,930
tipd at end, ft	9,501	-

Table 4. Output data for the base case and its full height map case.

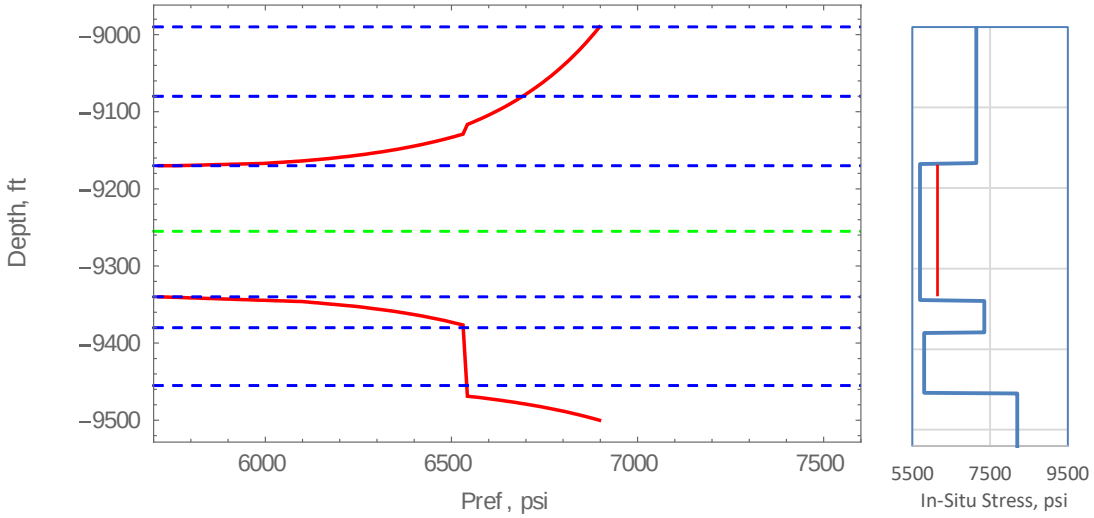

(a)

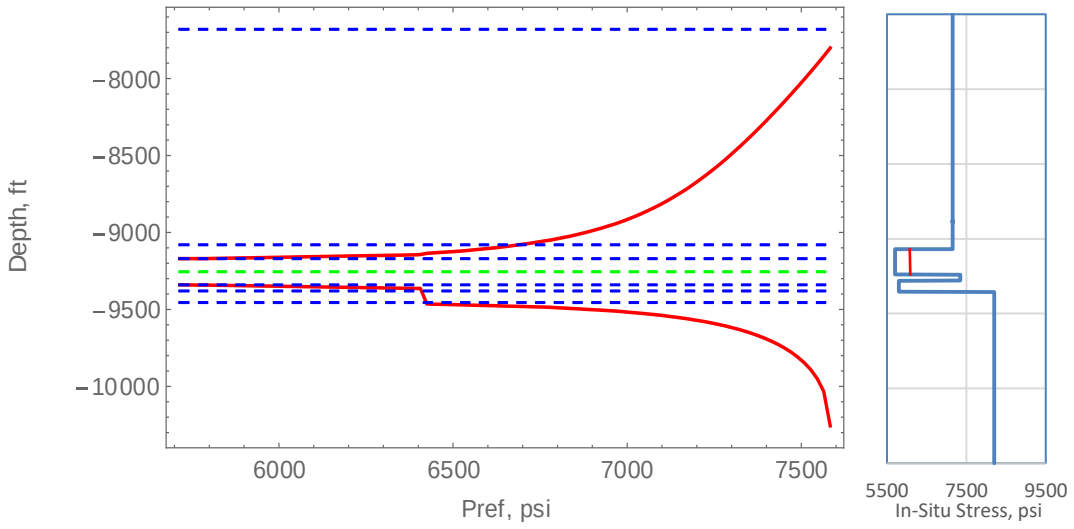

(b)

Fig. 6. (a) Height map of the base case, and (b) its full height map. Stress profiles on the right; Red bars represent perforation zones.

When we extend the thickness of top and bottom layers to large enough values of the input data, we can see the full height map **(Fig. 6b)**, i.e., the ultimate trend of height growth, when one fracture tip will grow to infinity. This suggests the maximum pressure to be used. The output parameters are shown in Table 4. In Fig. 5b, the calculation stops because the lower tip drops very quickly due to a small pressure increase. In other reservoir conditions with small upper barrier force, it may be the upper tip that loses stability.

4.4 Second Solution and Multiple Solutions in a 3-Layer Case

4.4.1 Investigate Second Solution Profile by Mathematical Experiment

Mathematically, there is a second solution pair of the tip locations above a certain net pressure (Valkó and Economides 1995; Liu and Valko 2015). To avoid confusion to our design job from this mathematical but impractical solution pair, we need to find when it will occur. Input data for a 3-layer case are in **Table 5**. Reference depth is 10,000 ft, and fracturing fluid density is 62.4 lb/ft^3. We found the second solution pair profile (dash lines in **Fig. 7**) by experimenting different initial values for solver in Excel. It occurs between 6666.5-6780.4 psi.

No. of Layer	Top Depth, ft	Thickness h_i, ft	In-Situ Stress σ_i, psi	Fracture Toughness K_{ICi}, psi$\sqrt{\text{in.}}$	Perforation
1	0	9975	6500	1000	False
2	9975	50	6000	1000	True
3	10025	1000	7000	1000	False
Fracturing fluid density ρ, lbm/ft^3			62.4		
Reference depth, d_{ref}, ft			10000		

Table 5. Reservoir data for the second solution pair study.

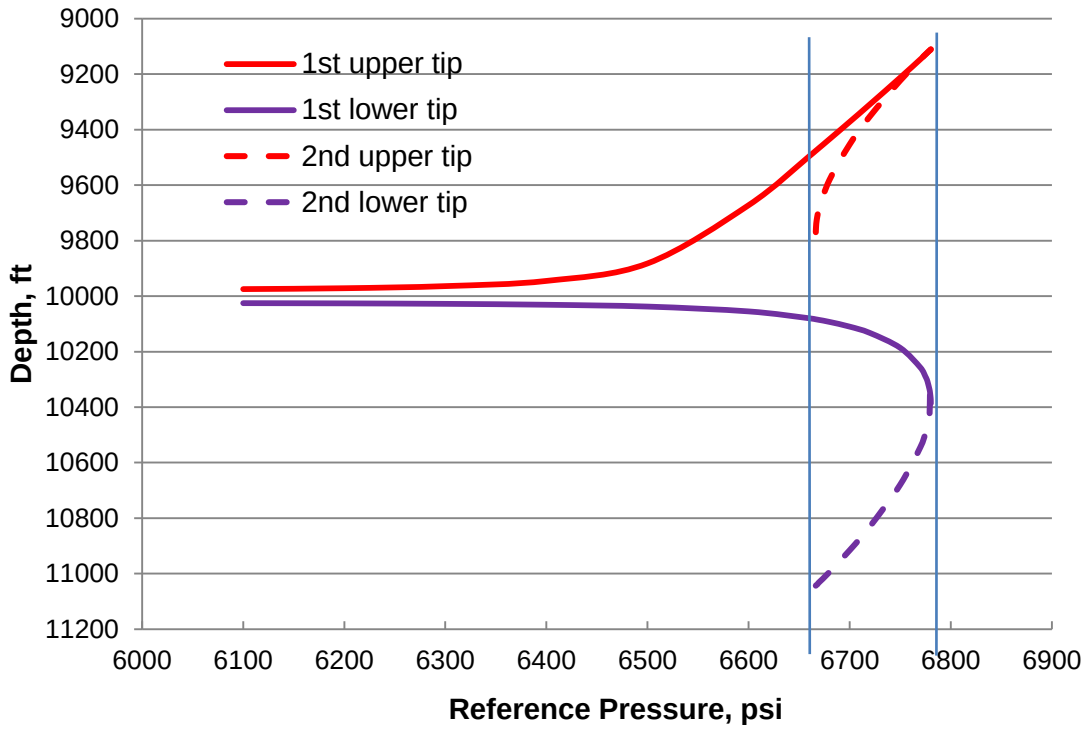

Fig. 7. Height map of the first and second solution pairs by experiment in Excel.

4.4.2 Predict Multiple Solution Profile

We also studied the appearance of second solution pair in this 3-layer case as in Table 5 using our *calcKIdiffs* subroutine model. In Mathematica, we used "RegionPlot" function to investigate where the equilibrium-height will occur, under each specified pressure, among all the combination of upper and lower tip locations (*tipu* and *tipd*) of the given 3-layer formation. Result is shown in **Fig. 8**. Tip locations *tipu* and *tipd* are in ft. Note that, the fracture starts from the lower left corner; the light blue area represents the tip-combination for upper tip to be stable (*diffu*<0), and the light red area represents the tip-combination for lower tip to be stable (*diffd*<0), the white area represents where the fracture exits, or, tips are unstable (*diffu*>0 and *diffd*>0), so the upper right corner of white area is the equilibrium-height tips (*diffu*=0 and *diffd*=0).

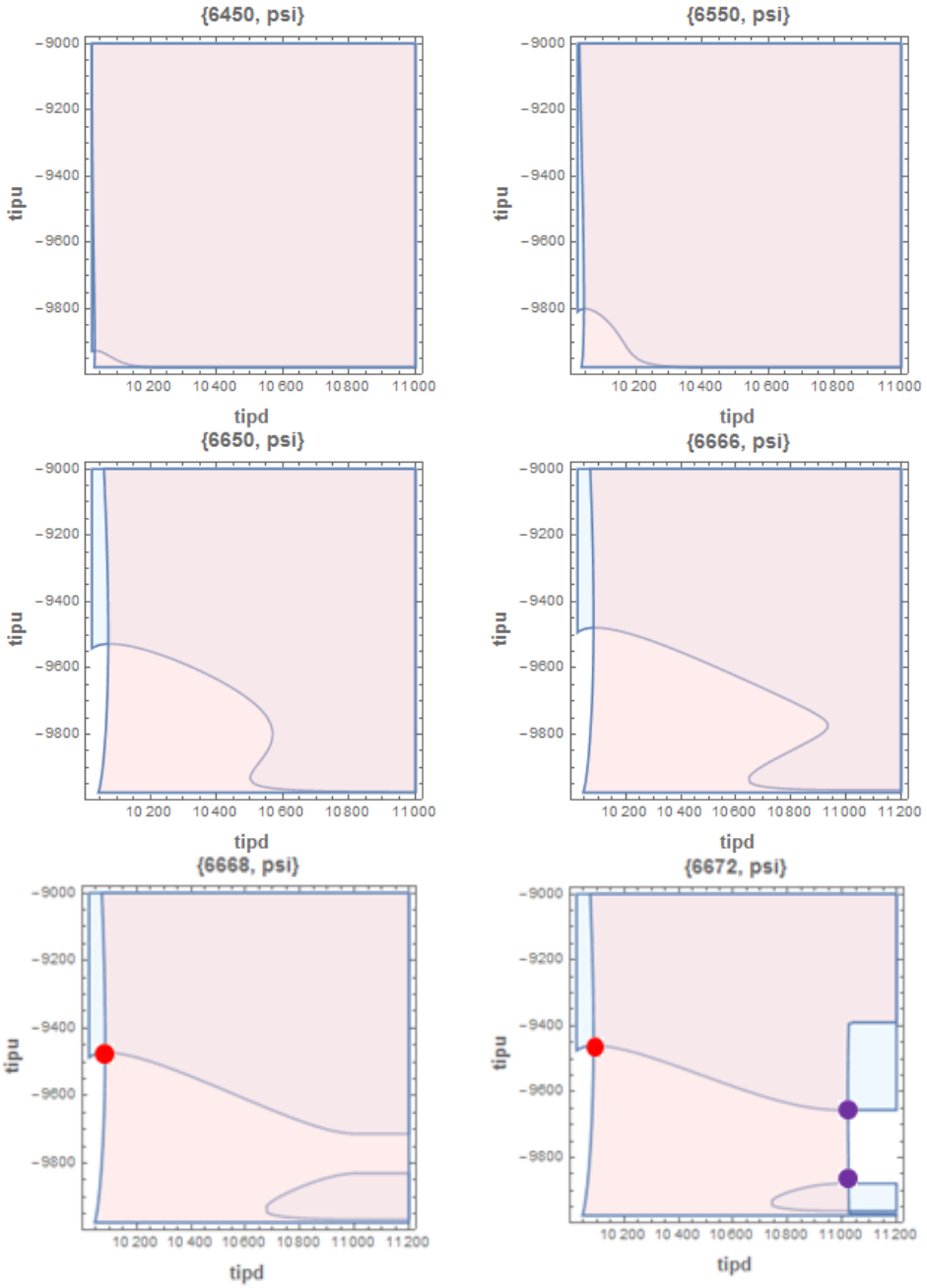

Fig. 8. Height map of the first and second solution pairs using our model. Red dots are primary solution pairs, purple dots are secondary solution pairs, which our model can avoid.

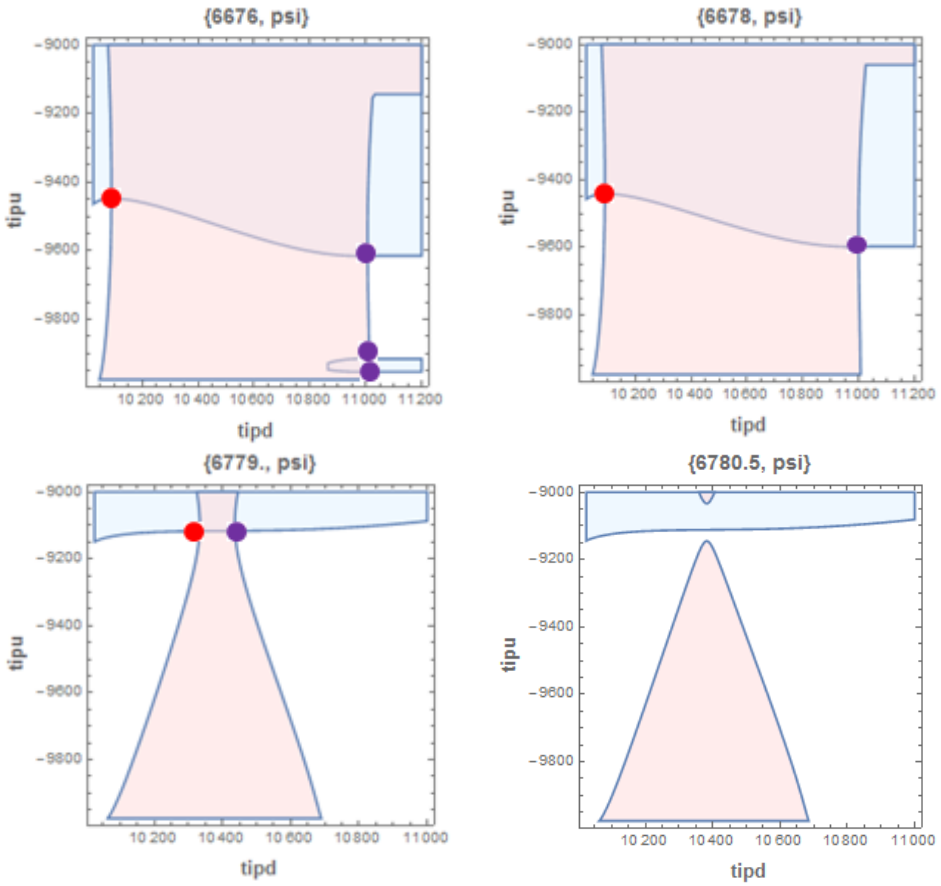

Fig. 8. Continued.

The same as in Fig. 7, the second solution pair occurs between 6666.5-6780.4 psi. At 6780.5 psi, there is no overlap between light blue (upper tip stable) and light red (lower tip stable) areas; upper tip location is sealed/limited by light blue area, when lower tip loses stability-shooting from 10400 ft to infinity, same in Fig. 7; so from now on, no solution exists, 6780.5 psi is the maximum treating pressure inside fracture we can use.

Interestingly, we see the *third and fourth* solution pairs occur between 6672-6676 psi. Because the two-equation system (*diffu*=0 and *diffd*=0) is highly nonlinear, and K_{ICi} can change abruptly from layer to layer. This is just a 3-layer case; for more layers, the multiple solutions will be more likely to appear.

From both Figs. 7 and 8, we can see that, if net pressure gradually increases and two tips gradually grow apart, it is impossible for the upper tip to recede back, and impossible for the lower tip to jump over a stable interval to a far, deep position. Therefore, this second solution pair is unrealistic, thus should be avoided in the fracture propagation simulator. Since our MFEH model always starts searching for the solution pair from the *lower left corner*, the secondary solution pairs can be avoided.

4.5 Comparison of the MFEH Model with Existing Models

4.5.1 Comparison with Previous Models with a 3-layer Symmetric Problem

To compare our model with existing models, we tested the models with a 3-layer symmetric problem, because some previous models apply to only 3-layer, symmetric formations. The input parameters and results are in **Tables 6 and 7**, respectively.

No. of Layer	Top Depth, ft	Thickness h_i, ft	In-Situ Stress σ_i, psi	Fracture Toughness K_{ICi}, psi$\sqrt{\text{in.}}$	Perforation
1	8962.5	1000	7700	1000	False
2	9962.5	75	7100	1000	True
3	10037.5	1000	8100	1000	False
Fracturing fluid density ρ, lbm/ft^3			62.4		
Reference depth, d_{ref}, ft			10000		

Table 6. Input data of the 3-layer case study for model comparison purpose.

Pnet , psi	Height Outside Perforated Interval, ft	MFEH Model	PPS/Newberry Method (Economides et al. 2012)	Error of Other models Over MFEH Model
200	Δh_u	3.76	2.79	26%
	Δh_d	1.62	0.97	40%
600	Δh_u	140	62.1	56%
	Δh_d	33	13.3	60%

Table 7. Comparison of fracture height with previous models for the 3-layer case.

The model in the book “Petroleum Production Systems” (PPS) (Economides et al. 2012) and Newberry et al. (1985) models obtained less fracture height, especially at higher net pressure (600 psi). The difference can be great (100 ft in total fracture height). The error ranges from 26~60% for the studied net pressure. The PPS model is not reliable due to the wrong derivation process and parameters (C1, C2, C3) listed in Table 1. The wrong height results can create unnecessary risk, if there are overlying and/or underlying aquifers, for it will cause problems of water production and contamination of drinking water. No solution can be obtained from the other methods (except MW model), because of the erroneous equations.

4.5.2 Comparison with MW Model with a 6-layer Asymmetric Problem

We also compared modified MW model (using the corrected equation (9) in Weng et al. paper (2011)) with our model on the 6-layer asymmetric problem, the base case, described in Table 3. We substitute our *calcKIdiffs* subroutine with SIF equations in modified MW model in Table 1, Eq. 9.

The height maps produced from two methods overlap very well, as shown in **Fig. 9**. In Fig. 9 we used fluid density as 1 SG (specific gravity); we also tested SG of 2 and 5, and again got very good overlapping between the two methods. Thus, modified MW method is a reliable model to calculate SIF, although the authors didn’t address the secondary solution issue.

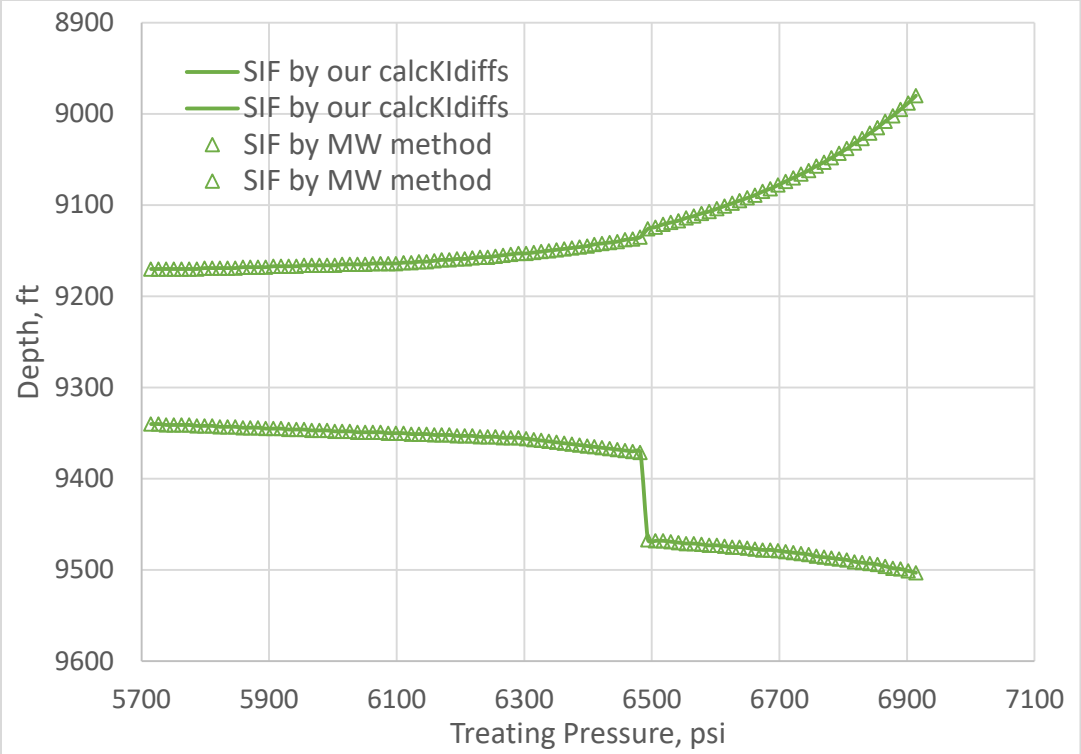

Fig. 9. Comparison of height map with stress intensity factor (SIF) using modified MW model and our calcKIdiffs subroutine.

4.5.3 Comparison with Commercial Software

We compared the near-wellbore height results of MFEH model with MShale and FracPro software, under the same ideal geology condition, for 2 stages in a horizontal well A, and a vertical well B with 4 vertical perforation intervals (2 intervals above and 2 below the middle non-perforated interval) (**Fig. 10**). The well data used for these modeling are from Fayetteville shale. The stress profiles for the different scenarios are shown in Fig. 10. There are generally 7 layers for each scenario. Red dots/lines represent the perforation locations.

Run the cases in MShale and FracPro with ideal conditions: No wellbore hydraulic, no heat transfer, no fracture friction, no wall roughness, no tip effect, no perforation erosion, no proppant solution, no fracture-proppant effect, 3-D model, one fracture/cluster, no fracture

interaction, same pump schedule for 3 clusters each stage, proppant distribution-uniform, no near wellbore effect, no mid-field fracture complexity, zero leakoff, same formation properties (thickness, TVD, E, Poisson ratio, fracture toughness, in-situ stress) between the software and MFEH.

We select fluid specific gravity (SG) as 1, viscosity at shear rate 100 1/s. The rheology data don't matter because we assume no friction anywhere, and we only look at the pressure and height at the wellbore. Use proppant A004 and A002 with the following properties. Final proppant is A002 with concentration 1.4 ppg.

1) Proppant A004: Atlas PRC 40/70 @250F, SG=2.41, Diameter= 0.01295 in
2) Proppant A002: Atlas PRC 20/40 @250F, SG=2.54, Diameter= 0.0256 in

In input data for MFEH model, to consider the initial perforated fracture height in horizontal well, we add a 5-ft layer into the pay zone which is the only layer to be perforated, thus splitting the pay zone into 3 layers. Use the same reference depth and density (1101.7 kg/m^3) as the software. To compare the results between MShale/FracPro with MFEH height map, take the highest bottomhole flowing pressure (BHFP) or net pressure from MShale/FracPro, and interpolate in MFEH height map, then compare the upper and low tips locations and total hf.

When wells are perforated at the low-stressed layers (Fig. 10a, 10b, 10c: 4025 psi in the 5th layer), the two commercial models give almost the same results of final wellbore height (**Fig. 11a, 11b**), with slightly difference (1.4-8.8 ft of difference). MShale calculated height around 4 ft smaller, and FracPro average 6 ft larger, than our MFEH model.

The discrepancy is much larger (20-60 ft of difference), when there are abnormally low stress in the adjacent layers (Fig. 10d, 10e: 3000 psi in overlying or underlying layers v.s. 4025

psi in the perforated layer), or abnormally high stress in adjacent layers (Fig. 10f: 6000 psi in underlying layers v.s. 4025 psi in the perforated layer). MShale shows much smaller height (Fig. 11c: average 39 ft shorter), while FracPro model much larger height (Fig. 11d: average 29 ft higher).

When we combine the 4 perforation intervals into 1 perforation interval, again MShale shows much shorter height (37 ft smaller), and FracPro model much larger height (25 ft larger) (the last columns in Fig. 11c & 11d).

The discrepancy is not because they consider other issues like weak formation interface, naturally fractured formations, as it can be demonstrated by running the software with these additional effects switched off. The discrepancy may be attributable to the different interpretation of the "net pressure", and how they solve the non-linear equilibrium height equation system for the multi-layered reservoir scenario. From **Table 8**, Bottomhole Flowing Pressure (BHFP), base pressure, and net pressure comparison of the software with our MFEH model, we find MShale uses thickness-weighted in-situ stress as the base pressure for net pressure, while FracPro uses in-situ stress at the center of perforation interval as the base pressure. However, when there are abnormally low/high stress in the adjacent layers, even the treating pressure (BHFP), base pressure, and net pressure are all the same respectively between the software and our MFEH model, there is still large discrepancy, meaning the difference mainly coming from how they discretize the multi-layer formations, solve the non-linear equation system, and how they deal with the abrupt change or large contrast in the formation properties. Since our model calculates fracture height for uniform, non-naturally fractured media without weak layer interface, thus provides upper limit of fracture height for all reservoir conditions, MShale is more acceptable.

(a)Pressure Comparison of MShale and MFEH model

	Model	Well A-Stg 1	Well A-Stg 2	Well B-Interval 1	Well B-Interval 2	Well B-Interval 3	Well B-Interval 4	Well B-One Total Interval	Stg 1-Overlying Low Stress	Stg 1-Underlying Low Stress	Stg 1-Underlying High Stress
BHFP	MShale	4288.9	4350.0	4240.4	4247.4	4262.9	4269.4	4378.1	4247.8	4353.7	4524.8
	MFEH	4288.6	4349.7	4240.4	4247.4	4262.9	4269.4	4378.2	4247.8	4353.7	4524.8
Base Pre	MShale	4024.8	4080.5	4017.4	4015.6	4015.5	4025.8	4018.1	4024.8	4024.8	4024.8
	MFEH	4024.5	4080.2	4014.9	4014.8	4017.8	4024.3	4014.6	4024.1	4024.5	4025.1
Net Pre	MShale	264.1	269.5	223.0	231.9	247.4	243.6	360.0	223.0	328.9	500
	MFEH	264.1	269.5	225.5	232.6	245.1	245.1	363.6	223.7	329.2	499.7

(b)Pressure Comparison of FracPro and MFEH model

	Model	Well A-Stg 1	Well A-Stg 2	Well B-Interval 1	Well B-Interval 2	Well B-Interval 3	Well B-Interval 4	Well B-One Total Interval	Stg 1-Overlying Low Stress	Stg 1-Underlying Low Stress	Stg 1-Underlying High Stress
BHFP	FracPro	4429.0	4494.0	4429.9	4453.8	4414.6	4381.1	4596.0	4381.0	4488.0	4636
	MFEH	4429.3	4494.5	4429.9	4453.8	4414.6	4381.1	4596.0	4381.0	4488.0	4636.0
Base Pre	FracPro	4025.2	4080.5	4014.9	4014.8	4018.6	4024.1	4024.5	4024.4	4025.2	4024.8
	MFEH	4025.5	4081.0	4014.9	4014.8	4018.6	4024.1	4014.9	4025.1	4024.5	4024.8
Net Pre	FracPro	403.8	413.5	415.0	439.0	396.0	357.0	571.5	356.6	462.8	611.2
	MFEH	403.8	413.5	415.0	439.0	396.0	357.0	581.1	355.9	463.5	611.2

Table 8. Bottomhole Flowing Pressure (BHFP), base pressure, and net pressure comparison between the software (a) MShale and (b) FracPro with our MFEH model. BHFP is the highest treating pressure outside the perforation obtained in MShale and FracPro for all the scenarios.

For the same scenario, e.g., Well A-Stage 1, our model produced different heights as in Fig. 11a and 11b. This is because our model needs the highest fracture pressure during the whole fracturing process to get the largest fracture height; and this largest height is used to compare with the final height calculated in the software. While somehow the two pieces of software yield different highest fracture pressure for the same scenario (BHFP in Table 8). So we need to adjust the pressure to get different heights for two comparisons.

For the underlying layer, with increasing in-situ stress, both software applications show we need larger final highest treating pressure (see Table 8 and Fig. 11e): MShale from 4353.7 to

4524.8 psi, FracPro from 4488 to 4636 psi. MFEH model got different results and trends (see 2nd and 3rd columns in Fig. 11c and 11d) for corresponding pressures read from MShale (2 green lines in Fig. 11e) and FracPro (2 blue lines in Fig. 11e), because higher underlying stress will push the whole fracture upwards. However, whether the total fracture height will be higher or not depends on the competition of higher treating pressure and higher underlying in-situ stress, and the upper in-situ stresses relative to the underlying ones.

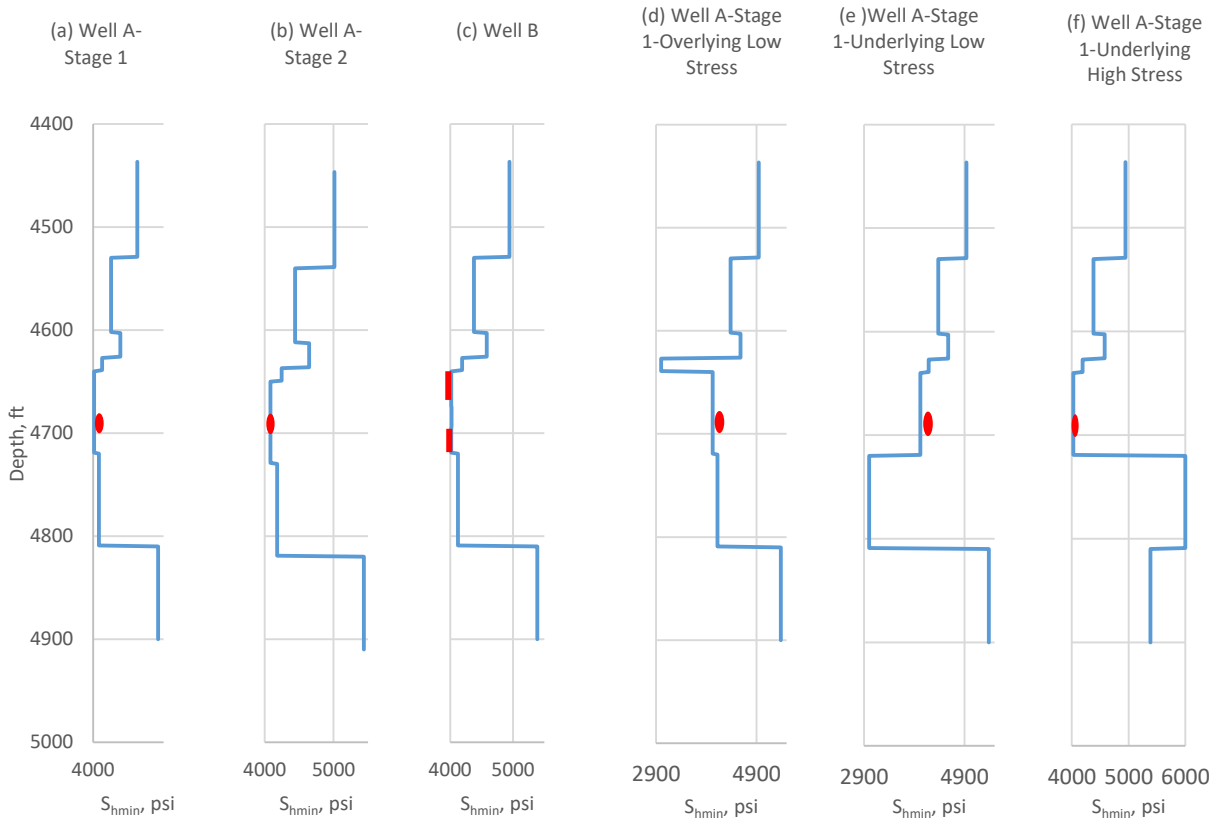

Fig. 10. Stress profiles for (a) & (b) two stages of the horizontal well A, (c) the vertical well B with 4 perforation intervals (2 intervals above and 2 below the middle non-perforated interval); For Well A-Stage 1: (d) low stress in overlying layer above perforation interval, (e) low stress in underlying layer below perforation interval, and (f) high stress in underlying layer below perforation interval. Red dots/lines represent the perforation locations.

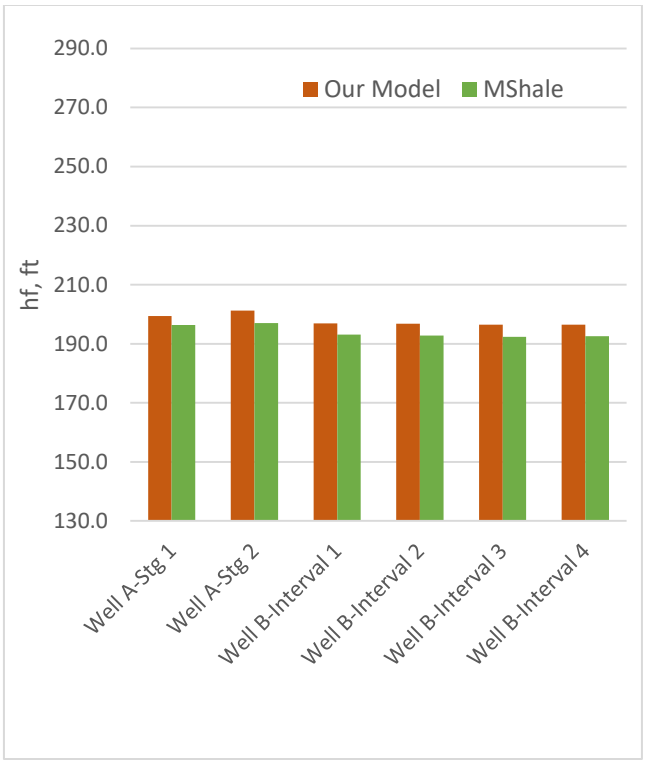

(a) MShale vs MFEH

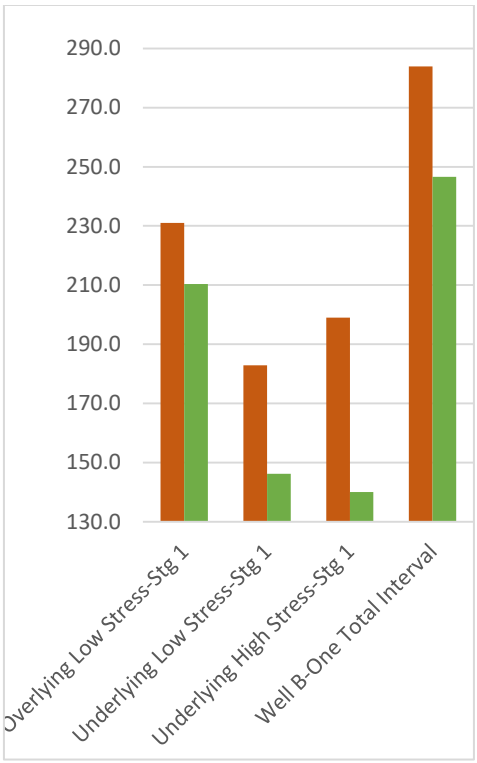

(c) MShale vs MFEH

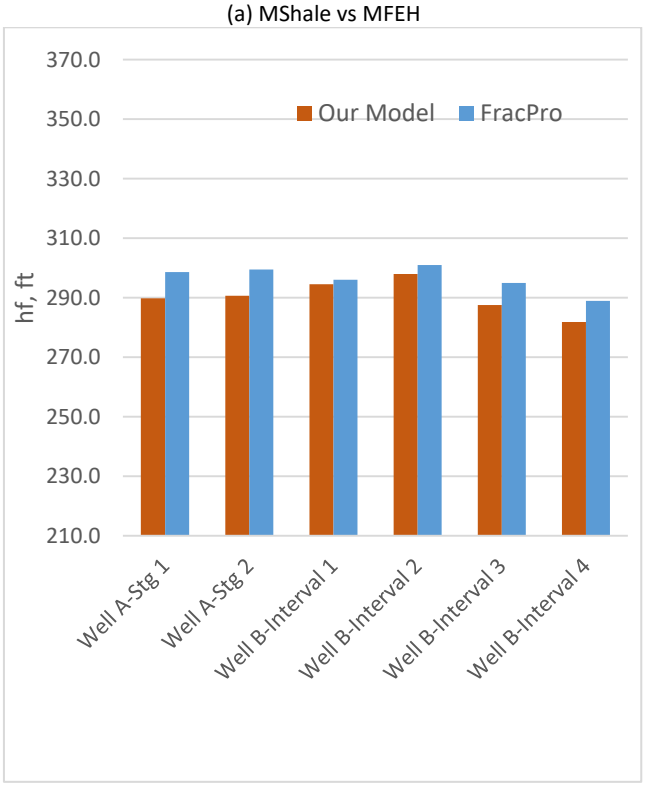

(b) FracPro vs MFEH

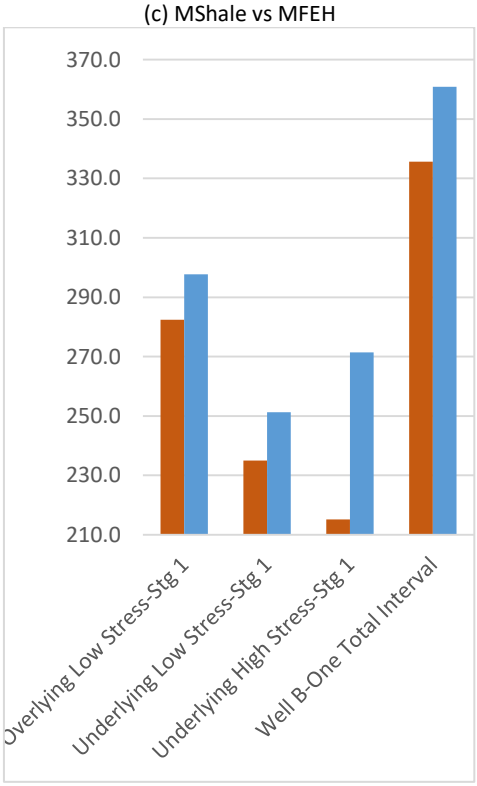

(d) FracPro vs MFEH

Fig. 11. Height comparison of (a) & (c) MShale and (b) & (d) FracPro software with our model. (e) MFEH heights for underlying low and high stresses scenarios with different highest treating pressure obtained from MShale (2 green lines) and FracPro (2 blue lines).

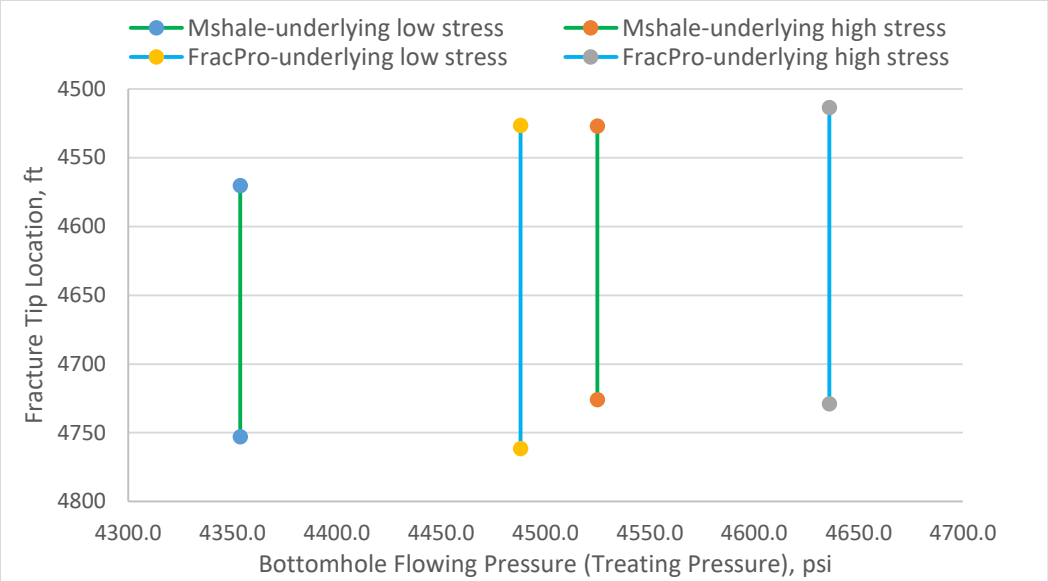

(e) MFEH heights for underlying low and high stresses scenarios and different treating pressure obtained from MShale and FracPro

Fig. 11. Continued.

4.6 Influence of Rock and Fluid Properties

Among the many factors mentioned in the "Introduction", here we only look at the factors that affect the equilibrium-height migration: in-situ stress, σ; fracture toughness, K_{IC}; fluid density, ρ; and their interactive effects. Based on the base case data in Table 3, we extended the top and bottom layer thicknesses as needed, and kept other parameters the same, while changing one parameter to be evaluated. P_{net} is used for x-axis, with 5700 psi calculated as the net pressure base.

4.6.1 Effect of In-situ Stress in Underlying Layers

We set σ_6= 5,200, 8,200, 10,000, 30,000 psi, to investigate the effects of in-situ stress in the underlying layers **(Fig. 12)**. When the in-situ stress, σ_6, in underlying layers is very small, the lower tip drops down to infinity (Fig. 12a); as σ_6 increases, the lower tip grows steadily (Fig. 12b); when σ_6 is large, the lower tip will stay at the interface of layer 5 and 6 for large net pressures (Figs. 12c and 12d); then, it may grow downward, to infinity, if the net pressure is

large enough (Fig. 12e). When σ_6 is extremely large, e.g. 30,000 psi, the in-situ stress barrier fully stops the downwards growth of the fracture (Fig. 12f).

4.6.2 Effect of In-situ Stress in Overlying Layers

We set σ_1= 5,150, 7,150, 10,000, 30,000 psi, to investigate the effects of in-situ stress in the overlying layers **(Fig. 13)**. When the in-situ stress, σ_1, in overlying layers is too small, the upper tip shoots to infinity (Fig. 13a). As σ_1 increases, the upper tip grows slowly (Fig. 13b); when σ_1 is large, the upper tip will be confined, even at large net pressure (Figs. 13c and 13d), and the lower tip will lose stability.

4.6.3 Effect of Fracture Toughness in Underlying Layers

We set K_{IC6}= 500, 2,000, 20,000, 50,000 psi$\sqrt{\text{in.}}$, to investigate the effects of fracture toughness in the underlying layers **(Fig. 14)**. When K_{IC6} in underlying layers is small, the lower tip propagates steadily but not abruptly, and eventually to infinity at large net pressure (Figs. 14a and 14b). When K_{IC6} is large, the lower tip will stay at the boundary of layers 5 and 6 for a long period, until it has accumulated enough net pressure to overcome the fracture toughness. Then, the lower tip will grow downward, and the upper boundary may be reached before the lower tip loses stability (Figs. 14c, 14d).

4.6.4 Effect of Fracture Toughness in Overlying Layers

We set K_{IC1}= 500, 2,000, 20,000, 50,000 psi$\sqrt{\text{in.}}$, to investigate the effects of fracture toughness in the overlying layers **(Fig. 15)**. When K_{IC1} in overlying layers is small, it does not affect the overall height map (Figs. 15a and 15b); this is different from effect of overlying σ_1,

where small σ_1 will cause the upper tip to jump up and lose stability, because fracture toughness is an integration of pressure/stress. When K_{IC1} is too large, the upper tip will stay at the boundary of layers 1 and 2 for a long period (Figs. 15c and 15d), until it has accumulated enough net pressure to overcome the fracture toughness. At the same time, the lower tip will continue to grow downward in an unlimited manner.

4.6.5 Interaction of In-situ Stress and Fracture Toughness

High σ and Low K_{IC}

We set σ_5=10,000 psi, K_{IC5}=500 psi$\sqrt{\text{in.}}$, and σ_1=10,000 psi, K_{IC1}=400 psi$\sqrt{\text{in.}}$, to study the interaction of high in-situ stress and low fracture toughness in the boundary layers **(Fig. 16)**. Fracture tips grow slowly in the associated layers because of the high in-situ stress, and they do not jump even though the fracture toughness is smaller in these layers. Therefore, small K_{IC} doesn't affect the profile significantly, whereas high σ dominates the tip growth.

Low σ and High K_{IC}

We set σ_5=5,000 psi, K_{IC5}=10,000 psi$\sqrt{\text{in.}}$, and σ_1=6,050 psi, K_{IC1}=10,000 psi$\sqrt{\text{in.}}$, to study the interaction of low in-situ stress and high fracture toughness in the boundary layers **(Fig. 17)**. Fracture tips stay at the boundaries of layers for a period because of high K_{IC}, and then they jump because of low σ. Thus, high K_{IC} affects the profile at the associated boundary initially; then, the low σ becomes the controlling factor.

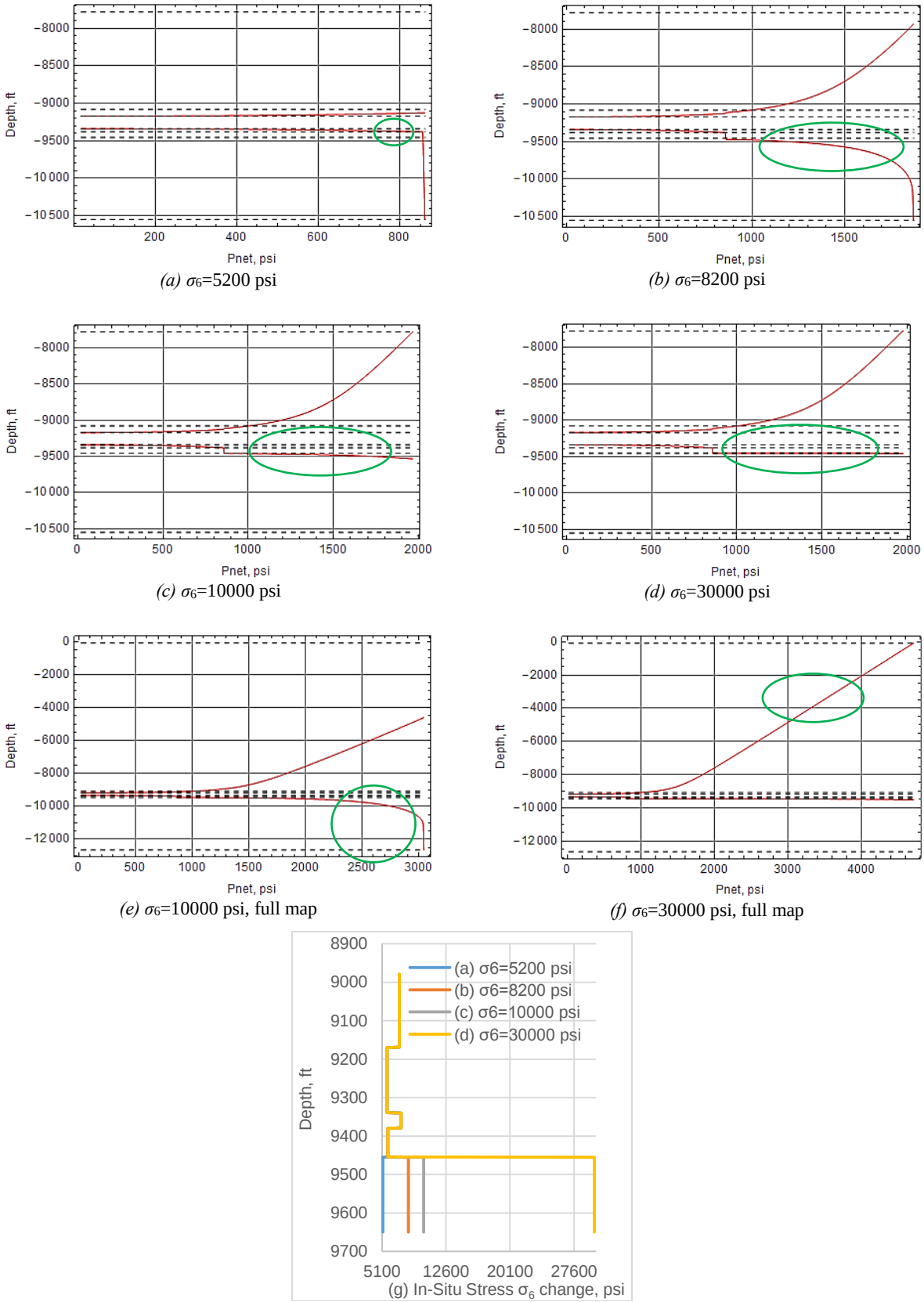

Fig. 12. Effects of in-situ stress in underlying layers on the induced fracture height map.

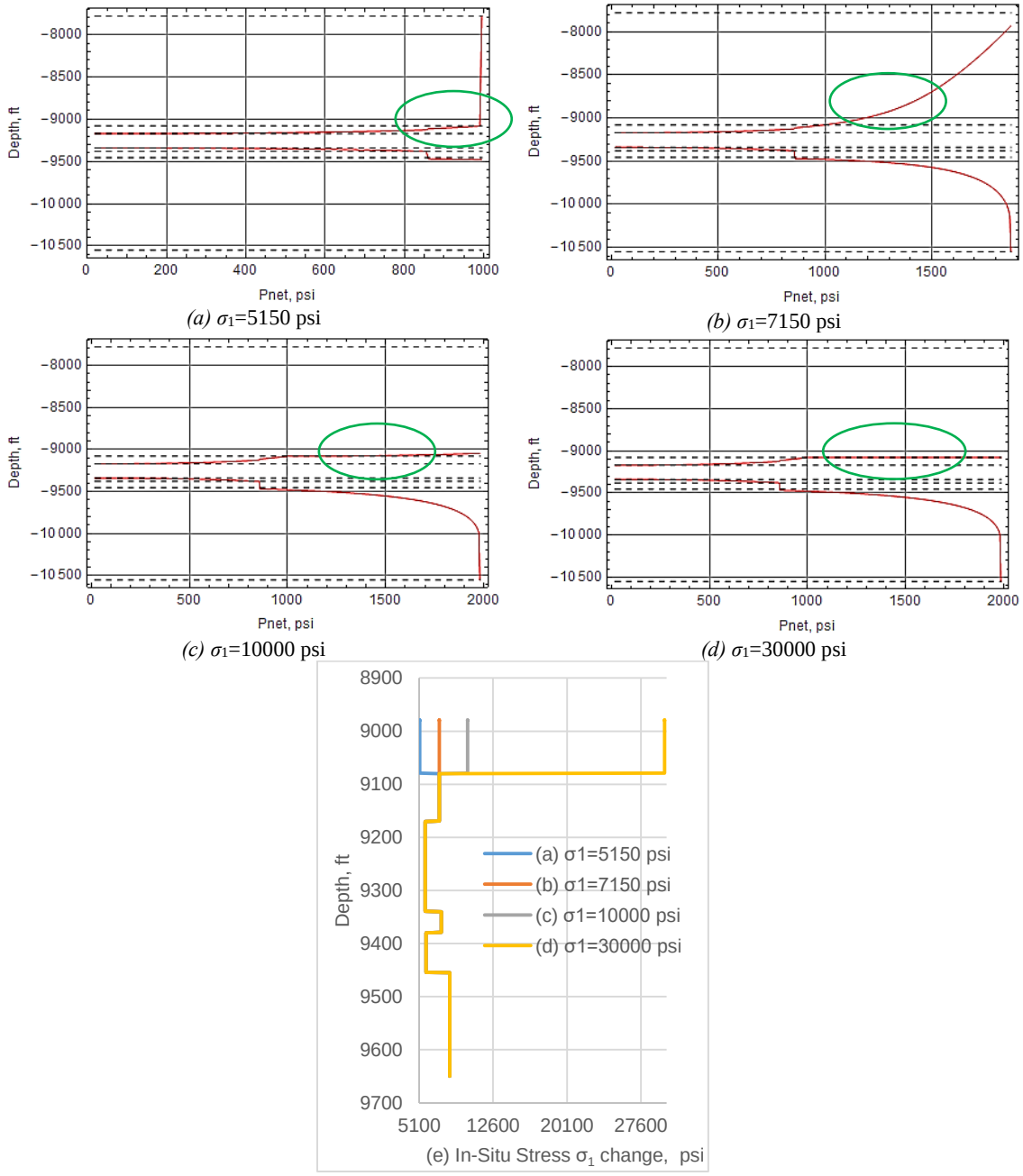

Fig. 13. Effects of in-situ stress in overlying layers on the induced fracture height map.

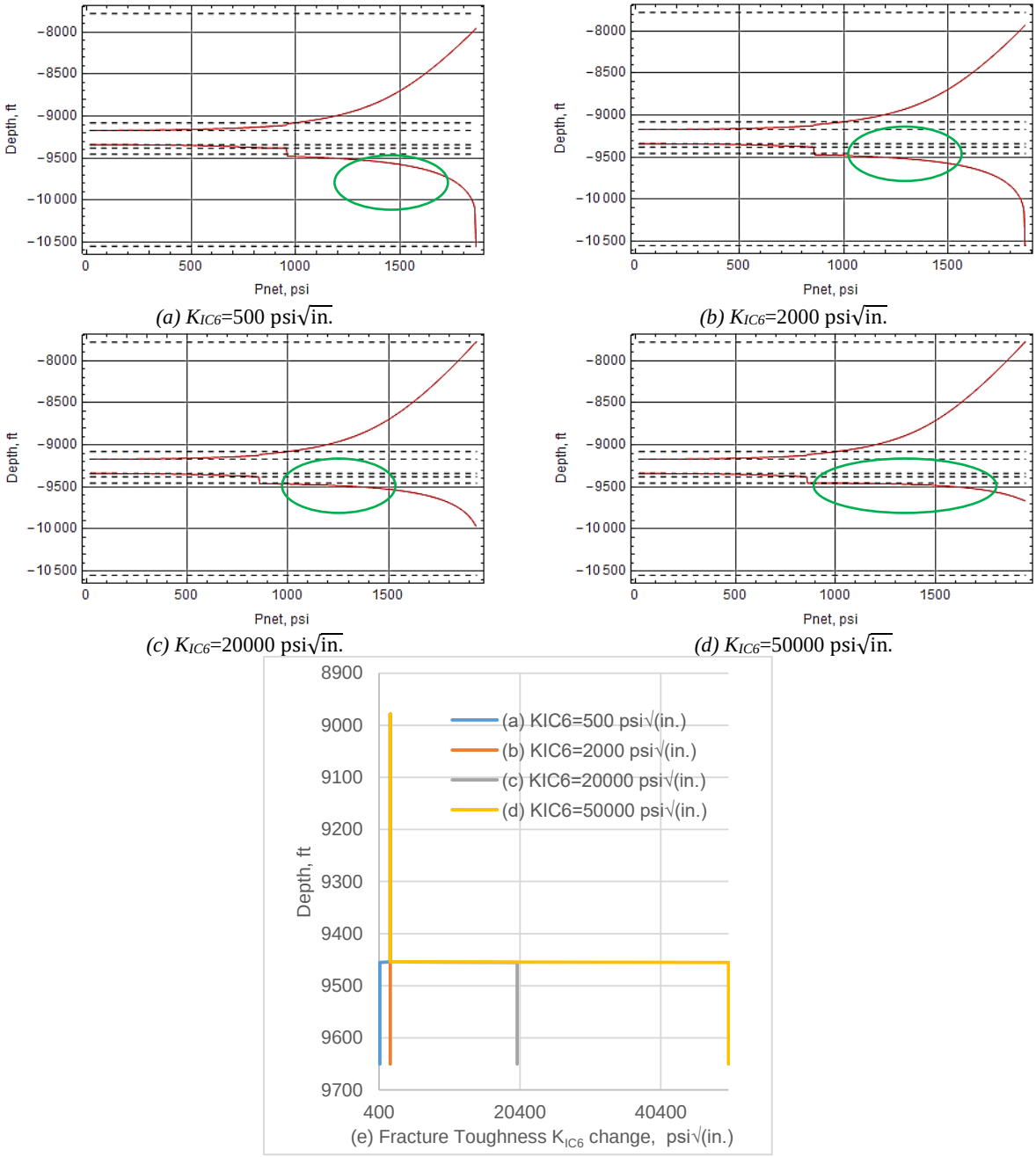

Fig. 14. Effects of fracture toughness in underlying layers on the induced fracture height map.

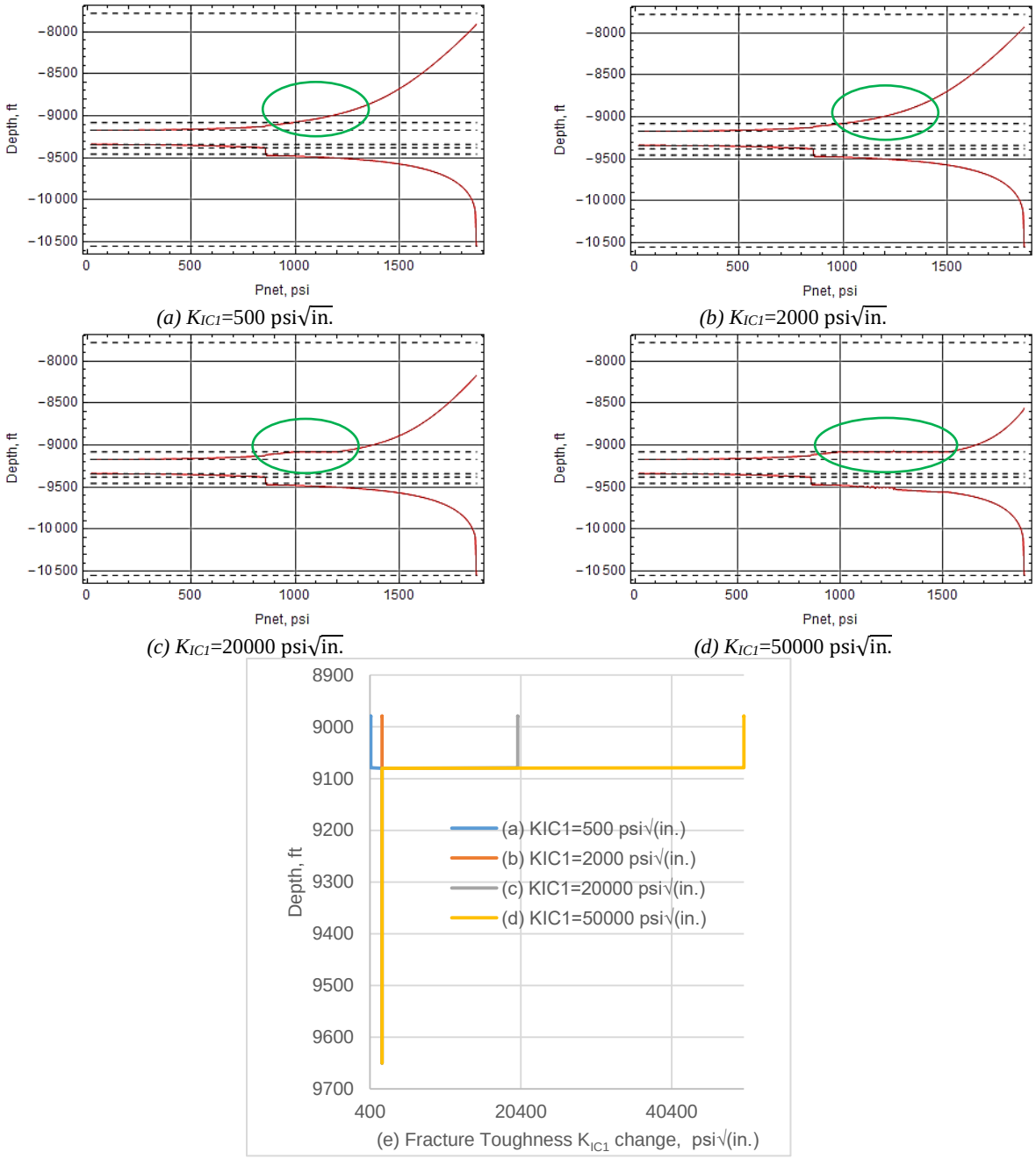

Fig. 15. Effects of fracture toughness in overlying layers on the induced fracture height map.

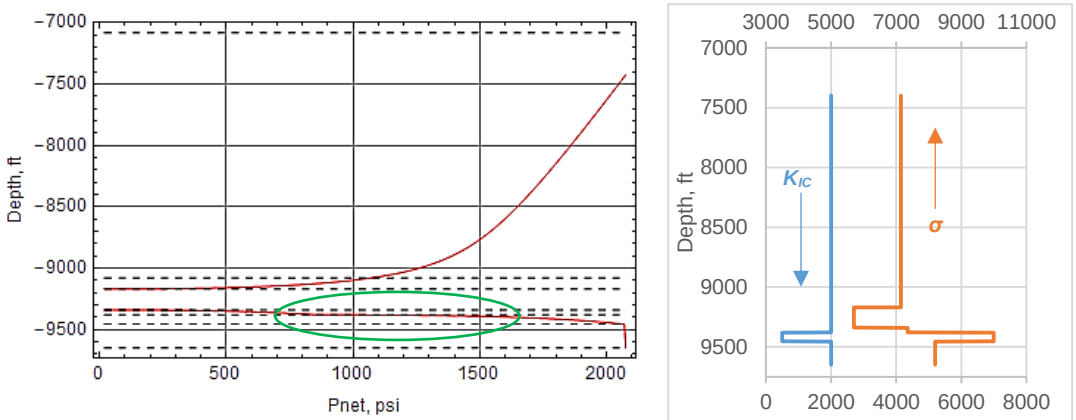

(a) σ_5=10000 psi, K_{IC5}=500 psi$\sqrt{in.}$

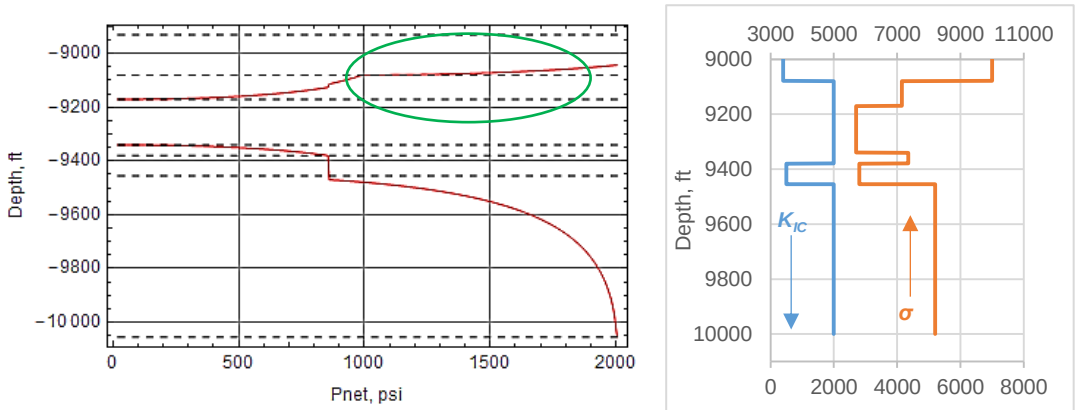

(b) σ_1=10000 psi, K_{IC1}=400 psi$\sqrt{in.}$

Fig. 16. Interactive effects of High σ and low K_{IC} on the induced fracture height map.

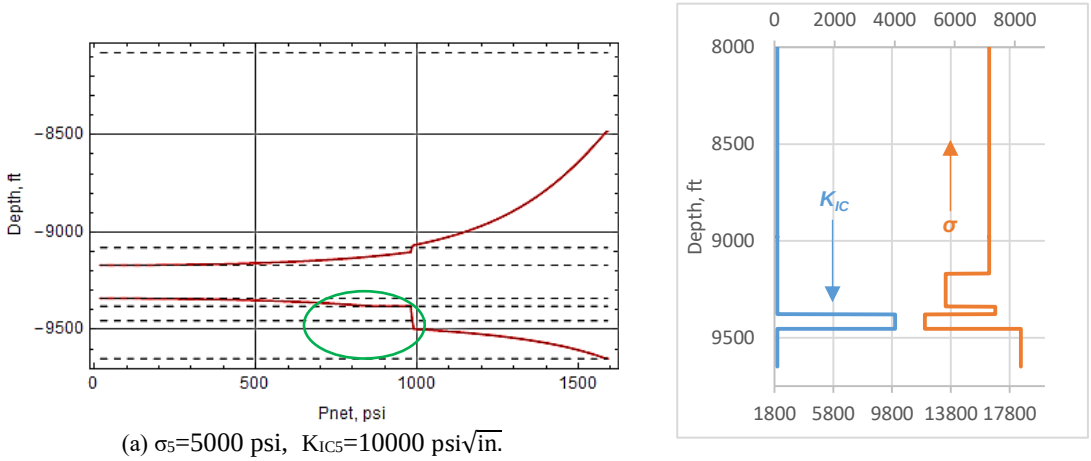

(a) σ_5=5000 psi, K_{IC5}=10000 psi$\sqrt{in.}$

Fig. 17. Interactive effects of low σ and high K_{IC} on the induced fracture height map.

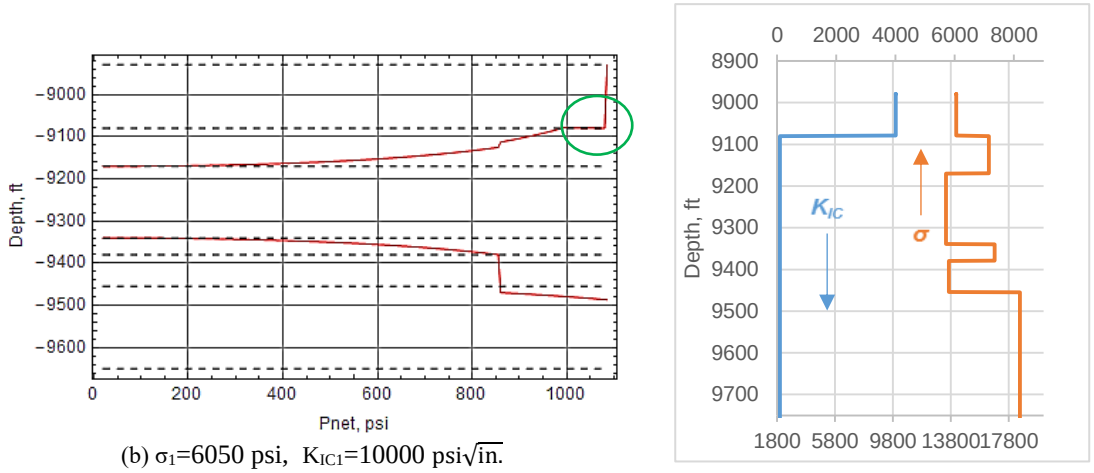

(b) σ_1=6050 psi, K_{IC1}=10000 psi$\sqrt{in.}$

Fig. 17. Continued.

4.6.6 Effect of Fluid Density

We set the specific gravity of fracturing fluid SG=0, 1, 2, to investigate the effects of fluid density on height growth **(Fig. 18)**. In the base case, if SG=0, the upper tip will lose stability first, while lower tip will grow in an unlimited manner if SG=1 and 2. Thus, if we ignore or give the wrong value of the fracture fluid density in the pre-fracturing design, the results can be misleading.

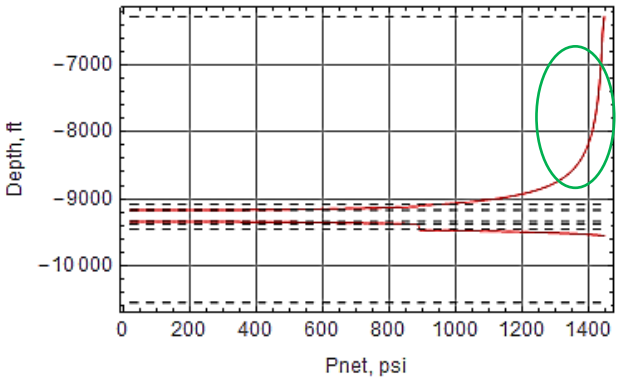

(a) SG=0

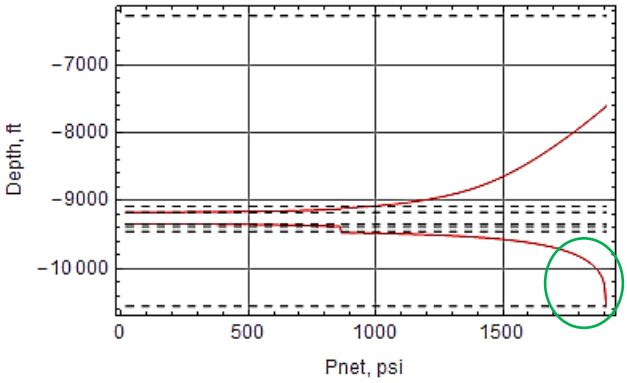

(b) SG=1

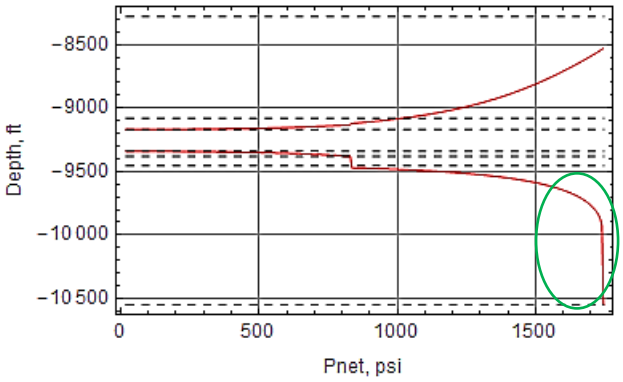

(c) SG=2

Fig. 18. Effects of fluid density on the induced fracture height map.

4.7 Outer and Inner Height Map Envelopes

There are many uncertainties in the available reservoir data, due to the geologic heterogeneity and measurement technology. Therefore, it is advantageous to know the outer and inner envelopes of the height map of a specific multilayer formation.

We determine the *outer* envelope by selecting the *minimum* in-situ stress, and fracture toughness, in each of overlying and underlying layers to establish a pseudo 3-layer problem; similarly, we make the *inner* envelope by selecting the *maximum* in-situ stress, and fracture toughness, to establish another pseudo 3-layer problem **(Table 9)**.

From **Fig. 19**, we can see the outer envelope stopped calculation at 55 psi net pressure, because the lower tip drops down in an unlimited manner; the inner envelope stopped calculation at 1,610 psi net pressure, because the upper tip reached the boundary; while the original 6-layer problem stopped calculation at 1,000 psi net pressure, because the upper tip lost stability. The inner envelope gives us the maximum net pressure we may need to fracture the formation, and the outer envelope tells us the minimum net pressure we may need. The difference between them can be hundreds of psi; therefore, we should determine the reservoir properties as precisely as possible, to avoid the invalid design.

	No. of Layer	Top Depth, ft	Thickness h_i, ft	In-Situ Stress σ_i, psi	Fracture Toughness K_{ICi}, **psi$\sqrt{\text{in}}$.**	Perforation
Original Problem	1	8580	500	6150	2000	False
	2	9080	90	7150	2000	False
	3	9170	170	5700	2000	True
	4	9340	40	7350	2000	False
	5	9380	75	5800	2000	False
	6	9455	500	8200	2000	False
Outer Envelope	1	8580	590	6150	2000	False
	2	9170	170	5700	2000	True
	3	9340	615	5800	2000	False
Inner Envelope	1	8580	590	7150	2000	False
	2	9170	170	5700	2000	True
	3	9340	615	8200	2000	False

Table 9. Reservoir data for the outer and inner envelopes study.

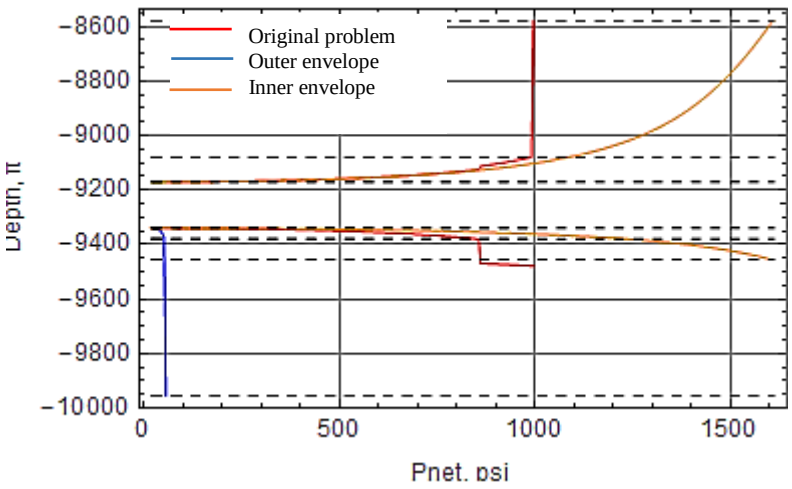

Fig. 19. Outer and inner height map envelopes for a specific multilayer formation.

4.8 Conclusions

1)A literature review revealed limitations of current models for determining equilibrium-height of hydraulic fractures. We developed a Multilayer Fracture-Equilibrium-Height Model (MFEH) that rapidly and rigorously solves for equilibrium-height under various formation minimum in-situ stress (σ), fracture toughness (K_{IC}), and fluid density (SG). The detailed derivation of stress intensity factors (SIFs) K_I clearly demonstrates the physical meaning of SIFs. This model is based on equilibrium height theory, so provides upper limit for fracture height.

2)Comparison with previous models and commercial software (MShale and FracPro) was made. When there is abruptly high or low stress or fracture toughness in the adjacent layers of perforated interval, current models predict the wrong height. Generally, MShale calculated shorter height, and FracPro higher height, than our MFEH model. While our model is robust to calculate the correct height under those circumstances, no matter how many perforation intervals and whether they are placed in high- or low-stressed layers. Modified Mack and Warpinski's model (modified MW) is right in the calculation of K_I although they didn't show the clear derivation.

3)The secondary solutions were investigated using mathematical experiment and this model, and can be eliminated in the MFEH model. They are physically unrealistic and misleading in the fracture propagation design, even though mathematically right.

4)The proposed new definition of net pressure base Pbase can make sure the initial fracture always grows under positive net pressure Pnet, whereas the common practice of Pbase definition will result in fracture growth under negative Pnet; when it is the simple 1+2 layer case it gives back the usual definition of net pressure, minimum in-situ stress σ_{min} at the middle layer.

5)Tip jump can be induced by low σ, but not low K_{IC}; tip stability is imposed by high K_{IC} and/or high σ. Decreasing σ, will induce tip jump/instability at the boundary, whereas decreasing fracture toughness, K_{IC}, will not cause tip jump, but still a smooth growth. Increasing K_{IC} and/or σ will hinder the fracture growth, or even keep tips stable at the layer boundary.

6)It was found that fracturing fluid density affects which tip starts to grow to infinity when treating pressure reaches a critical value.

7)A full-height map with very large top and bottom formation thicknesses shows the ultimate trend of fracture height map when the fracture tip will grow to infinity, and suggests the maximum treating pressure to be used. The model will detect and stop the calculation, if tips touch the top or bottom boundary, or if tip starts to grow to infinity.

8)The outer and inner envelopes of the height map can be a useful tool to assess the potential effects of parameter uncertainties.

5. USING MICROSEISMIC CLOSURE WINDOW TO CHARACTERIZE FRACTURE GEOMETRY AND SRV*

5.1 Summary

Many studies have assessed microseismic (MS) interpretation in hydraulically fractured shale wells. However, to derive stimulated reservoir volume (SRV) and fracture geometry from MS data is still enigmatic, for MS events come not only from the induced main fractures of the current stage, but also from non-relevant sources. MS data of adjacent stages tend to overlap each other severely. Simulated hydraulic fracture (HF) networks using MS data always yield higher production than actually reported. We addressed these issues by evaluating MS data from the "Closure Window."

Using an Excel-VBA program, we divided the MS events from each fracture stage into three windows: the Pad Window, the Proppant Window, and the Closure Window, based on the fracture stimulation record of each stage. The Closure Window includes only MS events during the shut-in period (from the end of slurry pumping until before flowback of that stage). During the Closure Window, leakoff and fracture closing are the dominant phenomena. Leakoff into the formation matrix can cause shear slippage of pre-existing natural fractures (NF) and tensile opening of micro pores. These secondary fractures have potential to transport fluid and facilitate the induced major fractures. The fracture will close when the fluid inside leaks off. Both leakoff and fracture closing can trigger MS events near the major fractures, thus can better capture the effective fracture geometry of current stage.

*Part of this chapter is reprinted with permission from "Microseismic Closure Window Characterizes Hydraulic-Fracture Geometry Better" by Songxia Liu, Peter P. Valkó, Steven McKetta, and Xiaoda Liu. 2016. SPE Reservoir Evaluation & Engineering, Volume 20, Issue 02, page 423 – 445. SPE 179116-PA.

We developed a Mathematica program to calculate area and volume of SRV for 3 individual windows and the entire window of each stage. The area ratio of Closure/Entire window is avg. 0.7. The volume ratio of Closure/Entire window is avg. 0.75.

The Closure Window method was applied on 5 shale wells. Unique characteristics in the Closure Window were observed. The Closure Window reduced the fracture dimensions of each stage and MS cloud overlap among stages. Comparing the Closure Window with the entire window, fracture width (W_f) decreased the most by an average of 230 ft (26.6%), fracture height (h_f) decreased by an average of 89.6 ft (25.7%), and lastly fracture length (x_f) decreased by an average of 41.6 ft (4.9%). The three windows shifted from each other, with Closure Window shifting from the previous stages. Cumulative production history-match error dropped from 30% in entire window to 2% in Closure Window. By using the Closure Window, we eliminated those events induced by previous stages, reactivation of NFs, and pumping noise detected by Pad and Proppant Windows. We suggest that Closure Window MS collected after proppant pumping, provide unique insights into fracture stimulation.

The VBA and Mathematica program developed in this study can be used to process MS data from any fracture stimulation job, segregate the three MS event windows, and calculated SRV area and volume. The Closure MS Window will indicate fracture geometry more accurately, and thus enhance optimization of hydraulic fracturing design and the prediction of hydrocarbon production. Infill wells and re-fracturing may be considered in the light of indicated fracture geometry reduction.

5.2 Closure Window Theory

Having realized MS events at different times may be triggered by different mechanisms, we divided the MS events into three windows: ***Pad Window, Proppant Window,*** and ***Closure Window***, based on the fracture stimulation job record. The Pad Window is when the pad fluid is injected; the Proppant Window is when proppant-laden slurry is injected; and the Closure Window includes only the MS events during shut-in time, i.e. after the pumping of proppant slurry and before flowback for the current stage. We extracted MS events in the Closure Window to characterize effective fracture geometry, and eliminated those induced by the previous stages, NFs, and pumping noise. Using this approach on 1 Fayetteville Shale well and 4 Eagle Ford Shale wells, we reduced MS cloud overlap of the different stages and increased the accuracy of inferred fracture geometry and SRV.

Closure Window better characterize the SRV and geometry for several reasons. During shut-in time, high pressure is maintained in fractures, so leakoff and fracture closing surrounding current stage fractues are the dominant phenomena (Busetti and Reches 2014):

1) Leakoff into the formation causes ***shear slippage*** of pre-existing fractures or weak planes (Warpinski and Teufel 1987; Busetti and Reches 2014; Seth Busetti 2014), because the pore pressure is increased by leakoff and the effective normal stress decreases, and thus shear strength of the fracture interface decreases (Barree and Mukherjee 1996; Ramurthy et al. 2009; Davies et al. 2013; Palmer et al. 2013). Shear slippage triggers MS events (Busetti and Reches 2014) with double-couple (DC) source (Baig and Urbancic 2010; Eyre and van der Baan 2015). Shear slippage can also open pre-existing fractures and enhance their porosity and permeability, and these fractures can be large enough to accept small mesh-size proppant (Olsson and Barton 2001; Palmer et al. 2013).

2) Leakoff into the matrix can pressurize small pores and cause ***tensile opening*** (Warpinski and Teufel 1987; Seth Busetti 2014; Sharma and Manchanda 2015), resulting in MS events with compensated linear vector dipole (CLVD) and isotropic (ISO) sources (crack opening mechanisms) (Baig and Urbancic 2010; Warpinski et al. 2013; Eyre and van der Baan 2015).

3) When all the fluid leaks away from the fracture, the fracture will ***close***, which may also trigger MS events with CLVD and ISO source mechanisms (Baig and Urbancic 2010; Eyre and van der Baan 2015). The leakoff and fracture closing activities and resultant MS events occur in the sphere of the main HFs of the current stage (Busetti and Reches 2014), which can be uniquely captured by the Closure Window. Whereas, the Pad and Proppant Windows, under active frac job excecution and high pressure perturbation, may contain MS events caused by reactivation of NFs far away and previously created HFs, and operation noise. These non-relevant MS events can be minimized in Closure Window.

Manchanda and Sharma (2013) introduced the concept of an induced, un-propped (IU) fracture network, which is created around the main propped fractures during the process of hydraulic fracturing, does not receive proppant, but can produce oil and gas (Manchanda and Sharma 2013). Here, we extend the concept to shut-in time (Closure Window), to explain the flow from fractures created by leakoff. Those IU fractures, or secondary fractures, have the potential to transport fluid and facilitate induced major propped fractures, and even play a dominant role in some shales (Palmer et al. 2013; Busetti and Reches 2014; Sharma and Manchanda 2015).

Therefore, the MS data collected during Closure Window can provide accurate information about the effective fracture network around the main induced fractures of the current stage, which contributes to fluid flow.

5.3 Data Processing Method

5.3.1 Division of 3 Windows Using a VBA Program

The MS data were divided into 3 windows by the following steps using a VBA program.

1) Copy the MS data into the first worksheet of the Excel template: “Total MS”.

2) Create an empty sheet for each fracture stimulation stage to input the fracture treatment records.

3) Copy the fracture stimulation job records into the newly created worksheets, in at least 3 columns: date, time, and proppant concentration. Proppant concentration is the criterion to decide the start and end of Proppant Window.

4) For each stage, the program detected the start of each window (Pad, Proppant and Closure) according to the proppant concentration; by comparing the dates and times to those events in the “Total MS” MS data were divided into three windows.

5) For each stage, the 3 individual windows were plotted in plan view (to show fracture length and width of the SRV) and in side view (to show fracture height) of MS clouds. These views showed the relative positions of the 3 windows.

6) For comparison, the entire window (consisting of Pad, Proppant and Closure) for all stages were plotted in plan and side views; then similarly, only the Closure Window for all stages were plotted in plan and side views. The Closure Window reduced overlap among the stages.

7) Adjust the scales of the plots to make the x and y axes equal, so that the fracture geometry could be read correctly.

5.3.2 SRV Area and Volume Using a Mathematica Program

Then the SRV area (plan view, in x-y plane) and volume of 3 individual windows and the entire window are calculated using a Mathematica program.

Calculate SRV Area

1) Import data for one well from Excel into Mathematica, find the stage numbers; for each stage, divide the MS data into 3 windows, then use the function "ConvexHullMesh" to make boundary meshes of the smallest 2D convex hull region from all the points in each window. This 2D convex hull is a projected convex area in x-y plane, so we only need x and y coordinates of each point. Then use the function "Area" to calculate the area of each window.

2) To calculate the entire window area, we plot the 3 individual windows together by using "Show" function on the 3 convex hull windows; then use "BoundaryDiscretizeGraphics" to make one 2D convex hull for the entire window eliminating the overlap of the three windows.

Calculate SRV Volume

1) For each of the 3 windows (Pad, Proppant, Closure) of one stage, divide the data points into groups with 4 (or 5) points each group.

2) Calculate the projected area in x-y plane, calculate height of each group by Zmax-Zmin, then multiply them to get the SRV volume for each data group.

3) Add all groups together to get SRV volume for this window. Do the same thing for the entire window to obtain SRV volume of this stage.

5.4 Results and Discussion

We studied five wells regarding the MS clouds and the resulting three windows; one in the Fayetteville Shale, and four in the Eagle Ford Shale. Plug & Perf completion method was used in these wells. They have 1-4 clusters/stage, with 6 shot/ft shot density for Well 1, 0.36 shot/ft for Well 2 & 3, 4 shot/ft for Well 4 & 5. Stage spacing is 138 ft for Well 1, 53 ft for Well 2 & 3, 78 ft for Well 4 & 5. For those wells, average measured duration of Closure Window ranged from 25-64 minutes; maximum measured duration ranged from 39-109 minutes (**Table 10)**. These results are based on selected stages that had sufficient Closure Window data; we excluded stages with no Closure Window data or with too few data points.

Typically, microseismic recording continues during pump down of plug and perforation guns at very low rate (e.g., 4-10 bbl/min). Events recorded during pump down will either be delivered as a subset of data identified as pump down events, or they will be ignored. Therefore, the Closure Window events shown here don't include the period of pumping down of plugs and perforating guns, thus won't be affected by it. Closure Window lasts during shut-in and stops before the plug and perf period of the next stage.

Complete results for Fayetteville Shale (Well 1) and Eagle Ford Shale (Wells 2-5) wells analyses are in the Appendix (**Figs. A-1 through A-10**)**.** The following discussion provides observations of unique characteristics of Closure Window MS data, based on selected figures among those in the Appendix.

Well No.	Location	Average Duration, min	Maximum Duration, min	Year of Measurement	Number of Stages Studied	Avg. Error, ft	Avg. Noise/SNR
1	Fayetteville	64.4	69.7	2007	4 (2-5)	20.66	NA
2	Eagle Ford	36.4	50.7	2011	7 (13-19)	NA	29.5/4.7
3	Eagle Ford	54.1	108.7	2011	4 (12-15)	NA	26.7/4.7
4	Eagle Ford	25.7	38.8	2012	8 (13-20)	NA	12.4/3.9
5	Eagle Ford	32.7	56.0	2012	7 (13-19)	NA	17.9/3.9

Table 10. Duration of Closure Window Measurements for 5 Shale Wells.

5.4.1 Characteristics of Closure Window MS Data

Reduced Overlap Among Stages in the Closure Window

Overlap among stages is much less in the Closure Window (compare **Fig. 20a** with **20b**, **Fig. 20c** with **20d**), because the Closure Window area in each stage is smaller; overlap for all three windows is severe. This indicates that when one stage has finished and injection has begun in the next stage, the induced fractures and weak interfaces in the sphere of the previous stage were reactivated, thus, enlarging the area or SRV of the subsequent stage. The Pad and Proppant Windows operated during the early time of a subsequent fracture stage will detect this reactivated or overlapping area. Therefore, by using the Closure Window, we reduced this overlap area. Due to the possible fracture connection of two stages, the Closure windows of adjacent stages still overlap each other, but much less severe than the entire window.

Appendix Figs. A-3a, A-3b, A-5a, A-5b, A-7a, A-7b, A-9a, A-9b, for Eagle Ford wells 2 through 5, respectively, demonstrate the same trend and conclusion.

Shift of the 3 Windows

We plotted the 3 individual windows separately for each stage. In **Fig. 21**, the plan views of stage 2, 4 and 5 of Fayetteville Well 1 and stage 12 of Eagle Ford Well 3 show the Pad Window, the Proppant Window and the Closure Window clearly shift from each other. The

Closure Windows move away from the previous stage locations, whereas Pad and Proppant Windows are closer to previous stages.

The distance between the centers of two adjacent stages in Well 1 is 420 ft, while the shift between Pad Window and Closure Window is 410 ft, 406 ft, 491 ft, respectively for stage 2, 4 and 5. The distance between the centers of two adjacent stages in Well 3 is 305 ft, while the shift between Pad Window and Closure Window of Well 3 is 540 ft. The shift of Closure/Pad Window is equal or larger than the distance between two adjacent stages. This conceivably results from the influence of previous fractures or natural fractures. Thus, the influence of previous fracture stages is diminished in the Closure Window. The same trends are present in Figs. A-6a, A-8m, A-10e, etc., in the Appendix.

Pad Window of Next Stage Overlap Closure Window of Previous Stage

Fig. 22 shows the plan view of 3 individual windows of stage 1-4 for Fayetteville Well 1, with Pad Window of next stage plotted on each stage. We can see Pad Window of next stage (red circles) almost overlap exactly Closure Window of previous stage (yellow dots).

Narrower Closure Window

Plan views of the 3 individual windows for selected stages of Eagle Ford Wells 2, 3 and 5 show the area of the Closure Window is narrower than the entire window of the stage **(Fig. 23)**. This is reasonable because, during shut-in, the dominant phenomena of leakoff and fracture closing occur only near the current main induced fractures. Other figures in the Appendix show the same phenomenon, e.g., Figs. A-4e, A-4k, A-6c, A-6g, A-8m, A-10c, etc.

Less Fracture Height in Closure Window

As shown by the side views in **Figs. 24a and 24b**, also, Figs. A-2d and A-2h, fracture height in the Closure Window is less than that of the entire window. For example, the range of depth for stage 5 diminishes from 500 ft (Fig. 24a) to 300 ft (Fig. 24b). Some far points (circled) are absent in the Closure Window, and they may not connect to the main HF. Also, there is less overlap of stages and the Closure Window is narrower than the entire window. Again, the Closure Window filtered out the enlarged area due to the previous stages, pre-existing NFs, and other noise. The same phenomenon is present in the other wells (Appendix Figs. A-3c, A-3d, A-5c, A-5d, A-7c, A-7d, A-9c, A-9d, etc.)

Closure Window Represents Entire Window, in Some Cases

In some cases the Closure Window does not shift or shrink, relative to the entire window (**Fig. 25).** The Closure Window can still be used to characterize the entire window of a stage. This implies that, in the extreme case, we do not need to monitor the Pad or Proppant Windows for fracture geometry, but may monitor only the Closure Window for a sufficient time, e.g. 30-60 minutes; thus cost and time can be minimized. We may still need to measure the Pad and Proppant Windows for analysis and future study, but in the past, Closure Window data have been a neglected resource that can provide additional insights and more effectively capture SRV. The same phenomenon is present also in Appendix Figs. A-4a, A-4c, A-4g, A-4i, A-4m, A-6e, A-8k, A-10i, A-10k, etc.

Pad Window Often Covers the Entire Window

While it is reasonable to anticipate that Pad Window covers a smaller volume than the Proppant Window and entire window-because the fractures may not have fully developed yet-in the given 5-well examples often the opposite happened. Surprisingly, Pad Window (blue dots) is very often as tall and long as the entire window (Figs. 21c, 25, A-4, etc.), which may indicate that before pumping sand slurry, we have already created fractures over the entire window, and the velocity of fracture growth is great. We noticed in the field measurement and simulation that, the net or treating pressure in the Proppant Window was no higher than the Pad Window, which may confirm fracture height is mainly determined by net pressure (Liu and Valko 2015).

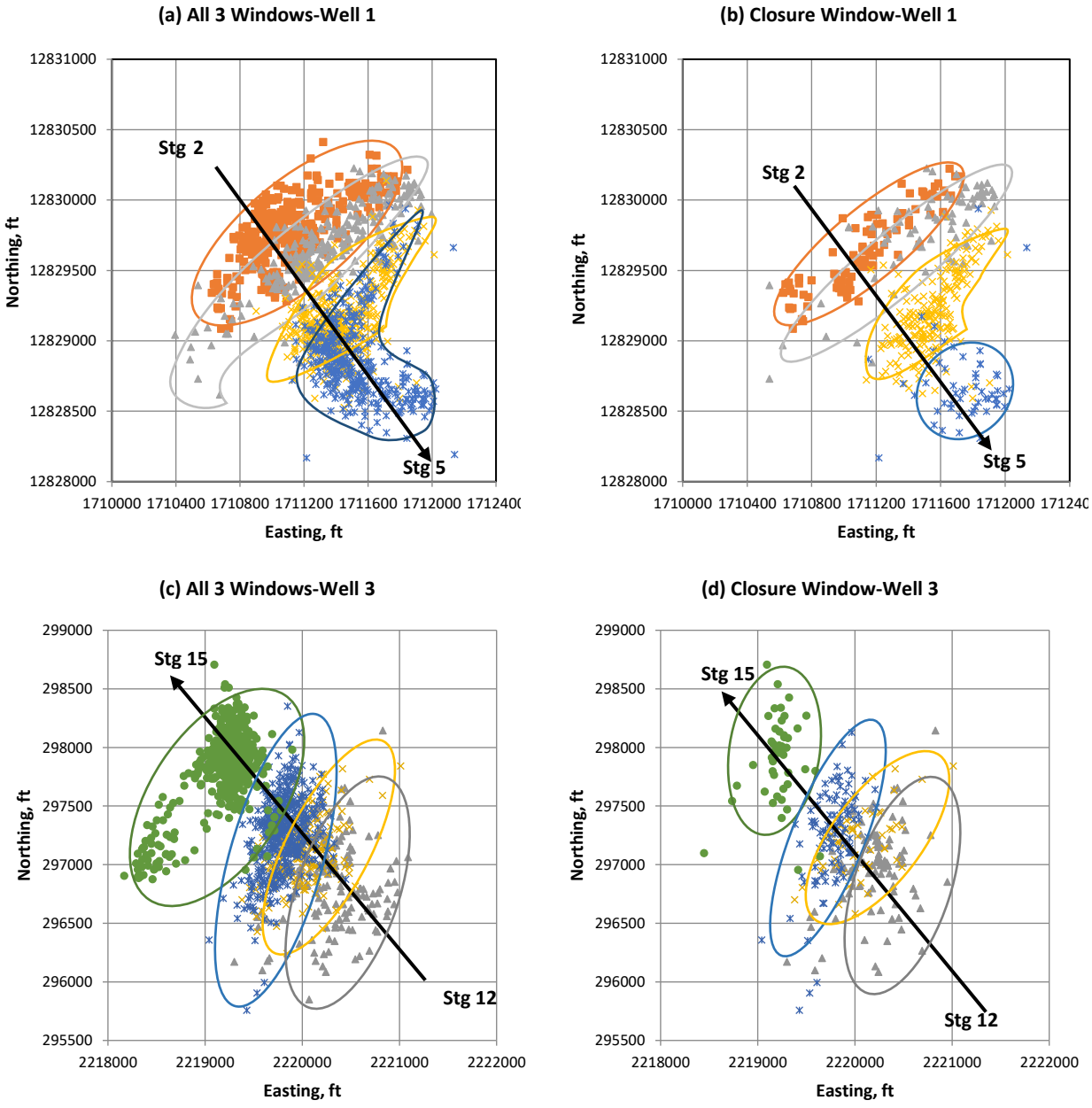

Fig. 20. Plan view of (a) all 3 windows and (b) Closure Window for stages 2-5 of Fayetteville Well 1. Plan view of (c) all 3 windows and (d) Closure Window for stages 12-15 of Eagle Ford Well 3. Overlap among stages in Closure Window is significantly less than that of all 3 windows.

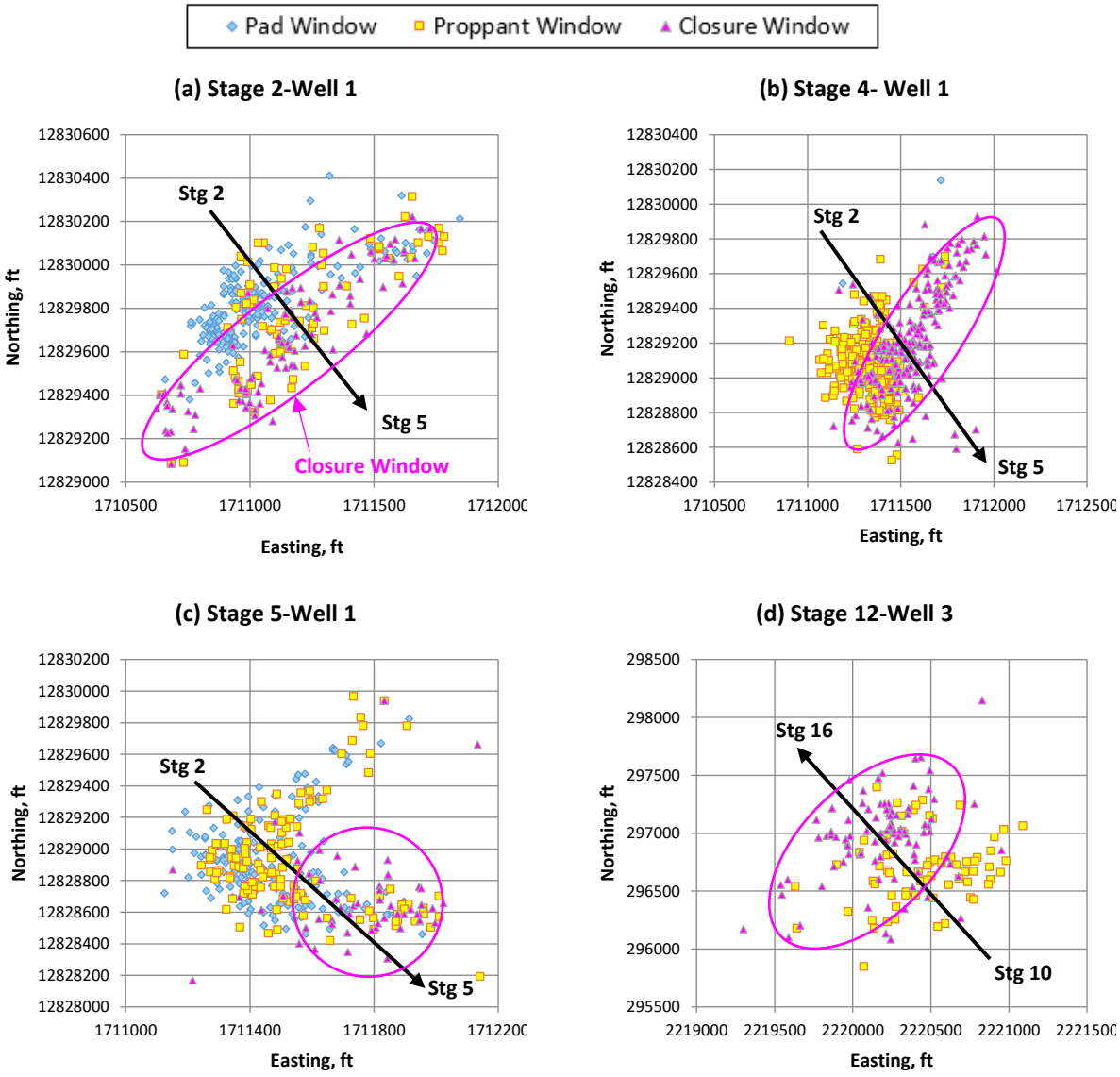

Fig. 21. Plan view of the 3 MS event windows for (a-c) stages 2-5 of Fayetteville Well 1 and (d) Stage 12 of Eagle Ford Well 3. Closure window (pink envelop) shifts from the other two windows, and away from the previous stages.

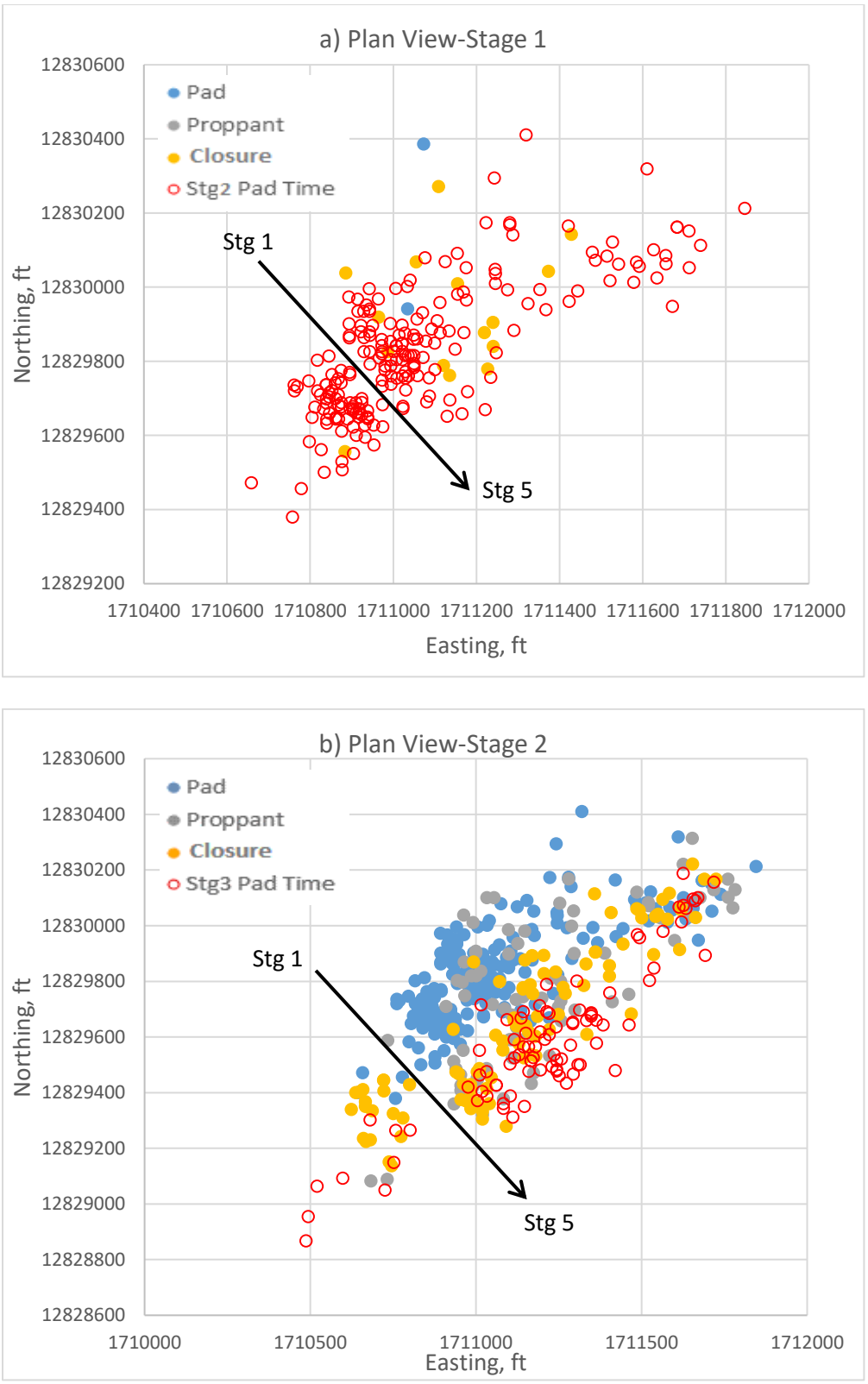

Fig. 22. Plan view of 3 individual windows of stage 1-4 of Fayetteville Well 1, with Pad Window of next stage plotted on each stage.

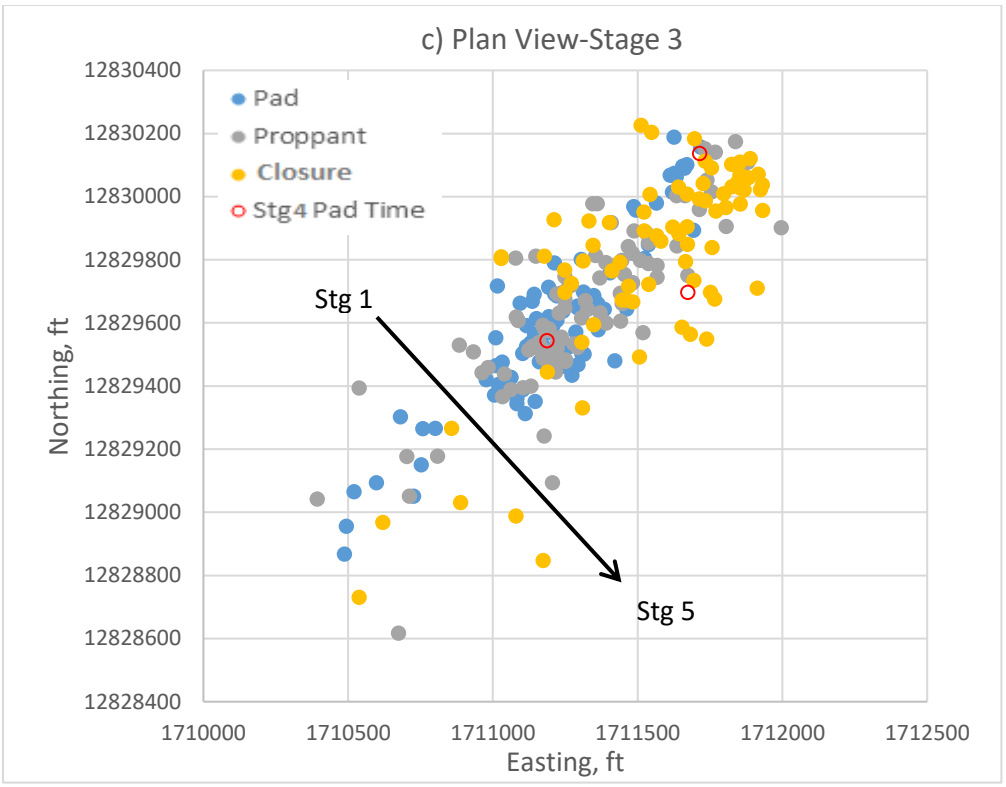

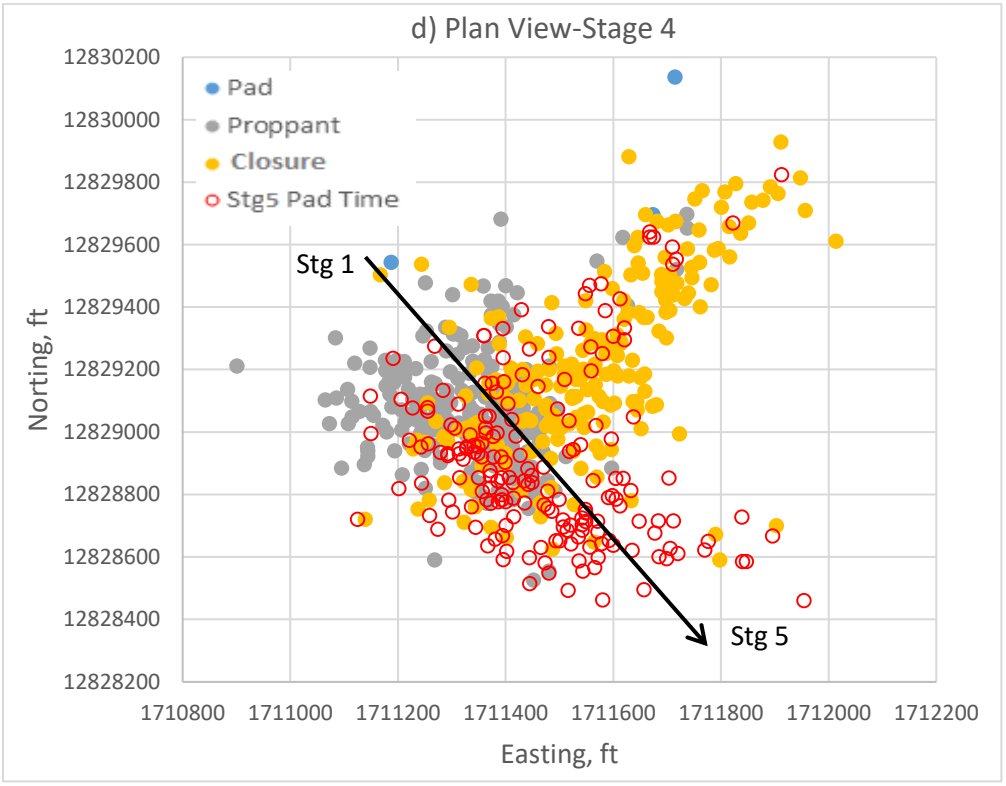

Fig. 22. Continued.

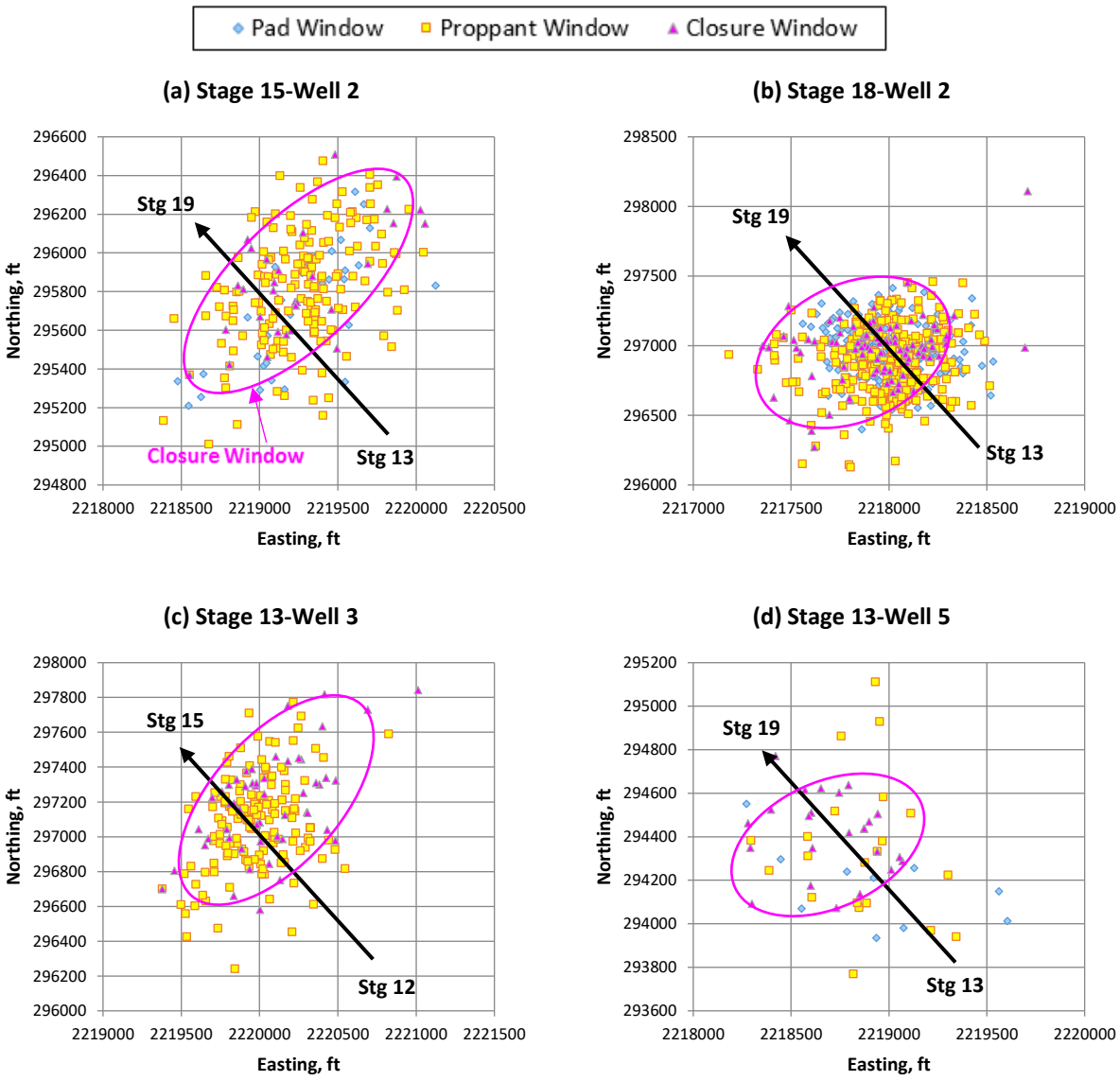

Fig. 23. Plan view of the 3 individual windows for selected stages of Eagle Ford Wells 2, 3 and 5. Closure window (pink envelop) is narrower than the entire window, and it shifts away from the other two windows, and from the previous stages.

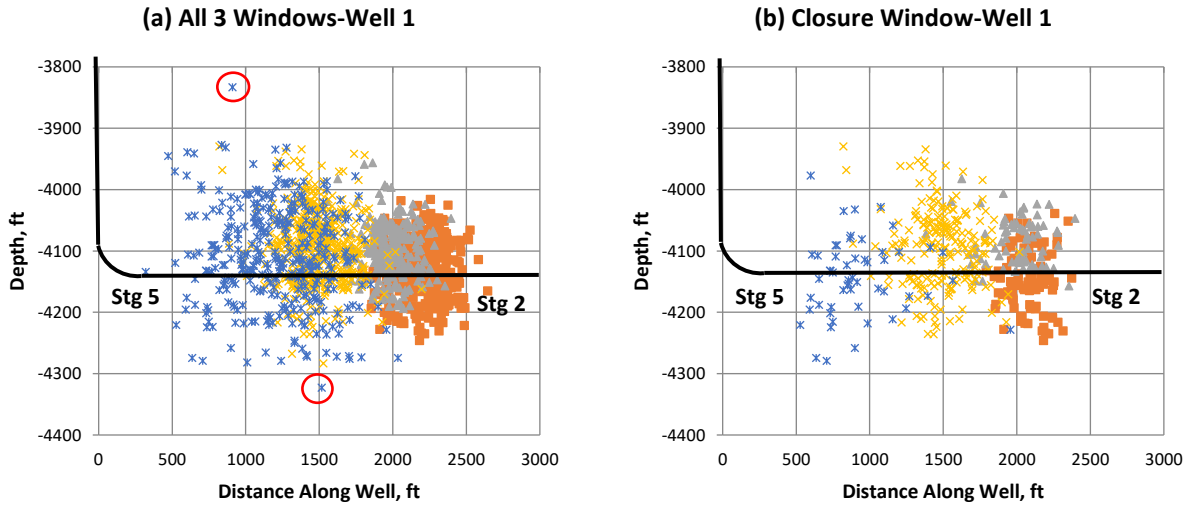

Fig. 24. Side view of (a) all 3 windows and (b) Closure Window for stages 2-5 of Fayetteville Well 1. Closure window is shorter than the entire window, and it is narrower with less overlap of each stage.

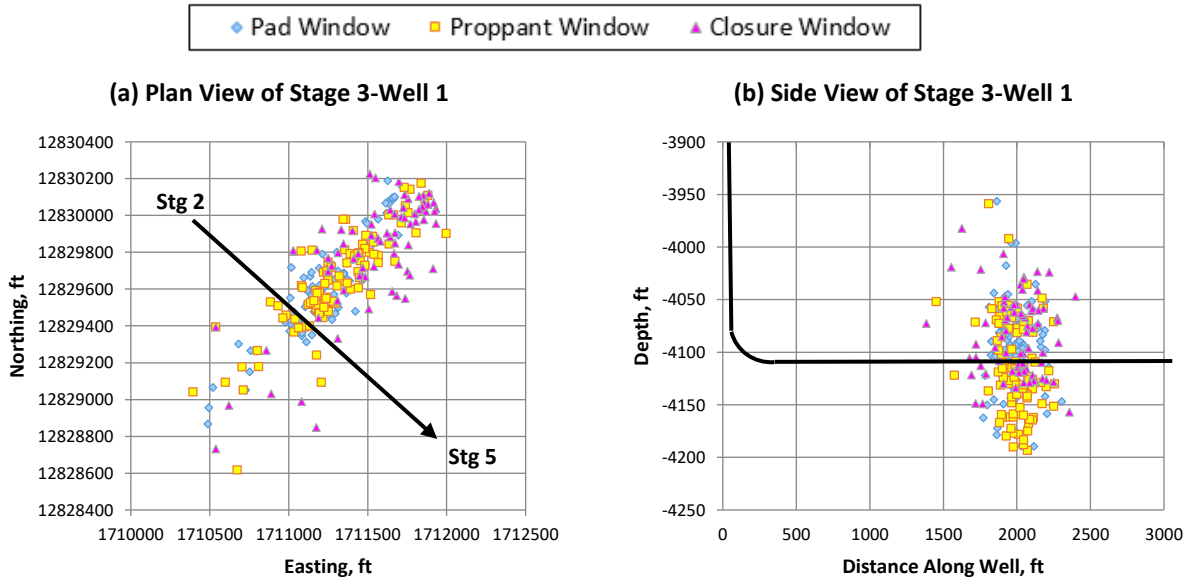

Fig. 25. Plan view and side views of the 3 individual windows for (a and b) stage 3 of Well 1 and (c and d) stage 17 of Well 2. In some cases, the Closure Window may represent the entire window of a stage, if it does not shrink or shift.

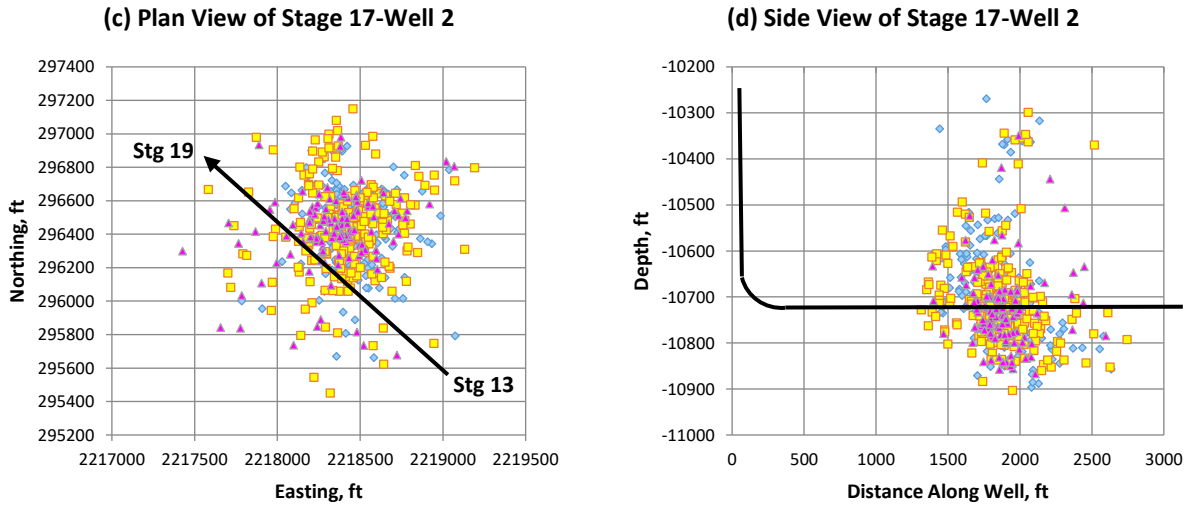

Fig. 25. Continued.

5.4.2 Reduced Fracture Geometry from Closure Window Matches Production History

Two problems persist with application of MS data: the MS clouds of stages overlap severely; and it is difficult to history match production and fracture geometry using the large fracture geometry read from the entire MS window. Using Closure Window method, the two problems are mitigated.

The Fracture Geometry and Overlap are Reduced

Fig. 26 shows the reduction in fracture width (W_f), height (h_f), and length (x_f) in Closure Window, as compared to the entire window, for Well 1; the corresponding numbers are listed in Appendix **Table A-1**. Especially, width decreased significantly, by 100-370 ft (17-35%), which is why there is much less overlap. This means that the Closure Window can eliminate the influence from previous stages and reactivated NFs. Comparing the Closure Window with the entire window, fracture height was reduced by 23-188 ft (10-42%); fracture length decreased by 0-100 ft (0-12%). W_f decreased the most by an average of 230 ft (26.6%), h_f decreased by an average of 89.6 ft (25.7%), and lastly x_f decreased by an average of 41.6 ft (4.9%). So, based on

the reduced, effective fracture geometry, infill wells and re-fracturing could be considered. The Closure Window provides abundant information for us to optimize well performance and field development.

Production is Matched Fairly Well

We simulated the gas production with fracture geometry inferred from the entire MS window and from Closure Window, for Fayetteville Well 1 (**Fig. 27**), using reservoir simulator MProd; and history-matched the cumulative production against measured data Initial reservoir pressure=2,143 psi, initial BHP=1,300 psi, bottmhole reservoir temperature 131 °F, porosity=2.07%, permeability=45 nD, water saturation 45.6%, rectangular reservoir drainage area 160 acre, net pay 170 ft.

The gas rate determined from the entire window was much higher than that determined from the Closure Window. The error of cumulative gas production (up to Day 2,850) between the measurement and simulation by entire window was 29.5%, whereas the error of simulation by Closure Window was -1.96%. Based on OGIP 177.7 MMSCF, the recovery factor (RF) of actual production on Day 2850 is 20.2%, RF of simulaton by Closure Window on Day 5000 (13.7 years) is 25.3%. The fracture geometry matched by the two methods is in Appendix Table A-1. The larger fracture dimensions (SRV) of the entire MS data result in large simulated cumulative production.

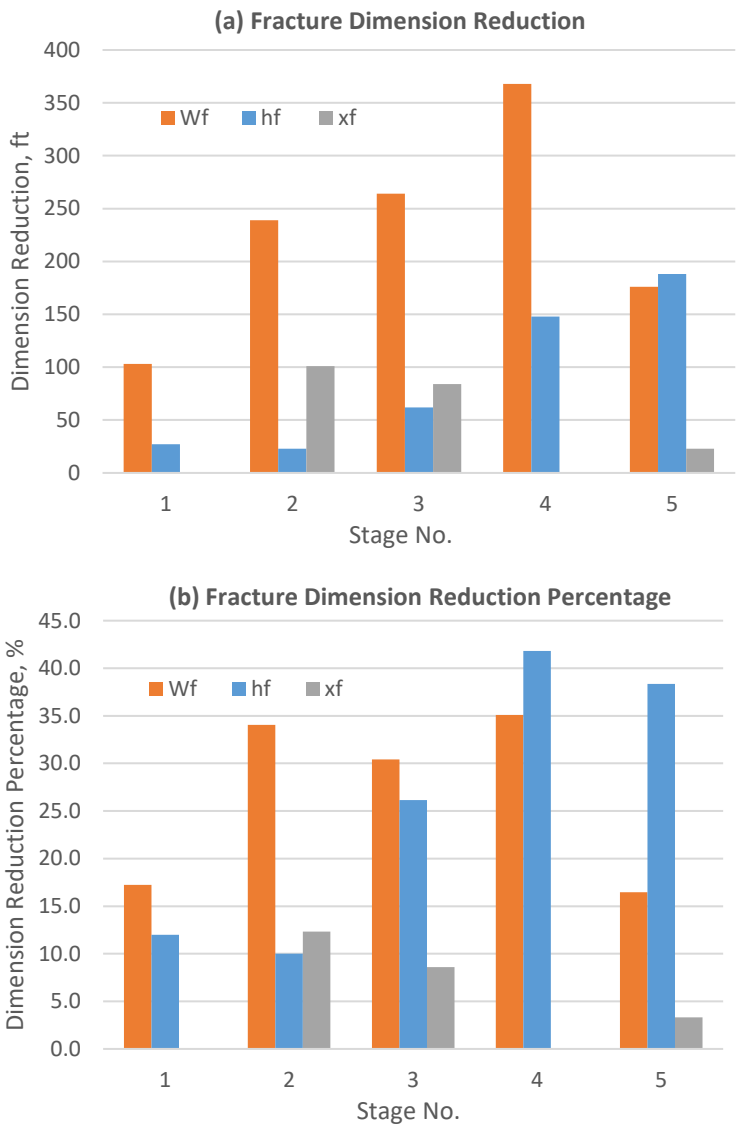

Fig. 26. (a) Fracture geometry reduction and (b) percentage of reduction in Closure Window, for Fayetteville Well 1 (W_f: fracture width of a stage, ft; h_f: fracture height of a stage, ft; x_f: fracture half length of a stage, ft).

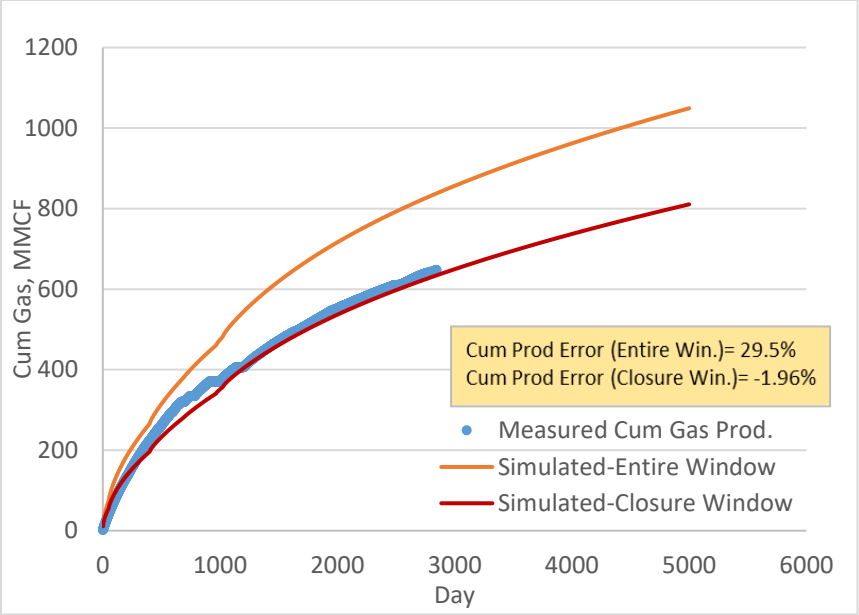

Fig. 27. Comparison of cumulative gas production history match between the entire window and Closure Window SRV, for Fayetteville Well 1.

5.4.3 SRV Area of 3 Individual Windows of Each Stage of the Studied Wells

We calculated the SRV area occupied by MS data events for the 3 individual windows of each stage of the five studied wells. Results are shown in **Table 11**. Then the average SRV area ratios of Pad, Proppant, Closure Windows over the entire window for each well and the average ratios of five wells are calculated in **Table 12**. The average SRV area ratio of Closure/entire window is 70% (range of 44~87%), meaning if Closure Window represents the effective productive reservoir area of each stage, then 30% of the SRV area measured by total MS data will not produce hydrocarbon. The SRV area ratio of Pad/entire window is 55% (range of 46~63%), the smallest among the three windows; and the ratio of Proppant/entire window is 73.3% (range of 67~82%), the largest among the three. Some example figures of SRV area of three MS convex windows plot by the Mathematica program are shown in **Fig. 28**.

	Stg NO	Entire Area	Pad Area	Proppant Area	Closure Area	Pad /Entire	Proppant/Entire	Closure/Entire
Well 1	1	222444	0	0	222444	0.00	0.00	1.00
	2	768799	540219	615133	524224	0.70	0.80	0.68
	3	1246176	514464	959224	1191163	0.41	0.77	0.96
	4	1076805	103960	585147	913071	0.10	0.54	0.85
	5	1316076	792945	977589	1107350	0.60	0.74	0.84
	Avg.					**0.44**	**0.63**	**0.87**
Well 2	**Stg NO**	**Entire Area**	**Pad Area**	**Proppant Area**	**Closure Area**	**Pad /Entire**	**Proppant/Entire**	**Closure/Entire**
	11	1306179	1116801	627045	331939	0.86	0.48	0.25
	12	773309	432092	647860	212215	0.56	0.84	0.27
	13	1114636	321009	943288	743641	0.29	0.85	0.67
	14	1589402	1571449	1233932	924848	0.99	0.78	0.58
	15	1660901	890649	1596870	913389	0.54	0.96	0.55
	16	2101309	1168346	1805790	1716824	0.56	0.86	0.82
	17	2043808	1253716	1880242	1551597	0.61	0.92	0.76
	18	1298375	731722	1237434	903295	0.56	0.95	0.70
	19	1201067	851506	917834	955120	0.71	0.76	0.80
	Avg.					**0.62**	**0.84**	**0.64**
Well 3	**Stg NO**	**Entire Area**	**Pad Area**	**Proppant Area**	**Closure Area**	**Pad /Entire**	**Proppant/Entire**	**Closure/Entire**
	10	3394809	0	662667	3394809	0.00	0.20	1.00
	12	2108318	0	1368642	1967060	0.00	0.65	0.93
	13	1443027	0	1315719	1016219	0.00	0.91	0.70
	14	1679932	128001	1281842	1344290	0.08	0.76	0.80
	15	1684978	136165	1564826	1275180	0.08	0.93	0.76
	Avg.					**0.03**	**0.74**	**0.84**
Well 4	**Stg No**	**Entire Area**	**Pad Area**	**Proppant Area**	**Closure Area**	**Pad /Entire**	**Proppant/Entire**	**Closure/Entire**
	12	304506	0	196299	175094	0.00	0.64	0.58
	13	380401	0	321798	235011	0.00	0.85	0.62
	14	644925	114476	62188	576922	0.18	0.10	0.89
	15	216214	0	118007	189301	0.00	0.55	0.88
	17	1619854	241524	1281318	893621	0.15	0.79	0.55
	18	551062	0	525005	396943	0.00	0.95	0.72
	20	506498	202815	413664	467316	0.40	0.82	0.92
	Avg.					**0.10**	**0.67**	**0.74**

Table 11. SRV area of 3 individual windows of each stage of the studied wells.

	Stg No	Entire Area	Pad Area	Proppant Area	Closure Area	Pad /Entire	Proppant/Entire	Closure/Entire
Well 5	12	226412	0	70733	163266	0.00	0.31	0.72
	13	898762	384870	771036	385478	0.43	0.86	0.43
	14	1159756	0	1097393	557167	0.00	0.95	0.48
	15	458843	249259	293416	93479	0.54	0.64	0.20
	16	851090	235505	744634	231280	0.28	0.87	0.27
	17	1850923	1611458	1161134	776961	0.87	0.63	0.42
	18	2333257	380606	2252155	1574699	0.16	0.97	0.67
	19	3186617	270459	2915388	965319	0.08	0.91	0.30
	Avg.					**0.36**	**0.77**	**0.44**

Table 11. Continued.

Well No.	Pad /Entire	Proppant/Entire	Closure/Entire
1	0.573	0.714	0.865
2	0.630	0.822	0.599
3	-	0.690	0.839
4	-	0.670	0.737
5	0.456	0.767	0.438
Avg.	0.553	0.733	0.696

Table 12. Average SRV area ratios of Pad, Proppant, Closure Windows over the entire window for each well and the average ratios of five wells.

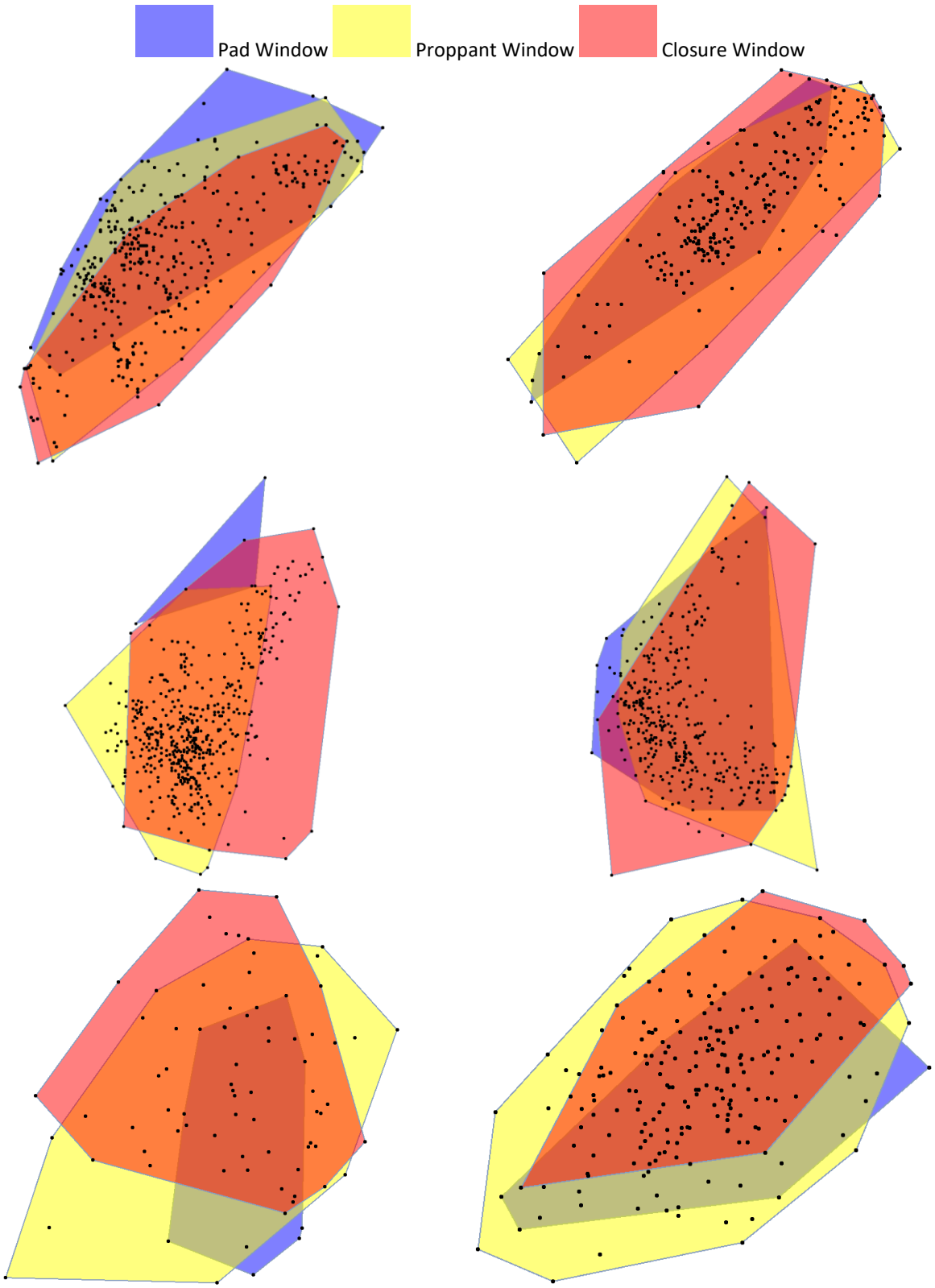

Fig. 28. Some examples of plan-view SRV areas of three microseismic windows in one stage plot by the Mathematica program.

5.4.4 SRV Volume of 3 Individual Windows of Each Stage of the Studied Wells

We calculated the SRV volume occupied by MS data events for the 3 individual windows of each stage of the five studied wells. Results are shown in **Table 13**. Then the average SRV volume ratios of Pad, Proppant, Closure Windows over the entire window for each well and the average ratios of five wells are calculated in **Table 14**. The SRV volume ratio of Closure/entire window is 75%, meaning if Closure Window represents the effective productive reservoir volume of each stage, then 25% of the SRV volume measured by total MS data will not produce hydrocarbon. The SRV volume ratio of Pad/entire window is 50%, the smallest among the three windows; and the ratio of Proppant/entire window is 79%, the largest among the three. Some example figures of SRV volume of three MS convex windows plot by the Mathematica program are shown in **Fig 29**.

	Stg No.	Entire Volume	Pad Vol	Prop Vol	Closure Vol	Pad/Entire	Prop/Entire	Clos/Entire
Well 1	2	17525700	10379070	13352400	13424850	0.592	0.762	0.766
	3	23798250	14970500	23318500	31583250	0.629	0.980	1.000
	4	22619300	5799950	13034600	18651650	0.256	0.576	0.825
	5	50081250	32397700	28707550	31623350	0.647	0.573	0.631
	Avg					0.531	0.723	0.806
Well 2	Stg No.	Entire Volume	Pad Vol	Prop Vol	Closure Vol	Pad/Entire	Prop/Entire	Clos/Entire
	11	106489500	95300250	162872600	114981950	0.895	1.000	1.000
	12	73346900	71965800	59032350	28893100	0.981	0.805	0.394
	13	109387250	29710400	109671550	85869000	0.272	1.000	0.785
	14	132057500	125778000	108238800	193149000	0.952	0.820	1.000
	15	132660450	120184500	109243300	138509500	0.906	0.823	1.000
	16	181866000	90980550	139010050	106219200	0.500	0.764	0.584
	17	76343850	54709500	84641750	100922350	0.717	1.000	1.000
	18	122045000	57057750	116565950	163787000	0.468	0.955	1.000
	19	71671300	50099050	51723800	78004750	0.699	0.722	1.000
	Avg					0.710	0.877	0.863

Table 13. SRV volume of 3 individual windows of each stage of the studied wells.

	Stg No.	Entire Volume	Pad Vol	Prop Vol	Closure Vol	Pad/Entire	Prop/Entire	Clos/Entire
Well 3	10	115947600	0	31923100	126023750	0.000	0.275	1.000
	12	51028550	0	42918350	30561600	0.000	0.841	0.599
	13	41544950	0	41886200	30604600	0.000	1.000	0.737
	14	62199850	18195400	58250700	54295300	0.293	0.937	0.873
	15	65601450	7856735	61137600	57926300	0.120	0.932	0.883
	16	86696300	64059250	48323250	3729690	0.739	0.557	0.043
	Avg					0.384	0.757	0.689
Well 4	Stg No.	Entire Volume	Pad Vol	Prop Vol	Closure Vol	Pad/Entire	Prop/Entire	Clos/Entire
	12	46452300	0	73516950	53767800	0.000	1.000	1.000
	13	50546400	0	46076200	10392430	0.000	0.912	0.206
	14	72551400	19303200	29205300	42761100	0.266	0.403	0.589
	15	9074025	0	7184325	19969600	0.000	0.792	1.000
	16	30135950	907128	37110000	10239740	0.030	1.000	0.340
	17	55377550	35141050	53812400	44441000	0.635	0.972	0.803
	18	27096150	0	26804050	18666650	0.000	0.989	0.689
	19	28806150	5704855	18877100	37324150	0.198	0.655	1.000
	20	32107650	5859290	21014200	30148200	0.182	0.654	0.939
	Avg					0.262	0.820	0.729
Well 5	Stg No.	Entire Volume	Pad Vol	Prop Vol	Closure Vol	Pad/Entire	Prop/Entire	Clos/Entire
	12	177163000	0	16033800	44016050	0.000	0.091	0.248
	13	100234400	43458900	63795100	66816650	0.434	0.636	0.667
	14	54747350	0	52939400	59623500	0.000	0.967	1.000
	15	36110300	24956700	35877300	20149550	0.691	0.994	0.558
	16	34564850	31226200	22190850	17512600	0.903	0.642	0.507
	17	70979300	148908500	87710000	35315700	1.000	1.000	0.498
	18	62549350	20231800	87972100	84250700	0.323	1.000	1.000
	19	55559000	11355335	40746050	49478500	0.204	0.733	0.891
	Avg					0.593	0.758	0.671

Table 13. Continued.

Well No.	Pad/Entire	Proppant/Entire	Closure/Entire
1	0.531	0.723	0.806
2	0.710	0.877	0.863
3	0.384	0.757	0.689
4	0.262	0.820	0.729
5	0.593	0.758	0.671
Avg.	**0.496**	**0.787**	**0.752**

Table 14. Average SRV volume ratios of Pad, Proppant, Closure Windows over the entire window for each well and the average ratios of five wells.

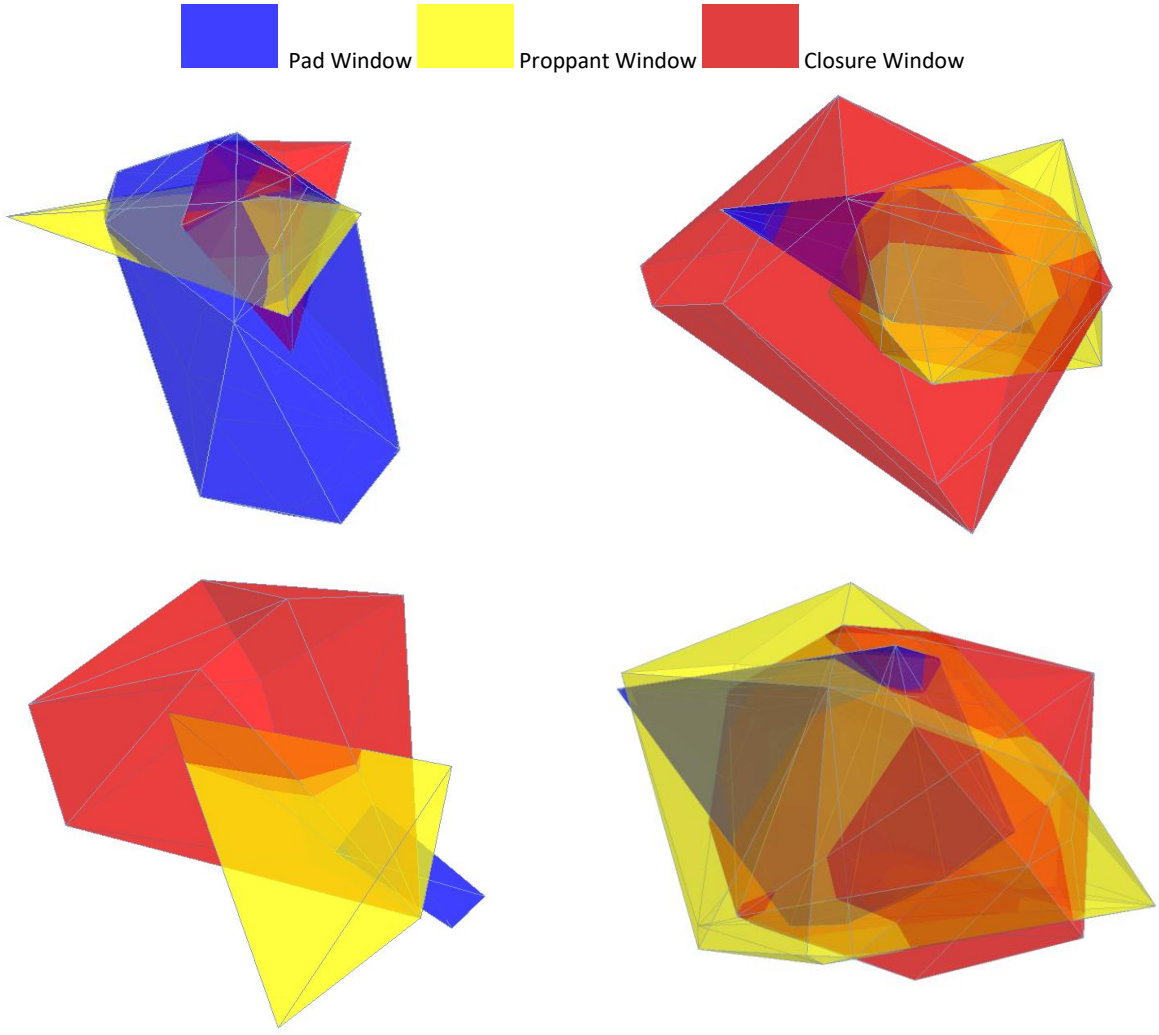

Fig. 29. Some examples of 3D-view SRV volumes of three microseismic windows in one stage plot by the Mathematica program.

5.5 Conclusions

1)By using Closure Window data, we reduced the fracture dimensions and matched the cumulative production very well. Wf decreased the most by an average of 230 ft (26.6%), hf decreased by an average of 89.6 ft (25.7%), and lastly xf decreased by an average of 41.6 ft (4.9%). Cumulative production history match error dropped from 30% to 2%. Infill wells and re-fracturing may be considered in the light of geometry reduction.

2)By dividing the MS events of hydraulic fracture treatments into three windows: the Pad, Proppant, and Closure Windows, we found Closure Window data have been a neglected resource that provide unique and significant insights and more effectively characterize SRV.

3)The Excel-VBA program developed in this study can be used to process any MS data and associated fracture stimulation job data, and to plot the three MS event windows.

4)The Mathematica program developed can calculate area and volume of SRV for 3 individual windows and the entire window of each stage. The area ratio of Closure/Entire window is avg. 0.7. The volume ratio of Closure/Entire window is avg. 0.75.

5)The overlap among stages is smaller in the Closure Window than the overlap in the entire window, due to the shrinkage and shift of the Closure Window. Because, the induced fractures and weak interfaces around the previous stage will be reactivated by pumping pad and proppant, in addition to pump noise, thus, enlarge the SRV of the next stage.

6)The 3 windows shift apart from each other, with Closure Window moving toward the current stage, while Pad and Proppant Windows moving toward the previous stage. Clear shifts among the 3 Windows indicate reactivation of previously induced HFs and/or pre-existing NFs, and operation noise recorded in the Pad and Proppant Windows. Therefore, a more accurate depiction of the fracture geometry (SRV) can be determined by using the Closure Window.

7)The Pad Window of next stage can exactly overlap the Closure Window of the previous stage, indicating the Pad Window MS events reflect the reactivation of fractures of the previous stage, and not quite represent the current stage.

8)Closure Window is usually narrower in width and shorter in height than the entire window, and offset from the other two, because the dominant phenomena of leakoff and fracture closing occur near the main induced fractures.

9)In some cases the Closure Window is as large as the entire window; then the Closure Window represents the fracture geometry of the entire fracture stimulation stage.

6. INTEGRATED STUDY OF FRACTURE PROPAGATION AND RESERVOIR PRODUCTION IN FAYETTEVILLE SHALE

6.1 Summary

To evaluate fracture effectiveness, predict well productivity, improve future fracture treatment design, and gain insights into hydraulic fractures in shale reservoirs, we studied two Fayetteville fractured horizontal wells-FAY Well #1 and #2 operated by Southwestern Energy (SWN) using Meyer hydraulic fracturing software suite —MShale (fracture simulator) and MProd (reservoir simulator). The workflow of integrated hydraulic fracturing simulation study is proposed.

We prepared input data by integrating geology data, reservoir properties from well logs and well test, perforation and well survey, fracture pump schedule, MS monitoring data, as well as data from the literature for the same Fayetteville formation. Then we built the fracture propagation model in MShale and reservoir production model in MProd.

Next we did parametric study to determine the most influential and uncertain parameters to adjust and how to adjust them. Then we history matched fracture geometry and production data for the two hydraulically fractured horizontal wells, and determined some uncertain variables (e.g. number of fractures per stage, in-situ stress gradient, leakoff coefficient, reservoir permeability, proppant damage factor, etc.). We also found the interaction of the variables, for example, how permeability influences fracture number per stage, fracture wall roughness, fracture conductivity and width, etc.

By comparison of the two studied wells, we found the following preliminary means to increase production: longer lateral length, higher cluster density, more cluster NO/stage, smaller

sand size, less fluid and sand per cluster or per foot since we have higher cluster density, and less pad/total fluid ratio, etc. Note that these means are based on the two wells.

6.2 Objectives

Use software—MShale (fracture simulator) and MProd (reservoir simulator)— to history match the fracture geometry and production data for the hydraulically fractured horizontal wells, to determine uncertain variables from history match, including: matrix permeability, stress gradient, leak-off coefficients, fracture wall roughness, number of transverse fractures, proppant settling mode, proppant damage factor, propped length/height, fracture conductivity, etc. Predict well productivity, evaluate frac effectiveness, improve future frac treatment design, and gain insights into hydraulic fractures in shale reservoirs.

6.3 Workflow of Integrated Hydraulic Fracturing and Reservoir Production Study

The workflow of the integrated study of hydraulic fracturing and reservoir production is shown in **Fig. 30**. Then in the following sections, we show how to collect all the data needed to prepare the input data for the fracture propagation software MShale, and reservoir simulation software MProd, both belonging to Meyer Hydraulic Fracturing software suite.

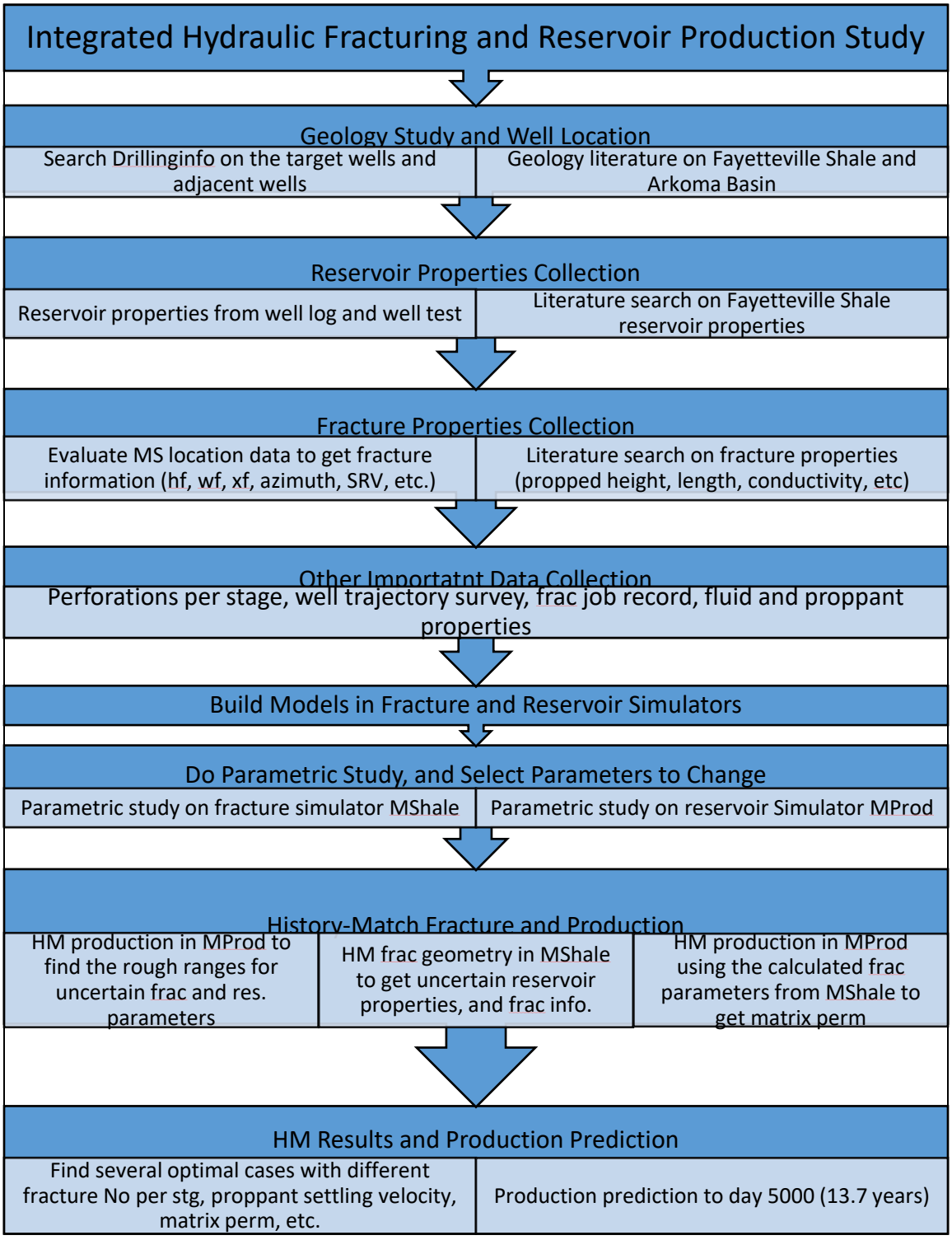

Fig. 30. Workflow of Integrated Hydraulic Fracturing and Reservoir Production Study

6.4 Preparation of Input Data for Model Building

6.4.1 Fayetteville Shale Geology

The Fayetteville Shale is located in Central Arkansas, in Arkoma Basin. It extends from Ozark Uplift in the north to Ouachita thrust fault on the south, encompassing more than 2 million acres where Southwestern Energy (SWN) operates 888,000 acres. It is a Late Mississippian-age shale that is the geologic equivalent of the Caney Shale in Oklahoma, the Barnett Shale in north Texas (**Fig. 31**), with thickness ranging from 50 ~ 550 ft and depth of 1,500 ~ 6,500 ft (Shelby 2008; McDonald and Wright 2016).

Fayetteville Shale is located in Arkoma Basin, which is an EW-trending elongated synclinorium in southeast Oklahoma and west-central Arkansas. Arkoma Basin is a Pennsylvanian basin bounded on the north by the Boston Mountains of the Ozark uplift and on the south by the over-thrust Ouachita Mountain anticlinorium (**Fig. 32**). This basin produces dry gas exclusively, from stratigraphic traps in Atokan and Morrowan Sandstones (conventional) and Fayetteville Shale (Unconventional) (Adler 1970-1971).

Fayetteville Shale is overlain by Atoka, Bloyd, Hale, Pitkin formations, and underlain by Batesville, Hindsville, Moorefield, Boone formations (**Fig. 33**). Fayetteville Shale is divided into Upper (UFAY), Middle (MFAY), and Lower Fayetteville which is divided into 3 zones (LFAY, FL2, FL3). MFAY has higher content of illite and mixed-layer illite and smectite, and has higher fracture gradients and lower gas porosity. FL2 has the lowest clay content and highest gas porosity of the intervals, so it is the main target interval. Natural fractures (both open and mineralized) occur throughout the Upper and Lower Fayetteville, and are nearly parallel to maximum horizontal stress (NE-SW) (Ramakrishnan et al.).

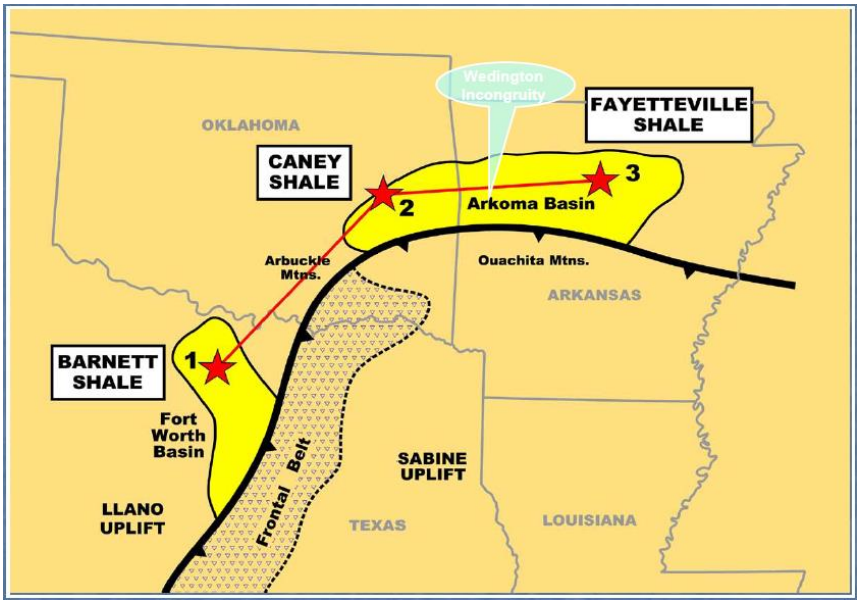

Fig. 31. Fayetteville Shale is a Mississippian-age shale, the geologic equivalent of Caney Shale (OK), and Barnett Shale (TX) (Shelby 2008).

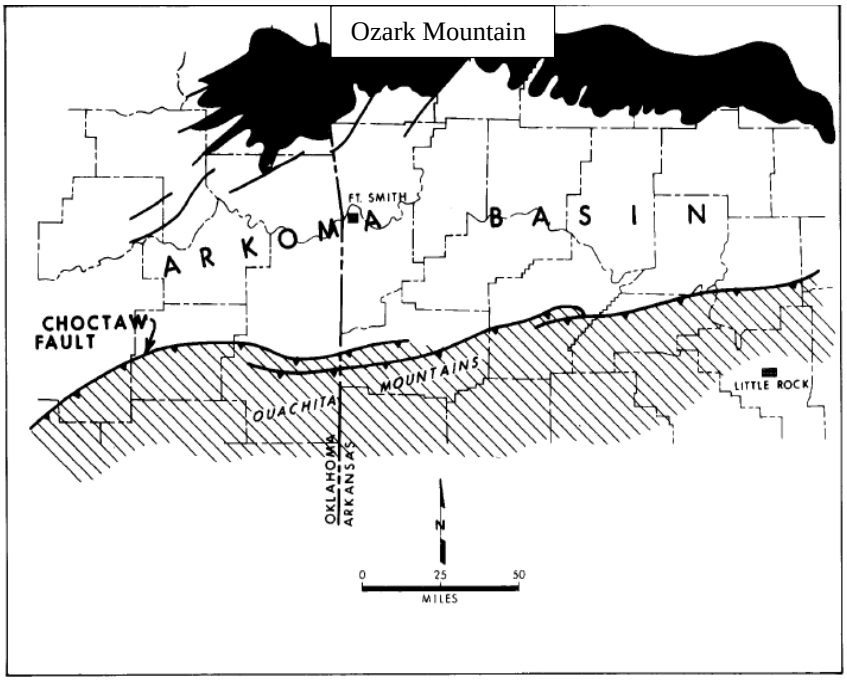

Fig. 32. Regional map of Arkoma Basin showing major tectonic features (Haines 1984).

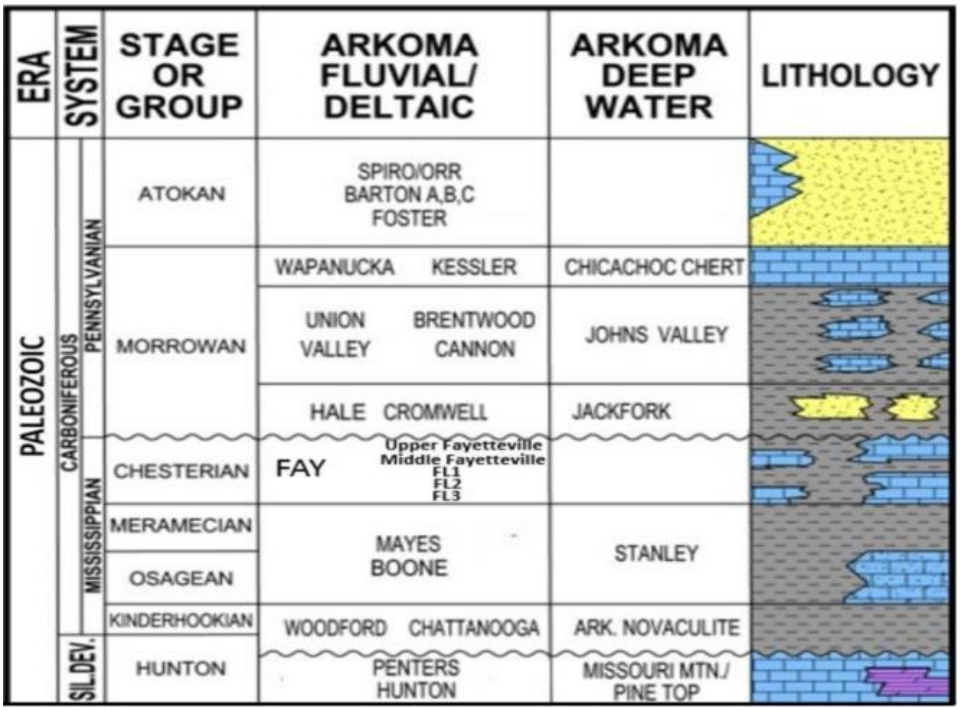

Fig. 33. Stratigraphic column showing the Fayetteville Shale.
Reprinted from McDonald and Wright (2016).

6.4.2 Well Locations

We found the two well locations (County, field, township, section, surface latitude, longitude, TVD, etc.) in DrillingInfo website using their API well numbers (**Table 15**, **Fig. 34**), and calculated their drainage areas roughly; we also found the completion and production information for adjacent wells, for future comparisons.

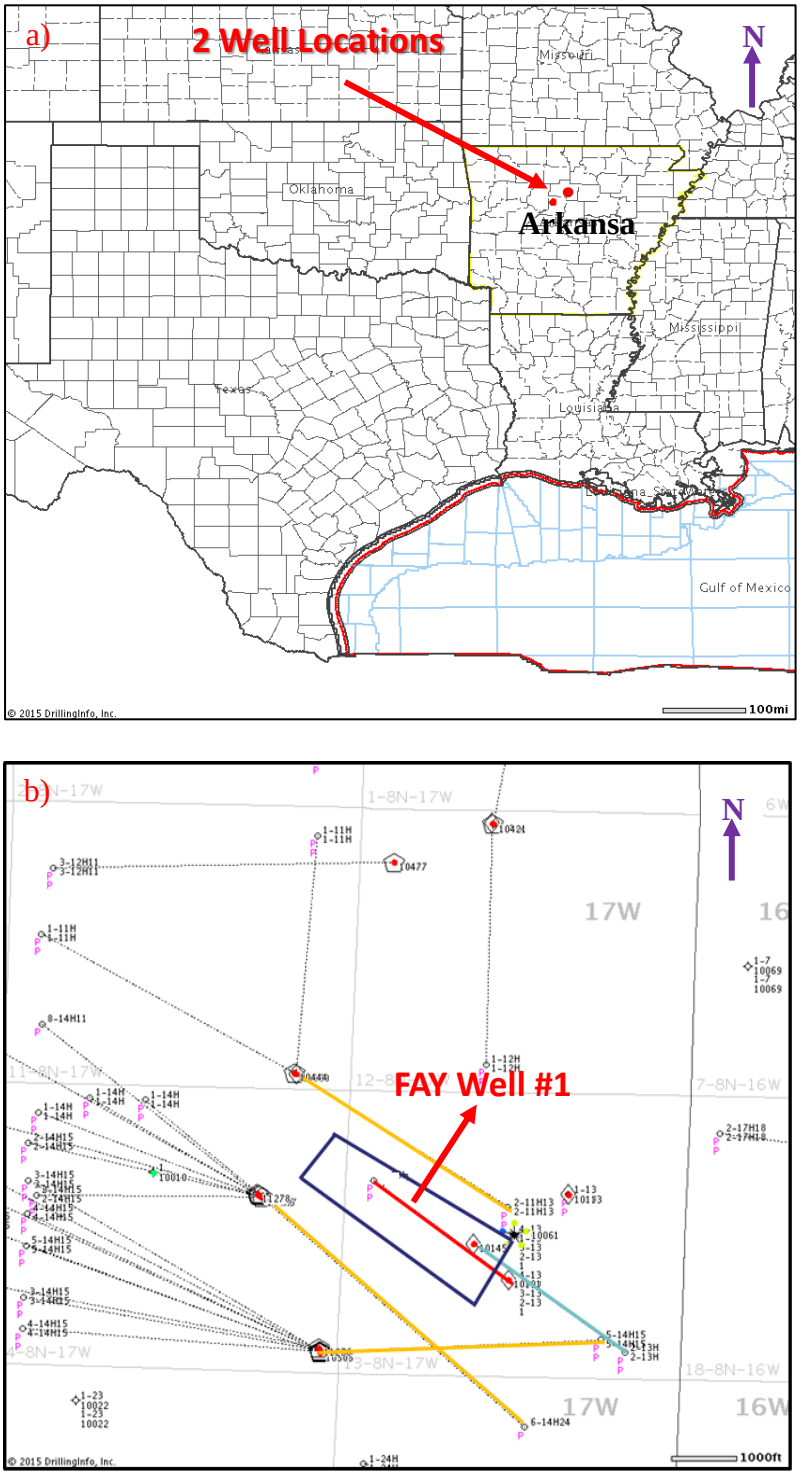

Fig. 34. Locations of a) the two studied wells in Arkansas; b) detail view of FAY Well #1 to roughly capture the drainage area (www.DrillingInfo.com).

Well Name	FAY Well #1	FAY Well #2
API Well Number	03-029-1xxxx	03-141-1xxxx
County	CONWAY, AR	VAN BUREN, AR
Field	F1	F2
Township	X	Y
Section	M	N
Spud Date	11/16/2006	3/5/2011
Surface Latitude	I	J
Surface Longitude	K	L
TVD	5400 ft	3585.6 ft

Table 15. Well Locations of the Two Studied Fayetteville Wells.

6.4.3 Well Survey and Perforation

Table 16 is a typical well trajectory by survey. **Table 17** summarizes the perforation information of the two wells.

MD	Inclination	Azimuth	Northing	Easting	TVD
1	0.1	0.1	0.000873	1.52E-06	0.999999
576	3.32	9.05	16.9497	2.62053	575.668
1044	1.32	156.35	25.3991	6.91672	1043.45
1530	0.8	95.28	19.959	12.5409	1529.38
2021	0.79	88.78	19.7156	19.3382	2020.33
2513.01	1.14	135.48	16.2981	26.1611	2512.28
3005.01	0.78	134.37	10.4666	31.9866	3004.21
3478.01	2.74	114.12	3.5945	44.6079	3476.97
3958.01	5.11	53.71	11.5622	72.3231	3955.98
4045.01	4.32	53.73	15.7939	78.0879	4042.69
4089.01	3.98	58.11	17.581	80.7205	4086.57
4133.01	1.61	48.17	18.8001	82.4779	4130.51

4177.01	4.27	277.92	19.4385	81.3151	4174.48
4220.01	10.4	269.03	19.5935	75.8436	4217.11

Table 16. An example of well trajectory of a horizontal well.

MD	Inclination	Azimuth	Northing	Easting	TVD
4264.01	16.07	268.39	19.355	65.7771	4259.92
4308.01	21.19	269.13	19.063	51.729	4301.6
4352.01	26.08	269.62	18.878	34.0955	4341.9
4395.01	30.93	268.64	18.5528	13.5837	4379.67
4439.01	35.89	268.67	17.9847	-10.6296	4416.39
4483.01	40.47	269.42	17.5406	-37.8162	4450.97
4527.01	44.45	270.39	17.5009	-67.5128	4483.43
4571.01	48.74	271.49	18.036	-99.4665	4513.65
4614.01	51.9	272.13	19.0854	-132.539	4541.11
4658.01	54.24	272.55	20.5233	-167.679	4567.54
4701.01	57.55	272.54	22.104	-203.244	4591.65
4745.01	60.83	272.42	23.7383	-240.994	4614.18
4789.01	63.64	272.28	25.334	-279.891	4634.68
4833.01	67.31	271.2	26.5437	-319.896	4652.94
4877.01	70.98	270.39	27.1106	-361.001	4668.6
4921.01	74.55	270.13	27.3003	-403.018	4681.63
4964.01	77.87	270.07	27.3731	-444.773	4691.88
5008.01	80.74	273.41	28.6915	-487.978	4700.05
5052.01	82.37	278.77	33.3112	-531.237	4706.52
5096.01	83.28	284.49	42.11	-573.977	4712.02
5139.01	83.83	289.99	54.7696	-614.769	4716.85
5183.01	85.21	295.4	71.6638	-655.159	4721.05
5227.01	86.15	301.26	92.4764	-693.761	4724.37
5271.01	86.7	306.18	116.848	-730.275	4727.11
5314.01	88.69	311.41	143.757	-763.748	4728.84
5358.01	90.86	317.26	174.491	-795.204	4729.02
5402.01	91.55	320.17	207.543	-824.226	4728.09
5490.01	90.72	321.89	275.945	-879.556	4726.35
5581.01	90.86	321.91	347.549	-935.701	4725.09
5668.01	91.27	323.15	416.585	-988.617	4723.48
5755.01	90	325.44	487.222	-1039.38	4722.51

Table 16. Continued.

Well Name	No. of Stg	Clusters/Stg	Length/ Cluster, ft	Cluster Spacing, ft	Shot Density, shot/ft	Shots/ Cluster	Perf Diameter, in
FAY Well #1	5	3	2	140	6	12	0.38

FAY Well #2	11	5	2	83.5	6	11	0.38

Table 17. Perforation summary of the two studied horizontal wells.

6.4.4 Reservoir Properties

Some reservoir properties were measured and provided by SWN, as shown in **Fig. 35**, and **Table 18 to Table 20**. We consider FL2 and FL3 as the pay zone. We also searched the literature for the same Fayetteville formation, to compare the provided parameter values with those in the literature, as in **Table 21**.

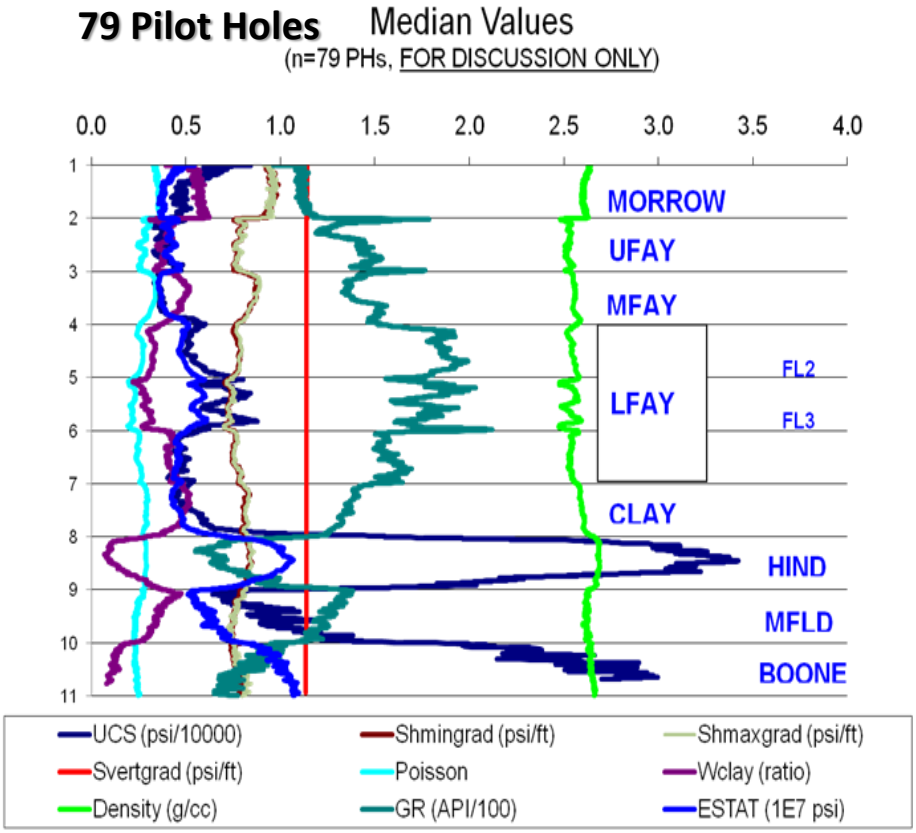

Fig. 35. Reservoir properties from 79 pilot holes measured by SWN.

Formation	E_static, 1E7 psi	Poison	σ_{hmin} Gradient, psi/ft	Fracture Toughness (Empirical)
Pitkin/Morrow	0.38	0.35	0.95	2000
UFAY	0.417	0.26	0.77	1500
MFAY	0.375	0.33	0.833	2000
LFAY	0.45	0.240	0.77	1500
FL2	0.5	0.25	0.76	1500
FL3	0.571	0.21	0.765	1500
Hindsville	0.9375	0.26	1	2000

Table 18. Reservoir properties read from 79 pilot holes for Fayetteville Shale.

Reservoir Properties	FAY Well #1	FAY Well #2
Azimuth of σ_{hmin}	144°	157°
RTA Permeability, nD	50-100	50
Gas Porosity	2.07%	2.66%
Reservoir Temperature, F	131	113.8
Initial Reservoir Pressure, psi	2143	1614
Gas Specific Gravity	0.58	0.58

Table 19. Other selected reservoir properties provided by SWN for FAY Well #1 and #2.

Formation	Lithology	Stage1 TVD		Stage2 TVD		Stage3 TVD		Stage4 TVD		Stage5 TVD	
		Top	Bottom	Top	Bottom	Top	Bottom	Top	Bottom	Top	Bottom
Pitkin	Limestone	4436.67	4530	4446.67	4540	4451.67	4545	4485	4580	4525	4615
UFAY	Shale/Sand	4530	4602.8	4540	4612.8	4545	4617.8	4580	4656.5	4615	4680.3
MFAY	Clay	4602.8	4627	4612.8	4637	4617.8	4642	4656.5	4682	4680.3	4702
LFAY	Shale/Sand	4627	4640	4637	4650	4642	4655	4682	4695	4702	4715
FL2	Shale/Sand	4640	4720	4650	4730	4655	4735	4695	4775	4715	4795
FL3	Shale/Sand	4720	4810	4730	4820	4735	4825	4775	4865	4795	4885
Hindsville	Limestone	4810	4860	4820	4840	4825	4845	4865	4885	4885	4905

Table 20. Example formation depths from the cross section maps of the well.

Parameters	Literature Values
Matrix Permeability	<1 nD (Burch et al. 2009); Shale matrix perm 100 nD (Palmer et al. 2014)
Total Porosity	7-12% (Burch et al. 2009)
Bottomhole Temperature	120-220°F for depth of 4,000-8,000 ft (Deville et al. 2011; Fritz and Jarrett 2012); average less than 175°F (Brady et al. 2013); geothermal gradient for Conway is 24-30 ^{o}C/km, 108-124 °F for depth of 4,728 ft (Byrnes and Lawyer 1999)
Initial Reservoir Pressure	1,150-2,500 psi (Brady et al. 2013) (Ramakrishnan et al. 2011; Xiao et al. 2011; Harpel et al. 2012; Palmer et al. 2014)

Table 21. Fayetteville formation properties in the literature.

6.4.5 Fracture Properties

To history-match fracture geometry in MShale, and estimate drainage area of each stage from fracture geometry for MProd, we need to get fracture properties (length xf, height hf, stage width for the fracture network y) from MS events (**Fig. 36**) and use the Closure Window data as described in Section 5. Fracture geometry read from MS events for FAY Well #1 is shown in **Table 22**.

For some parameters that are needed to build the model but not measured, and to make sure our input values are reasonable, we searched the literature to get some parameter values, as shown in **Table 23**.

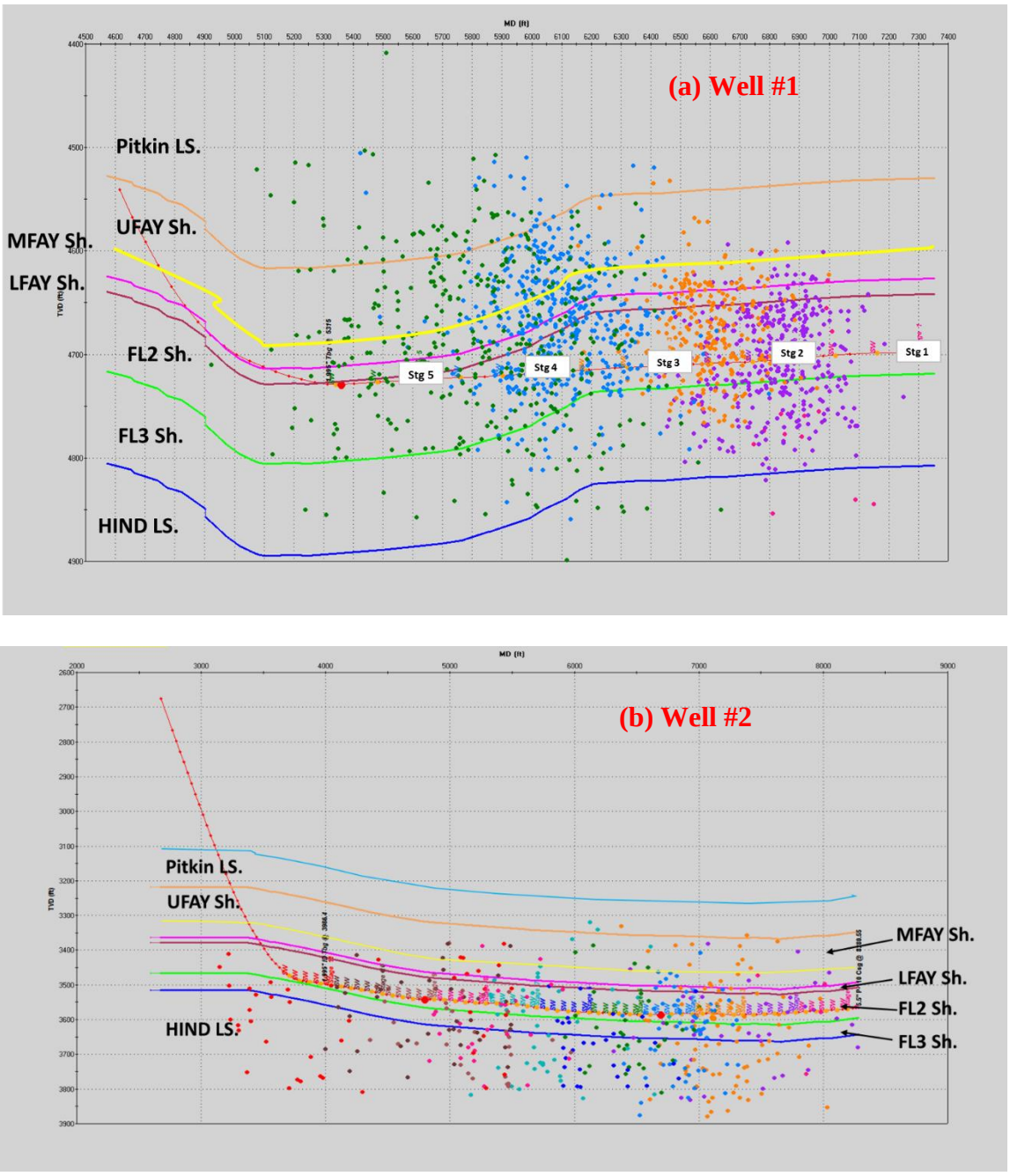

Fig. 36. Cross section geology map and MS events for (a) Well #1 and (b) Well #2. We read fracture geometry from (c) Closure Window of each stage.

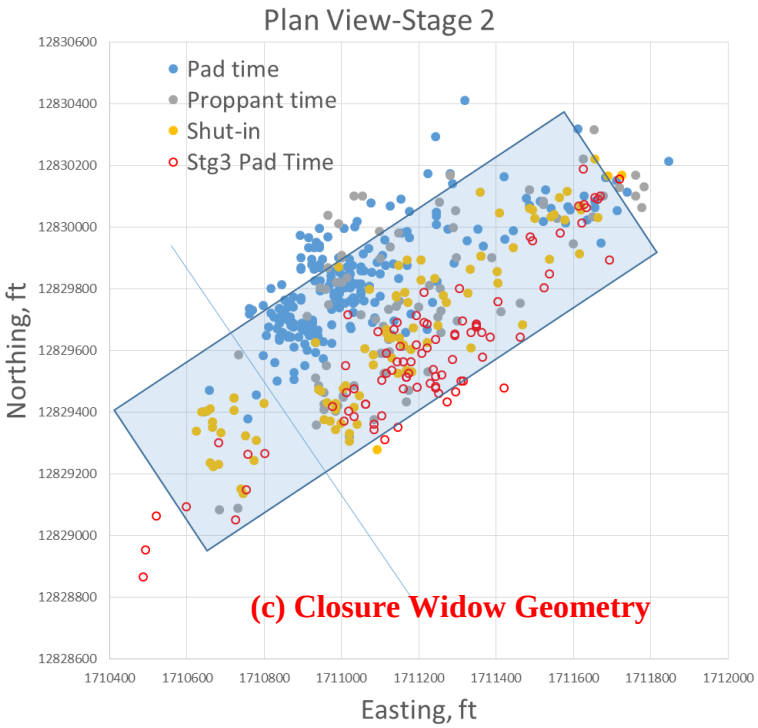

Fig. 36. Continued.

Stage No.	xf from MS, ft	hf from MS, ft	Stage Width y, ft	Reservoir Aspect Ratio 2xf/y	Drainage Area (160 acre Total), acre
1	525.0	300.0	493.8	2.13	25.19
2	717.5	207.0	463.2	3.10	23.63
3	894.0	174.5	604.0	2.96	30.82
4	668.1	317.0	681.2	1.96	34.76
5	670.2	310.0	893.6	1.50	45.60

Table 22. Fracture properties read from MS events for FAY Well #1. Same procedure for Well #2.

Parameters	Literature Values
Fracture height to spacing ratio h/d	0.5-3 (Sagy and Reches 2006; Tang et al. 2008) (Adda Bedia and Amar 2001)
Fracture half-length	300-600 ft (Ramakrishnan et al. 2011)
Propped height near wellbore from pulsed neutron capture and compensated neutron tools	60-100 ft (Duenckel et al. 2014; Saldungaray et al. 2014)
Fracture conductivity	Around 150 md-ft (Harpel et al. 2012); 3-10 md-ft (Ramakrishnan et al. 2011)
Fracture efficiency (flow back rate)	10-40% (Davies et al. 2013)

Table 23. Fracture properties from the literature.

6.4.6 Fracture Treatment Schedule

A typical fracturing treatment schedule for one stage of fracturing is shown in **Table 24**. We need to input them in the MShale software.

Stg #	Stage Name	Slurry Vol (bbl)	Slurry Rate (bbl/min)	Pump Time (min)	Fluid Name	Fluid Vol (gal)	PropName	Prop Concentration (PPA)	Prop Mass (lb)
1	Breakdown	6.2	4.2	1.5	Slickwater	256	None	0.0	0
2	Acid	17.6	8.0	2.2	15% HCl	737	None	0.0	0
3	Pad	177.1	26.6	6.7	Slickwater	7438	None	0.0	0
4	Acid	17.7	8.0	2.2	15% HCl	742	None	0.0	0
5	Pad	4270.4	75.5	56.5	Slickwater	179305	None	0.0	0
6	0.25 PPA	8.0	79.6	0.1	Slickwater	330	40/70 White	0.3	104
7	0.50 PPA	2246.2	80.2	28.0	Slickwater	92254	40/70 White	0.5	46132
8	0.75 PPA	3421.2	75.6	45.3	Slickwater	138989	40/70 White	0.7	103980
9	0.75 PPA	492.3	79.8	6.2	Slickwater	20001	20/40 White	0.7	14985
10	1.00 PPA	248.9	80.3	3.1	Slickwater	10009	20/40 White	1.0	9799
11	1.25 PPA	251.6	79.9	3.2	Slickwater	10007	20/40 White	1.2	12352
12	1.50 PPA	215.8	80.4	2.7	Slickwater	8520	20/40 White	1.4	12047
13	Flush	141.4	7.9	17.8	Slickwater	5992	None	0.0	22

Table 24. A typical fracturing treatment schedule for one stage of a fractured well.

6.5 Parametric Study on MShale and MProd

We need to match both fracture geometry and production with MShale and MProd, respectively. Therefore, we conducted parametric studies on both MShale and MProd, to know what parameters to change and how to change them to approach the measured values for fracture geometry and production. See **Table 25** and **26** for details. Symbol meanings in the table: ↑: increased; ↓: decreased; ↑↑: increased quickly, ↓↓: decreased quickly; ↑--: increased slightly; ↓--: decreased slightly; --: no change.

Fluid leakoff, Young's modulus, in-situ stress, fracture wall roughness or friction, fracture number/stage, fracture spacing, proppant distribution in fractures, DFN mode are the sensitive parameters for fracture propagation. Fracture number per stage, fracture spacing, pay zone permeability and height are the most sensitive parameters for production. Slow proppant settling velocity and small proppant damage factor can increase fracture conductivity, and increase propped fracture height and length.

From the above analysis, we decided the parameters (highlighted with green) that we will change to match fracture geometry in MShale (leakoff coefficients CL & Sp, in-situ stress gradient σ, fracture number/stage, fracture wall roughness, proppant settling mode, proppant damage factor), and parameters to match production in MProd (fracture number/stage, pay zone permeability, pay zone thickness, etc.).

NO	Parameter Change	xf	wf	hf	Fracture Efficiency	BHTP	WHTP
1	CL, Sp ↑	↓	↓	↓	↓	↑	↑
2	Fracture toughness ↑	↑--	↑	↓	↑	↑	↑
3	Young's modulus ↑	↓	↓	↑	↓	↑	↑
4	Poisson's ratio ↑	↓--	↓--	↑--	↓--	↑	↑
5	In-situ stress gradient↑	↑--	↑	↓	↓	↑	↑
6	Fracture wall roughness↑	↓	↑	↑--	↑	↑	↑
7	Tip effect ↑	↓	↑	↑--	↑	↑	↑
8	Fracture number/zones ↑	↓	↓	↑	↓	↑	↑
9	proppant settling: convective -> empirical	--	--	--	--	--	--
10	proppant damage factor ↑	--	--	--	--	--	--
11	Maximum fracture height to spacing ratio h/d ↑	↑--	↓	↑--	↓	↑	↑
12	Fluid loss Interaction %↑, or Empirical-> Full	↑	↓	↑	↑	↑	↑
13	Spacing along x ↑	↑	↑	↑--	↓	↑	↑
14	Spacing along y ↑	↑	↑	↓	↑	↓	↓
15	Aperture ratio of vertical fracture ↑	↓	↓	↓	↑	↓	↓
16	Aspect ratio ↑	↓	↓	--	↓	↓	↓
17	Proppant distribution: uniform-> dominant ↑	↓	↑	↓	↓	↑	↑
18	Separated --> Connected cluster DFN	↑↑	↑	↑↑	↓	↑↑	↑↑
19	Fracture Network: Cluster/complex -- >DFN ↑	↓	↓	↑	↓	↑	↑
20	Mid-field fracture complex ↑	--	--	--	--	↑	↑
21	Wellbore hydraulics (pipe roughness, friction loss multiplier) ↑	--	--	--	--	--	↑
22	Stage friction multiplier ↑	↓--	↓--	↓--	--	↓	↑
23	Fracture friction model: on (turbulent flow)	↑	↓	↓	↓	↓	↓
24	Perf friction-erosion rate ↑	--	--	--	--	--	--
25	Closure pressure on proppant ↑	--	--	--	--	--	--

Table 25. Parametric Study on Fracture Simulator MShale.

NO.	Parameters ↑	Cum Prod
1	Fracture NO./Stg	↑
2	Spacing	↑↑
3	Propped Length	↑--
4	Propped Height	↑--
5	Fracture Conductivity	↑--
6	Fracture Perm (if wf constant)	↑--
7	Reservoir Permeability	↑
8	Pay Zone Height	↑
9	Initial Pressure	↑
10	Drainage Area	--

Table 26. Parametric Study on Reservoir Simulator MProd.

6.6 History Match and Production Prediction

Now we try to history match fracture geometry in MShale and production in MProd. As described in the workflow (**Fig. 37**) in section 6.3: First, roughly match production in MProd to find the rough ranges for uncertain fracture and reservoir parameters. Then history-match fracture geometry in MShale to get uncertain reservoir properties, and fracture information. Next, history-match production in MProd using the calculated (output) fracture parameters from MShale (fracture height, length, width, conductivity, etc.) to get matrix perm. Next, find several optimal cases in MProd with different output of MShale by different setting of fracture number per stage, proppant settling velocity, matrix perm, proppant damage factor, etc. Finally, we can predict production to day 5000 (13.7 years) using the calibrated, optimal cases.

To summarize, our changing parameters to obtain history-match are: leakoff coefficients CL&Sp, in-situ stress gradient σ, fracture number/stage, fracture wall roughness, proppant settling mode, proppant damage factor, fracture number/stage, pay zone permeability, pay zone thickness. We start from the common values given in the field test, or literature, or empirical

values (see Section 6.4), and then change the values within reasonable range to achieve the history-match.

An example of simulated fracture geometry is shown in **Fig. 37**. And an example of simulated production of all stages of one well is shown in **Fig. 38**.

We need to match production in MProd first, to get rough ranges for propped height, length, conductivity, and especially transverse fracture number/stage. Then we match fracture geometry in MShale. Because production is our ultimate history-match goal. We match fracture geometry against the geometry read from Closure Window of MS data, and neglect treating pressure in MShale simulation.

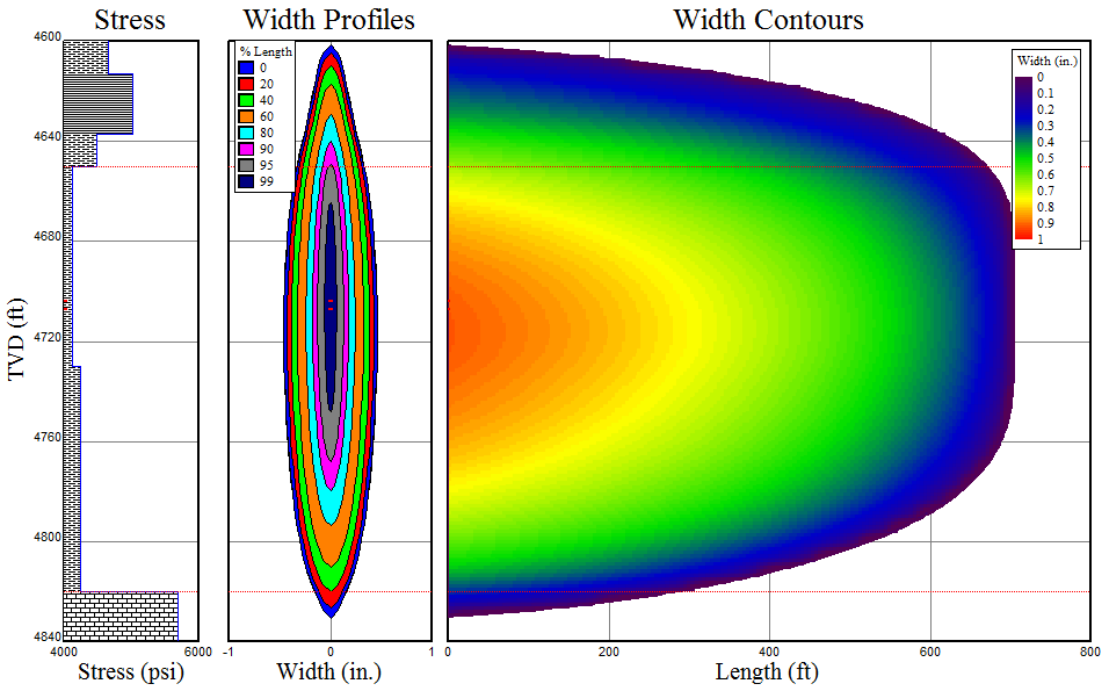

Fig. 37. Simulated fracture geometry in MShale.

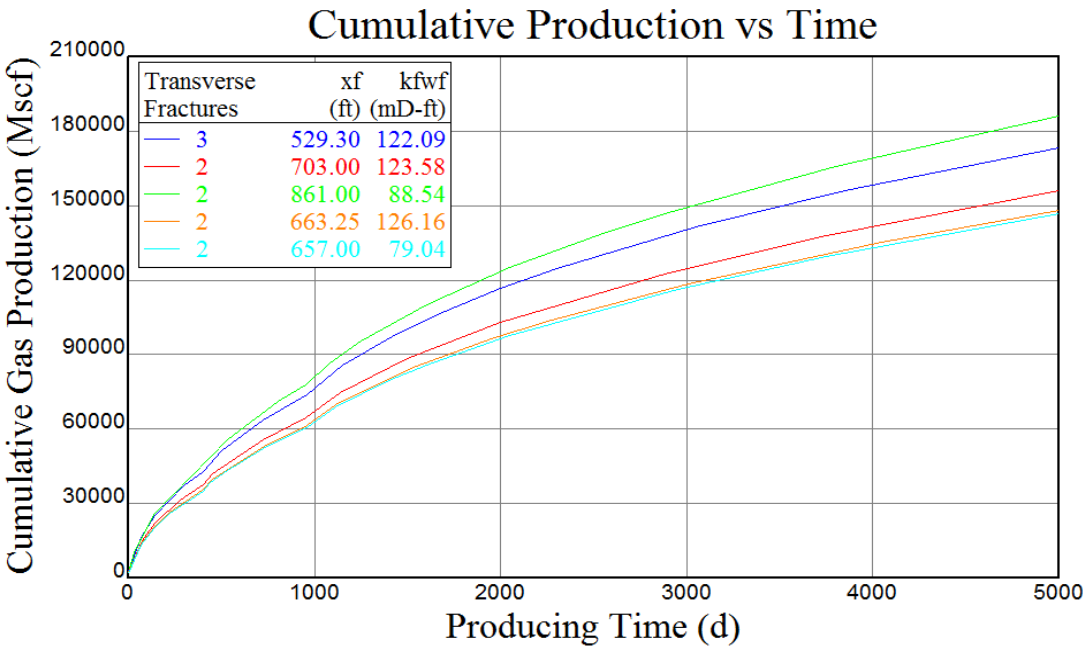

Fig. 38. Simulated production of all stages of a well in MProd.

6.6.1 FAY Well #1

We got 4 best matched cases. One of the optimal cases for Well #1 is shown below in **Table 27** and **Fig. 39**, with proppant settling mode as slow, damage factor 0.8, and permeability 50nD. The unit of stress gradient (σ) is psi/ft, leakoff coefficient (Cl) ft/min$^{0.5}$, spurt loss coefficient (Sp), gal/ft^2. A summary of 4 matched cases is in **Table 28**.

a) Input parameters to change in MShale to history-match fracture geometry. Units: stress gradient (σ), psi/ft; leakoff coefficient (Cl), ft/min$^{0.5}$; spurt loss coefficient (Sp), gal/ft^2. Proppant settling mode- slow, damage factor 0.8, and permeability 50nD.

Stage No.	Stage 1			Stage 2			Stage 3			Stage 4			Stage 5		
Frac Numbers	3			2			2			2			2		
Wall Roughness	16			10			0			22			30		
Formation	σ	Cl	Sp	σ	Cl	Sp	σ	Cl	Sp	σ	Cl	Sp	σ	Cl	Sp
Pitkin	1.1026	0.001	0.2	1.1554	0.0015	0.2	1.1539	0.0015	0.2	1.1539	0.001	0.2	1.1539	0.0010	0.2
UFAY	0.9592	0.0008	0.08	1.0104	0.001	0.1	1.0239	0.001	0.1	1.0039	0.0008	0.08	1.0239	0.0008	0.08
MFAY	0.9903	0.0006	0.05	1.0839	0.0009	0.07	1.0885	0.0009	0.07	1.0385	0.0007	0.05	1.0685	0.0006	0.05
LFAY	0.9001	0.0007	0.08	0.9646	0.0011	0.1	0.9862	0.001	0.1	0.9462	0.0009	0.08	0.9762	0.0008	0.08
FL2	0.8600	0.0007	0.08	0.87	0.0011	0.1	0.8400	0.001	0.1	0.9000	0.0009	0.08	0.9000	0.0008	0.08
FL3	0.8605	0.0007	0.08	0.8796	0.0011	0.1	0.8654	0.001	0.1	0.9058	0.0009	0.08	0.9058	0.0008	0.08
Hindsville	1.1036	0.001	0.2	1.1765	0.0015	0.2	1.1754	0.0015	0.2	1.1654	0.0011	0.2	1.1654	0.0010	0.2

b) Output fracture dimensions in MShale to be history-matched.

Stage No.	Stage 1	Stage 2	Stage 3	Stage 4	Stage 5
xf, ft	531.7	706.3	882	664.3	669.1
hf @well, ft	290.7	229	187.5	315.2	322.8

c) Output parameters from MShale and MProd after history-match.

Stage No.	Stage 1	Stage 2	Stage 3	Stage 4	Stage 5
Max wf, in	0.6733	0.9208	0.8718	0.7574	0.6633
Frac Efficiency	0.3845	0.3616	0.3713	0.3766	0.3636
Propped xf_avg	529.3	703	861	663.3	657
Propped hf_avg	119.9	114.4	88.5	130.7	157.2
Fracture Perm kf, mD	15013	13651	12530	15136	13815
Conductivity, mD-ft	61.03	61.80	46.06	63.08	39.51
Production, Mcf/d	142.60	126.57	150.64	120.17	118.59

Table 27. An optimal history-matched case for Well #1.

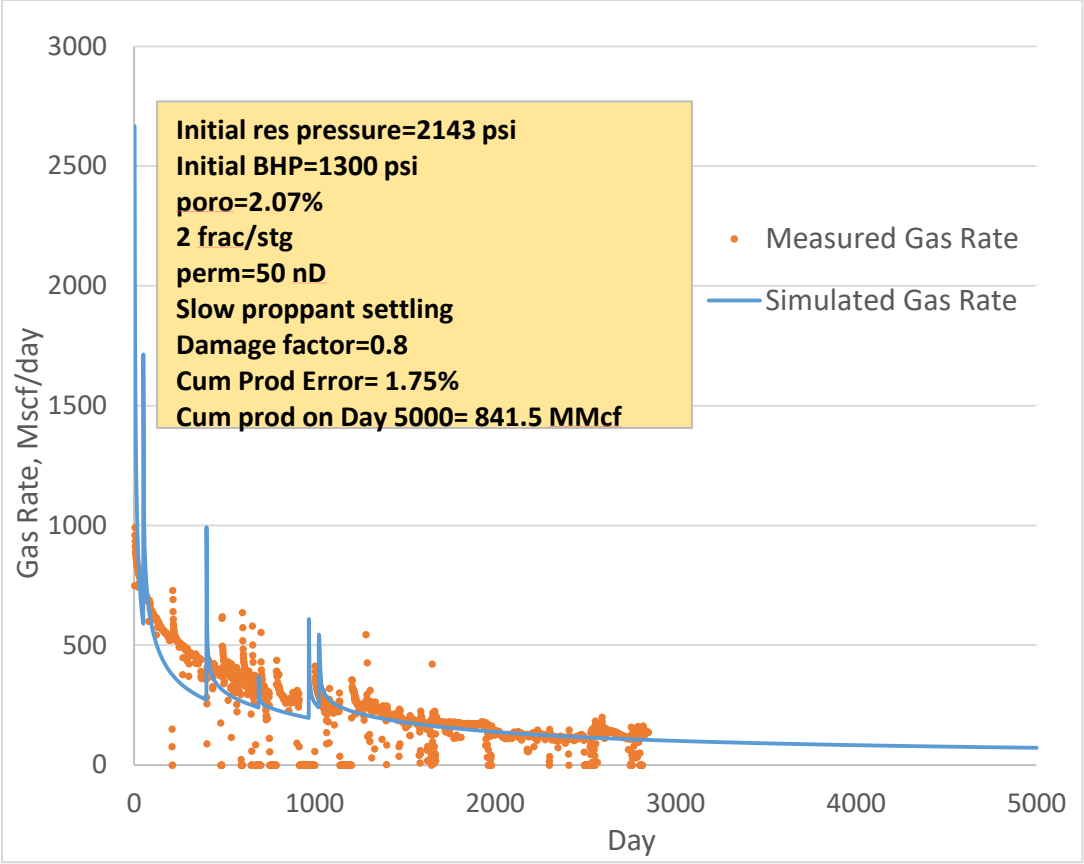

Fig. 39. Production history match and prediction for Well #1.

	Input Uncertain Parameters				Output Parameters			
Case NO.	**Matrix Perm, nD**	**NO. of Trans Frac**	**Prop Settling**	**Prop Damage Factor**	**Prop xf_avg, ft**	**Prop hf_avg, ft**	**Conductivity_avg, md-ft**	**Cum Prod, MMcf**
1	50	11	Slow	0.8	682.7	122.2	54.30	841.50
2	45	11	Slow	0.6	682.9	122.2	107.88	810.59
3	22	15	Slow	0.6	693.4	112.5	81.98	831.52
4	75	11	Fast	0.6	566.7	23.9	103.182	840.92

Table 28. Summary of 4 cases of history match for Well #1.

6.6.2 FAY Well #2

One of the optimal cases for Well #2 is shown below in **Table 29 & 30** and **Fig. 40**, with proppant settling mode as slow, damage factor 0.5, pay zone thickness 181 ft, and permeability 75 nD. A summary of 3 matched cases is in **Table 31**. Comparing the 3 cases, we see: As matrix

permeability decreases, number of open fractures increase (to match production history), conductivity and width decrease (to match the same xf and hf), fracture wall roughness decreases, created DFN increases, and cumulative production at Day 5000 decreases.

Compared with Well #1, in Well #2, MS events indicate that the Hindsville is not an effective frac barrier, and half of the MS events grew downward into Hindsville/Moorefield formations, and there are few events in Upper Fayetteville; Propped height lies largely in Hindsville; if not consider Hindsville, propped xf and hf will be too small; Well #2 has thinner FL3 (50 ft less), and lower matrix perm. Therefore, to be able to achieve history match, we include LFAY, FL2, FL3, and 10-30 % of Hindsville as pay zone, for we assume gas has migrated into Hindsville from overlying source shale. So pay zone height in Hindsville became an uncertain parameter to be matched as well. We need more well log and core data to verify this assumption, although.

	Input uncertain parameters		Parameters to be matched		Output parameters in MShale					
Stage No.	Open Clusters	Wall Roughness	hf @well, ft	xf, ft	wf_max, in	Fracture η	Propped xf_avg	Propped hf_avg	Fracture Perm kf, mD	Conductivity, mD-ft
1	1-5	20.0	354.4	714.8	0.3628	0.7341	688.7	22.5	10247	34.50
2	1-5	18.0	358.7	658.5	0.3415	0.7781	633.7	21.7	10327	38.66
3	2-5	40.0	467.5	661.2	0.3095	0.7751	649.8	29.7	11983	48.91
4	3-5	35.0	410	668.5	0.4508	0.7927	653.5	23.8	11115	58.94
5	2, 4, 5	30.0	367.8	676.5	0.5096	0.7824	647.2	22.0	10094	63.08
6	1-3	19.0	292.8	612	0.7326	0.7624	577.6	17.5	9311	66.09
7	1-3	37.0	365.5	658.9	0.5434	0.7934	634.2	21.9	7183	50.48
8	1-5	20.0	341.3	513.2	0.4544	0.7846	489.1	21.1	10647	53.32
9	1-5	21.0	373.2	679.8	0.3074	0.7991	656.1	21.6	10268	35.41
10	1-5	30.0	377.2	660.3	0.3113	0.796	637.6	21.9	10540	37.39
11	2-4	40.0	372.3	593.2	0.5413	0.7992	572.9	22.5	10782	71.02

Table 29. Fracture parameters of an optimal history-matched case for Well #2.

	Stage 1			Stage 2			Stage 3			Stage 4			Stage 5		
Formation	σ, psi/ft	Cl, ft/min^0.5	Sp, gal/ft^2	σ	Cl	Sp	σ	Cl	Sp	σ	Cl	Sp	σ	Cl	Sp
Pitkin	1.438	0.001	0.07	1.250	0.0009	0.07	1.120	0.00065	0.045	1.160	0.0007	0.062	1.210	0.0008	0.07
UFAY	1.165	0.0007	0.03	1.013	0.0005	0.03	0.903	0.00045	0.013	0.923	0.0004	0.022	0.973	0.0005	0.03
MFAY	1.260	0.0005	0.02	1.096	0.0004	0.02	0.964	0.00025	0.01	1.006	0.0002	0.012	1.056	0.0003	0.02
LFAY	1.165	0.0006	0.03	1.013	0.0005	0.03	0.903	0.00045	0.013	0.923	0.0004	0.022	0.983	0.0005	0.03
FL2	1.150	0.00065	0.03	1.000	0.00055	0.03	0.975	0.00045	0.013	1.000	0.0004	0.025	1.000	0.0005	0.03
FL3	1.158	0.0006	0.03	1.007	0.0006	0.03	0.965	0.00045	0.013	1.000	0.0004	0.025	1.010	0.0005	0.03
Hindsville	1.513	0.001	0.07	1.316	0.0009	0.07	1.149	0.00065	0.045	1.206	0.0007	0.065	1.276	0.0008	0.07
Avg	**1.264**	**0.00072**	**0.04**	**1.099**	**0.00062**	**0.04**	**0.997**	**0.00048**	**0.022**	**1.031**	**0.00046**	**0.033**	**1.073**	**0.00056**	**0.040**

	Stage 6			Stage 7			Stage 8			Stage 9			Stage 10			Stage 11		
Formation	σ	Cl	Sp	σ	Cl	Sp	σ	Cl	Sp	σ	Cl	Sp	σ	Cl	Sp	σ	Cl	Sp
Pitkin	1.328	0.0015	0.08	1.335	0.0008	0.072	1.385	0.0010	0.08	1.318	0.0007	0.065	1.380	0.0007	0.062	1.370	0.0007	0.063
UFAY	1.083	0.0008	0.04	1.074	0.0005	0.03	1.144	0.0007	0.04	1.064	0.0004	0.025	1.115	0.0004	0.022	1.105	0.0004	0.023
MFAY	1.175	0.00055	0.03	1.166	0.0003	0.018	1.236	0.0005	0.03	1.153	0.0002	0.015	1.208	0.0002	0.012	1.200	0.0002	0.013
LFAY	1.083	0.0009	0.04	1.074	0.0004	0.03	1.144	0.0008	0.04	1.064	0.0004	0.025	1.105	0.0004	0.022	1.105	0.0004	0.023
FL2	0.990	0.0009	0.04	1.100	0.0004	0.03	1.100	0.0007	0.04	1.070	0.0004	0.025	1.120	0.0004	0.022	1.140	0.0004	0.023
FL3	1.087	0.0008	0.04	1.087	0.0004	0.03	1.137	0.0007	0.04	1.077	0.0004	0.025	1.120	0.0004	0.022	1.110	0.0004	0.023
Hindsville	1.373	0.0015	0.08	1.407	0.0008	0.072	1.457	0.0010	0.08	1.408	0.0007	0.065	1.444	0.0007	0.062	1.450	0.0007	0.063
Avg	**1.160**	**0.00099**	**0.050**	**1.178**	**0.00051**	**0.0403**	**1.229**	**0.000771**	**0.050**	**1.165**	**0.00046**	**0.035**	**1.213**	**0.00046**	**0.032**	**1.211**	**0.00046**	**0.033**

Table 30. Stress and leakoff coefficients as uncertain input data in MShale for an optimal history-matched case for Well #2.
Units: stress gradient (σ), psi/ft; leakoff coefficient (Cl), ft/min$^{0.5}$; spurt loss coefficient (Sp), gal/ft^2.

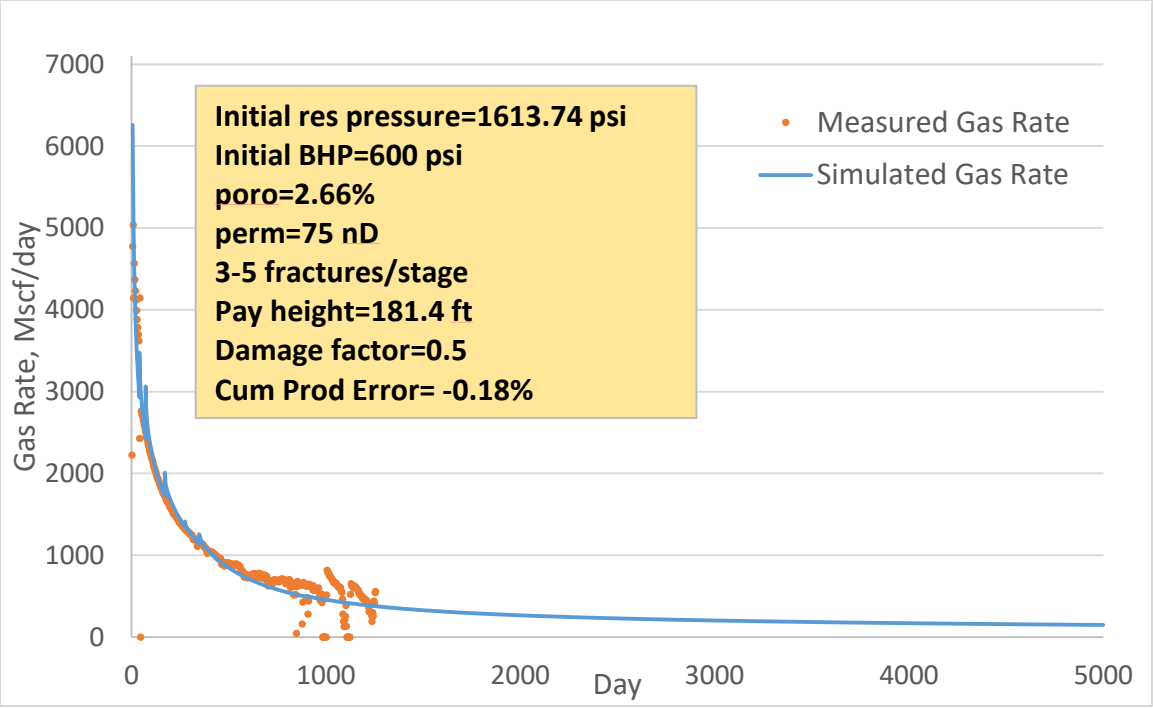

Fig. 40. Production history match and prediction for Well #2.

	Input Uncertain Parameters				Output Parameters				
Case NO.	Matrix Perm, nD	NO. of Trans Frac	Pay Zone	Frac Wall Roughness_avg	Prop xf_avg, ft	Prop hf_avg, ft	Conductivity_avg, md-ft	DFN Volume @End of Job, MMgal	Cum Prod, MMcf
1	75	44	LFAY+FL2+FL3+30 ft HIND LS =181 ft	28.2	622	22	50.71	3.140	2107.25
2	50	55	LFAY+FL2+FL3+15 ft HIND LS =166 ft	22.8	623	22	41.19	3.141	2043.22
3	35	88	LFAY+FL2+FL3+30 ft HIND LS =181 ft	5.0	611	21	27.78	3.184	1888.32

Table 31. Summary of history match results for Well #2. Set proppant settling as slow. Proppant damage factor is 0.5.

6.7 Analyze Fracturing Effectiveness of the Two Wells

We compared the fracture treatment and the production in the two wells in **Table 32**, to see how we can optimize fracture job to increase production or reduce fracturing cost. With almost the same porosity and pay zone thickness, Cumulative gas production/ft of Well #2 is 1.4 times of Well #1, and Cumulative gas production/drainage area is 1.82 times of Well #1. We found the following means just based on the two wells: longer lateral length, higher cluster density, more cluster NO/stage, smaller sand size, less fluid and sand per cluster or per foot since we have higher cluster density, and less pad/total fluid ratio, etc. Note that these means are only based on the two wells. We need to analyze more wells to get a better conclusion and understanding. Also, different geology condition may require different fracture treatment strategy.

In Well #2, half of the MS events grew downward into Hindsville/Moorefield formations, and there are few events in Upper Fayetteville (see Fig. 36b); Simulated propped height lies largely in Hindsville; Well #2 has thinner FL3 (50 ft less), and lower matrix perm. Therefore, to be able to achieve history match, we include LFAY, FL2, FL3, and 10-30 % of Hindsville as pay zone, for we assume gas has migrated into Hindsville from overlying source shale. So pay zone

height in Hindsville became an uncertain parameter to be matched as well. We need more well log and core data to verify this assumption, although.

Parameters	**Well #1**	**Well #2**	**Change of #2**
Frac date	1/15-17/2007	7/25-27/2011	Later
Fractured lateral length, ft	2110	4592.5	2.18 times
Pay depth (UFAY-FL3), ft	4550-4850	3350-3650	1200 ft Shallower
FL2+FL3 thickness, ft	170	133.2	40 ft thinner
Pay zone, ft	FL2+FL3=170 ft	LFAY+FL2+FL3+(15~30ft Hind)=166~181 ft	More layers
Frac gradient, psi/ft	0.874	1.06	1.21
Proppant concentration, PPA	0.25-1.5	0.25-2, 0.25-2	2 ramps
Sand size, mesh	40/70, 20/40	100, 30/70	Smaller
Max pump rate, bbl/min	80	100	1.25
Pump time/stg, min	171.8-199	92-100	Shorter time
Fluid volume/cluster, bbl	3683.8	1636.4	0.44
Pad volume/cluster, bbl	1397.9	153.2	0.11
Pad percentage	38%	9.20%	0.24
Sand /cluster, Mlb	64.02	55.25	Little less
NO of stage	5	11	
NO of cluster/stg	3	5	
Total clusters	15	55	3.67
Total sand, lb	1E+06	3E+06	3.16
Total clean fluid, bbl	6E+04	9E+04	1.66
Cum gas on Day 1256, MMcf	420.7	1304	3.10
Cum water on Day 1256, Mbbl	13.19	30.94	2.35
Cluster spacing, ft	140	83.5	1.68 denser
Interval of stage, ft	282	334	Same
Leak-off by simulation	62%	25%	Less
Fracture efficiency	38%	75%	Higher
Frac fluid recovered on Day 1250	37.26%	36.06%	Same

Table 32. Comparison of the fracture treatment and production of the two wells.

Parameters Nomalized by Length or Area	Well #1	Well #2	Ratio of #2 / #1
Fractured Lateral length, ft	2110	4592.5	2.18
Cross section drainage area, ft2	358700	610802.5	1.70
Cum gas/ft, MMCF	0.199	0.284	1.42
Cum gas/ft2, MMCF	0.0012	0.0021	1.82
Sand/ft, lb	0.152	0.132	0.87
Sand/ft2, lb	8.92E-04	9.95E-04	1.11
Fluid/ft, bbl	8.729	3.920	0.45
Cluster/ft (Cluster density)	0.007	0.012	1.68
Cluster/ft2	4.18E-05	9.00E-05	2.15

Table 32. Continued.

6.8 Conclusions

1)Comparing the two studied wells, with almost the same porosity and pay zone thickness, Cumulative gas production/ft of Well #2 is 1.4 times of Well #1, and Cumulative gas production/drainage area is 1.82 times of Well #1. We found the following preliminary means to increase production: longer lateral length, higher cluster density, more cluster NO/stage, smaller sand size, less fluid and sand per cluster or per foot since we have higher cluster density, and less pad/total fluid ratio, etc. Note that these means are only based on the two wells. We need to analyze more wells to get a better conclusion and understanding.

2)We need to match production in MProd first, to get rough ranges for propped height, length, conductivity, and especially transverse fracture number/stage. Then we match fracture geometry in MShale. Because production is our ultimate history-match goal.

3)To history match efficiently, we should do systematic parametric studies first, to find what parameters influence the results and how. Fluid leakoff, Young's modulus, in-situ stress, fracture wall roughness or friction, fracture number/stage, fracture spacing, proppant distribution in fractures, DFN mode are the sensitive parameters for fracture propagation. Fracture number per

stage, fracture spacing, pay zone permeability and height are the most sensitive parameters for production.

4)In Well #2, half of the MS events grow downward into Hindsville/Moorefield formations, simulated propped height lies largely in Hindsville; Well #2 has thinner FL3 (50 ft less), and lower matrix perm. Therefore, to be able to achieve history match, we include LFAY, FL2, FL3, and 10-30 % of Hindsville as pay zone, and we assume gas has migrated into Hindsville from overlying source shale. So pay zone height in Hindsville became an uncertain parameter to be matched as well. We need more well log and core data to verify this assumption, although.

5)Slow proppant settling velocity and small proppant damage factor can increase fracture conductivity, and increase propped fracture height and length.

6)As matrix permeability decreases, number of fractures increases (to match production history), conductivity and width decrease (to match the same xf and hf), fracture wall roughness decreases, created DFN increases, and cumulative production at Day 5000 decreases.

7. CONCLUSIONS AND FUTURE WORK

7.1 Conclusions

In this work, we addressed two problems in hydraulic fracturing: determination of the equilibrium-height in multilayered formations, and interpreting microseismic diagnostic data. Then we illustrated the use of the tools considering a case study.

Knowledge of equilibrium-height is crucial, because it provides an upper limit for the actually created fracture height. It is used in pseudo three dimensional fracture design programs as an important ingredient but can be also used independently, in the form of fracture height map indicating the relation between treating pressure and fracture height. Our present work focused on rigorous solution of the equilibrium height problem.

Originally the primary use of Microseismic diagnostics data related to fracture treatment was also related to assessment of fracture height. With the emergence of unconventional reservoirs the interpretation of microseismic data have been extended to obtain also the areal extent of the stimulation effect. The areal extent and vertical coverage together determine the stimulated reservoir volume (SRV). Our work focuses on improving the accuracy of the estimated SRV. To achieve this goal we introduced the Closure Window method.

The integrated application of the concepts in the evaluation of two shale gas wells illustrated the power and limitations of the current state of fracture modeling and diagnostics interpretation. In the following we list some of the more detailed conclusions.

7.1.1 Fracture Equilibrium Height

1a. A literature review revealed limitations of current models for determining equilibrium-height of hydraulic fractures. We developed a Multilayer Fracture-Equilibrium-Height Model (MFEH) that rigorously solves for equilibrium-height under various formation minimum in-situ stress (σ), fracture toughness (KIC), and fluid density (SG). The detailed derivation of stress intensity factors (SIFs) KI clearly demonstrates the physical meaning of SIFs. This model is based on equilibrium height theory, so provides upper limit for fracture height.

1b. Comparison with previous models and commercial software (MShale and FracPro) was made. When there is abruptly high or low stress or fracture toughness in the adjacent layers of perforated interval, current models predict the wrong height. Generally, MShale calculated shorter height, and FracPro higher height, than our MFEH model. Most of the difference is attributable to the different interpretation of Pnet, and how they solve the non-linear equilibrium height equation system for the multi-layered reservoir**.** While our model is robust to calculate the correct height under those circumstances, no matter how many perforation intervals and whether they are placed in high- or low-stressed layers. Modified Mack and Warpinski's model (modified MW) provides a correct formulation of the system of non-linear equations.

1c. The secondary solutions were investigated using mathematical experiment and this model, and can be eliminated in the MFEH model.

1d. We proposed a fracture-mechanics definition of the base level of treating pressure to be used in converting treating pressures to net pressures and vice versa. The new definition avoids the deficiency of commonly used definitions that might lead to fracture propagation under negative net pressure.

1e. Sensitivity analysis of the height map showed that tip jump can be induced by low σ, but not low KIC; tip stability is imposed by high KIC and/or high σ. Decreasing σ, will induce tip jump/instability at the boundary, whereas decreasing fracture toughness, KIC, will not cause tip jump, but still a smooth growth. Increasing KIC and/or σ will hinder the fracture growth, or even keep tips stable at the layer boundary. It was found that fracturing fluid density affects which tip starts to grow to infinity when treating pressure reaches a critical value.

1f. We showed the construction of outer and inner envelopes on the height map assisting the evaluation of reliability of a result coming from a "black box" simulator.

7.1.2 Microseismic Evaluation of Hydraulic Fracture

2a. The interpretation of microseismic data is a difficult task. In this work we suggest using the Closure Window technique to improve the production predictive capability of the estimated SRV. By dividing the MS events of hydraulic fracture treatments into three windows: the Pad, Proppant, and Closure Windows, we found Closure Window data have been a neglected resource that provide unique and significant insights and more effectively characterize SRV.

2b. The Excel-VBA program developed in this study can process any MS data and associated fracture stimulation job data, and plot the three MS event windows.

2c. By using Closure Window data, we reduced the fracture dimensions and could reduce the cumulative production history match error from 30% to 2%. Infill wells and re-fracturing may be considered in the light of geometry reduction.

2d. The Mathematica program developed can calculate area and volume of SRV for 3 individual windows and for the entire window of each stage. In the case study we found the area

ratio of Closure/Entire window to be about 0.7 and the volume ratio of Closure/Entire window to be about 0.75.

2e. The case study shows that the overlap among stages is smaller if the Closure Window approach is used. The 3 windows shift apart from each other, with Closure Window moving toward the current stage, while Pad and Proppant Windows moving toward the previous stage. Clear shifts among the 3 Windows indicate reactivation of previously induced HFs and/or pre-existing NFs, and operation noise recorded in the Pad and Proppant Windows. Therefore, a more accurate depiction of the fracture geometry (SRV) can be determined by using the Closure Window.

2f. Closure Window is usually narrower in width and shorter in height than the entire window, and offset from the other two, because the dominant phenomena of leakoff and fracture closing during shut-in period occur near the main induced fractures.

7.1.3 Integrated Study of Fracture Propagation and Reservoir Production

3a. We applied the previously developed tools to compare two gas wells from the Fayetteville Shale. The basic question was whether the difference in production performance can be attributed to difference in the fracture treatment and if improving the design may lead to better productivity.

3b. The simultaneous history match of microseismic and production data leads us to the assumption that well #2 had more downward fracture height growth and could tap into underlying layers, compared to well #1. However, we need more well log and core data to verify this assumption.

3c. Data uncertainty is a natural condition in hydraulic fracturing treatment design and evaluation, but data integration can provide additional insight and show ways to improve productivity.

7.2 Future work

Fracture height containment/growth continues to be a central issue in modeling and evaluation of hydraulic fracturing treatments. There is a need to better quantify additional physical phenomena involved. Data integration and refinement of existing diagnostic techniques should be further pursued in order to better understand the complexity of hydraulic fracture stimulation in unconventional reservoirs.

REFERENCES

Abbas, S., Gordeliy, E., Peirce, A. et al. 2014. Limited Height Growth and Reduced Opening of Hydraulic Fractures Due to Fractureoffsets: An Xfem Application. 2014/2/4/. http://dx.doi.org/10.2118/168622-MS.

Adda Bedia, M. and Amar. 2001. Fracture Spacing in Layered Materials. *Physical Review Letters* **86** (25): 5703-5706.

Adler, F.J. 1970-1971. Future Petroleum Provinces of the Mid-Continent. *Tulsa Geological Society Digest* **38**: 1077-1081.

Ahmed, U. 1984. A Practical Hydraulic Fracturing Model Simulating Necessary Fracture Geometry, Fluid Flow and Leakoff, and Proppant Transport. Paper presented at the SPE/DOE/GRI Unconventional Gas Recovery Symposium, Pittsburgh, PA. 13-15 May, 1984. SPE-12880-MS. http://dx.doi.org/10.2118/12880-MS.

Athavale, A.S. and Miskimins, J.L. 2008. Laboratory Hydraulic Fracturing Tests on Small Homogeneous and Laminated Blocks. Paper presented at the The 42nd U.S. Rock Mechanics Symposium (USRMS), San Francisco, California. 29 June-2 July, 2008. ARMA-08-067.

Baig, A. and Urbancic, T. 2010. Microseismic Moment Tensors: A Path to Understanding Frac Growth. *The Leading Edge* **29** (3): 320-324. http://dx.doi.org/10.1190/1.3353729.

Bao, J.Q., Fathi, E., and Ameri, S. 2015. Uniform Investigation of Hydraulic Fracturing Propagation Regimes in the Plane Strain Model. *International Journal for Numerical and Analytical Methods in Geomechanics* **39** (5): 507-523. 10.1002/nag.2320.

Barree, R.D. and Mukherjee, H. 1996. Determination of Pressure Dependent Leakoff and Its Effect on Fracture Geometry. Paper presented at the SPE Annual Technical Conference and Exhibition, Denver, Colorado, USA. 6-9 October, 1996. SPE-36424-MS. http://dx.doi.org/10.2118/36424-MS.

Biot, M.A., Medlin, W.L., and Masse, L. 1983. Fracture Penetration through an Interface. *SPE Journal* **23** (06): 857 - 869. SPE-10372-PA. http://dx.doi.org/10.2118/10372-PA.

Brady, J.W., Shattuck, D.P., Parker, M.H. et al. 2013. Video Production Logging and Polymer Gel Yields Successful Water Isolation in the Fayetteville Shale. 2013/9/30/. 10.2118/166301-MS.

Bunger, A., Detournay, E., Garagash, D. et al. 2007. Numerical Simulation of Hydraulic Fracturing in the Viscosity Dominated Regime. Paper presented at the SPE Hydraulic Fracturing Technology Conference, College Station, Texas, U.S.A. 29-31 January, 2007. SPE-106115-MS. http://dx.doi.org/10.2118/106115-MS.

Burch, D.N., Daniels, J., Gillard, M. et al. 2009. Live Hydraulic Fracture Monitoring and Diversion. *Oilfield Review*, 11/01/2009, 18-31.

Busetti, S. and Reches, Z.e. 2014. Geomechanics of Hydraulic Fracturing Microseismicity: Part 2. Stress State Determination. *AAPG Bulletin* **98** (11): 2459–2476. http://dx.doi.org/10.1306/05141413124.

Byrnes, A. and Lawyer, G. 1999. Burial, Maturation, and Petroleum Generation History of the Arkoma Basin and Ouachita Foldbelt, Oklahoma and Arkansas. *Natural Resources Research* **8** (1): 3-26. 10.1023/A:1021625526579.

Chitrala, Y., Moreno, C., Sondergeld, C.H. et al. 2011. Microseismic and Microscopic Analysis of Laboratory Induced Hydraulic Fractures. Paper presented at the Canadian Unconventional Resources Conference, Calgary, Alberta, Canada. 15-17 November, 2011. SPE-147321-MS. http://dx.doi.org/10.2118/147321-MS.

Chuprakov, D.A. and Prioul, R. 2015. Hydraulic Fracture Height Containment by Weak Horizontal Interfaces. Paper presented at the SPE Hydraulic Fracturing Technology Conference, The Woodlands, Texas, USA. 3-5 February, 2015. SPE-173337-MS. http://dx.doi.org/10.2118/173337-MS.

Clark, J.B. 1949. A Hydraulic Process for Increasing the Productivity of Wells. *Journal of Petroleum Technology* **1** (01): 1-8. SPE-949001-G. http://dx.doi.org/10.2118/949001-G.

Cohen, C.-E., Kresse, O., and Weng, X. 2015. A New Stacked Height Growth Model for Hydraulic Fracturing Simulation. Paper presented at the 49th U.S. Rock Mechanics/Geomechanics Symposium, San Francisco, California. 28 June-1 July, 2015. ARMA-2015-073.

Cohen, C.-E., Kresse, O., and Weng, X. 2017. Stacked Height Model to Improve Fracture Height Growth Prediction, and Simulate Interactions with Multi-Layer Dfns and Ledges at Weak Zone Interfaces. Paper presented at the SPE Hydraulic Fracturing Technology Conference and Exhibition, The Woodlands, Texas, USA. 24–26 January, 2017. SPE-184876-MS. https://doi.org/10.2118/184867-MS.

Daneshy, A.A. 1978. Hydraulic Fracture Propagation in Layered Formations. *Society of Petroleum Engineers Journal* **18** (01): 33 - 41. SPE-6088-PA. http://dx.doi.org/10.2118/6088-PA.

Davies, R., Foulger, G., Bindley, A. et al. 2013. Induced Seismicity and Hydraulic Fracturing for the Recovery of Hydrocarbons. *Marine and Petroleum Geology* **45** (0): 171-185. http://dx.doi.org/10.1016/j.marpetgeo.2013.03.016.

Detournay, E. 2004. Propagation Regimes of Fluid-Driven Fractures in Impermeable Rocks. *International Journal of Geomechanics* **4** (1): 35-45. 12916837. 10.1061/(ASCE)1532-3641(2004)4:1(35).

Deville, J.P., Fritz, B., and Jarrett, M. 2011. Development of Water-Based Drilling Fluids Customized for Shale Reservoirs. http://dx.doi.org/10.2118/140868-PA.

Dozier, G.C. 2009. Don't Let the Temperature Log Fool You-False Indications of Height Containment from Case Studies in a Tectonically Stressed Environment. *SPE Drilling & Completion* **24** (02): 346 - 356. http://dx.doi.org/10.2118/125869-PA.

Duenckel, R.J., Palisch, T.T., Han, X. et al. 2014. Environmental Stewardship: Global Applications of a Nonradioactive Method to Identify Proppant Placement and Propped-Fracture Height. *SPE Production & Operations*. http://dx.doi.org/10.2118/166251-PA.

Economides, M.J., Hill, A.D., Ehlig-Economides, C. et al. 2012. *Petroleum Production Systems*. Upper Saddle River, N.J. : Prentice Hall. Original edition. ISBN 9780137031580.

Economides, M.J. and Nolte, K.G. 2000. *Reservoir Stimulation*. Chichester, England; New York: Wiley. Original edition. ISBN 0471491926 9780471491927.

Eyre, T.S. and van der Baan, M. 2015. Overview of Moment-Tensor Inversion of Microseismic Events. *The Leading Edge* **34** (8): 882-888. http://dx.doi.org/10.1190/tle34080882.1.

Fisher, M.K. and Warpinski, N.R. 2012. Hydraulic-Fracture-Height Growth: Real Data. *SPE Production & Operations* **27** (01): 8 - 19. http://dx.doi.org/10.2118/145949-PA.

Fritz, B. and Jarrett, M. 2012. Potassium Silicate Treated Water-Based Fluid: An Effective Barrier to Instability in the Fayetteville Shale. 2012/1/1/. http://dx.doi.org/10.2118/151491-MS.

Fung, R.L., Vilayakumar, S., and Cormack, D.E. 1987. Calculation of Vertical Fracture Containment in Layered Formations. *SPE Formation Evaluation* **2** (04): 518-522. http://dx.doi.org/10.2118/14707-PA.

Gale, J.F.W., Laubach, S., Olson, J.E. et al. 2014. Natural Fractures in Shale: A Review and New Observations. *AAPG Bulletin* **98** (11): 2165-2216. http://dx.doi.org/10.1306/08121413151.

Garagash, D. 2006. Plane Strain Propagation of a Hydraulic Fracture During Injection and Shut-In: Asymptotics of Large Toughness. *Engineering Fracture Mechanics* **73** (4): 456-481. 10.1016/j.engfracmech.2005.07.012.

Garagash, D. and Detournay, E. 2005. Plane-Strain Propagation of a Fluid-Driven Fracture: Small Toughness Solution. *Journal of Applied Mechanics* **72** (6): 916-928. 10.1115/1.2047596.

Geilikman, M., Xu, G., and Wong, S.-W. 2013. Interaction of Multiple Hydraulic Fractures in Horizontal Wells. Paper presented at the SPE Unconventional Gas Conference and Exhibition, Muscat, Oman. 28-30 January, 2013. SPE-163982-MS. http://dx.doi.org/10.2118/163982-MS.

Green, C.A., Barree, R.D., and Miskimins, J.L. 2009. Hydraulic-Fracture-Model Sensitivity Analyses of a Massively Stacked, Lenticular, Tight Gas Reservoir. *SPE Production & Operations* **24** (01): 66 - 73. http://dx.doi.org/10.2118/106270-PA.

Gu, H. and Siebrits, E. 2008. Effect of Formation Modulus Contrast on Hydraulic Fracture Height Containment. *SPE Production & Operations* **23** (02): 170 - 176. http://dx.doi.org/10.2118/103822-PA.

Haines, R.A. 1984. *Middle Atokan Delta Systems in the Arkoma Basin of Arkansas*. 1981 Aapg Mid-Continent Regional Meeting. Oklahoma City Oklahoma City Geological Society. Original edition. ISBN.

Harpel, J.M., Barker, L.B., Fontenot, J.M. et al. 2012. Case History of the Fayetteville Shale Completions. 2012/1/1/. 10.2118/152621-MS.

Holditch, S.A. 2006. Hydraulic Fracturing. In *Petroleum Engineering Handbook*, Lake, L.W., Chapter 8: Society of Petroleum Engineers. Volume IV-Production Operations Engineering.

Hurt, R.S. and Germanovich, L.N. 2012. Parameters Controlling Hydraulic Fracturing and Fracture Tip-Dominated Leakoff in Unconsolidated Sands. 2012/1/1/. SPE-160140-MS. http://dx.doi.org/10.2118/160140-MS.

Jeffrey, R.G. and Bunger, A. 2009. A Detailed Comparison of Experimental and Numerical Data on Hydraulic Fracture Height Growth through Stress Contrasts. *SPE Journal* **14** (03): 413 - 422. http://dx.doi.org/10.2118/106030-PA.

Khanna, A. and Kotousov, A. 2016. Controlling the Height of Multiple Hydraulic Fractures in Layered Media. *SPE Journal* **21** (01): 256 - 263. SPE-176017-PA. http://dx.doi.org/10.2118/176017-PA.

Kim, G.-H. 2010. Interpretation of Hydraulic Fracturing Pressure in Low-Permeability Gas Reservoirs. Master of Science Thesis, The Pennsylvania State University.

King, G.E. and Leonard, R.S. 2011. Utilizing Fluid and Proppant Tracer Results to Analyze Multi-Fractured Well Flow Back in Shales: A Framework for Optimizing Fracture Design and Application. 2011/1/1/. http://dx.doi.org/10.2118/140105-MS.

Kovalyshen, Y. and Detournay, E. 2013. Fluid-Driven Fracture in a Poroelastic Rock. Paper presented at the ISRM International Conference for Effective and Sustainable Hydraulic Fracturing, Brisbane, Australia. May 20-22, 2013

Kresse, O. and Weng, X. 2013. Hydraulic Fracturing in Formations with Permeable Natural Fractures. Paper presented at the ISRM International Conference for Effective and Sustainable Hydraulic Fracturing, Brisbane, Australia. 20-22 May, 2013. ISRM-ICHF-2013-028.

Liu, S. and Valko, P.P. 2015. An Improved Equilibrium-Height Model for Predicting Hydraulic Fracture Height Migration in Multi-Layered Formations. Paper presented at the SPE Hydraulic Fracturing Technology Conference, The Woodlands, Texas, USA. 3-5 February, 2015. SPE-173335-MS. http://dx.doi.org/10.2118/173335-MS.

Mack, M.G. and Warpinski, N.R. 2000. Mechanics of Hydraulic Fracturing. In *Reservoir Stimulation*, 3rd Edition. Economides, M.J. and Nolte, K.G., Chapter 6, West Sussex, UK: John Wiley & Sons.

Manchanda, R. and Sharma, M.M. 2013. Time-Delayed Fracturing: A New Strategy in Multi-Stage, Multi-Well Pad Fracturing. Paper presented at the SPE Annual Technical Conference and

Exhibition, Orleans, Louisiana, USA. 30 September-2 October, 2013. SPE-166489-MS. http://dx.doi.org/10.2118/166489-MS.

McDonald, B. and Wright, T.H. 2016. Completion Optimization in the Fayetteville Shale Utilizing Rate Transient Analysis for Candidate Selection. Paper presented at the SPE Hydraulic Fracturing Technology Conference, The Woodlands, Texas, USA. 9-11 February, 2016. SPE-179160-MS. https://doi.org/10.2118/179160-MS.

Mendelsohn, D.A. 1984. A Review of Hydraulic Fracture Modeling—Ii: 3d Modeling and Vertical Growth in Layered Rock. *Journal of Energy Resources Technology* **106** (4): 543-553. http://dx.doi.org/10.1115/1.3231121.

Meyer, B.R. 1986. Design Formulae for 2-D and 3-D Vertical Hydraulic Fractures: Model Comparison and Parametric Studies. Paper presented at the SPE Unconventional Gas Technology Symposium, Louisville, Kentucky. 18-21 May, 1986. SPE-15240-MS. http://dx.doi.org/10.2118/15240-MS.

Meyer, B.R., Cooper, G.D., and Nelson, S.G. 1990. Real-Time 3-D Hydraulic Fracturing Simulation: Theory and Field Case Studies. Paper presented at the SPE Annual Technical Conference and Exhibition, New Orleans, Louisiana. 23-26 September, 1990. SPE-20658-MS. http://dx.doi.org/10.2118/20658-MS.

Morita, N., Whitfill, D.L., and Wahl, H.A. 1988. Stress-Intensity Factor and Fracture Cross-Sectional Shape Predictions from a Three-Dimensional Model for Hydraulically Induced Fractures. *JPT* **40** (10): 1,329 - 321,342. SPE-14262-PA. http://dx.doi.org/10.2118/14262-PA.

Newberry, B.M., Nelson, R.F., and Ahmed, U. 1985. Prediction of Vertical Hydraulic Fracture Migration Using Compressional and Shear Wave Slowness. Paper presented at the Low Permeability Gas Reservoirs, Denver, Colorado. 19-22 May, 1985. SPE-13895-MS. http://dx.doi.org/10.2118/13895-MS.

O'Brien, D.G., Larson, R.T., Parham, R. et al. 2012. Using Real-Time Downhole Microseismic to Evaluate Fracture Geometry for Horizontal Packer-Sleeve Completions in the Bakken Formation, Elm Coulee Field, Montana. *SPE Production & Operations* **27** (01): 27 - 43. http://dx.doi.org/10.2118/139774-PA.

Olsson, R. and Barton, N. 2001. An Improved Model for Hydromechanical Coupling During Shearing of Rock Joints. *International Journal of Rock Mechanics and Mining Sciences & Geomechanics Abstracts* **38** (3): 317-329. http://dx.doi.org/10.1016/S1365-1609(00)00079-4.

Palmer, I.D., Moschovidis, Z., and Schaefer, A.A. 2013. Microseismic Clouds: Modeling and Implications. *SPE Production & Operations* **28** (02): 181 - 190. SPE-154903-PA. http://dx.doi.org/10.2118/154903-PA.

Palmer, I.D., Moschovidis, Z.A., and Cameron, J.R. 2007. Modeling Shear Failure and Stimulation of the Barnett Shale after Hydraulic Fracturing. Paper presented at the SPE Hydraulic Fracturing Technology Conference, College Station, Texas, U.S.A. 29-31 January, 2007. SPE-106113-MS. http://dx.doi.org/10.2118/106113-MS.

Palmer, I.D., Moschovidis, Z.A., Schaefer, A. et al. 2014. Case Histories from Fayettville Shale: Srv Sizes, Fracture Networks, Spacing, Aperture Widths, and Implications for Proppant. Paper presented at the SPE Unconventional Resources Conference, The Woodlands, Texas, USA. 1-3 April, 2014. SPE-169015-MS. http://dx.doi.org/10.2118/169015-MS.

Ramakrishnan, H., Peza, E.A., Sinha, S. et al. 2011. Understanding and Predicting Fayetteville Shale Gas Production through Integrated Seismic-to-Simulation Reservoir Characterization Workflow. Paper presented at the SPE Annual Technical Conference and Exhibition, Denver, Colorado, USA. 30 October-2 November, 2011. SPE-147226-MS. http://dx.doi.org/10.2118/147226-MS.

Ramurthy, M., Lyons, W.S., Hendrickson, R.B. et al. 2009. Effects of High Pressure-Dependent Leakoff and High Process-Zone Stress in Coal-Stimulation Treatments. *SPE Production & Operations* **24** (03): 407 - 414. http://dx.doi.org/10.2118/107971-PA.

Rassenfoss, S. 2015. What Do Fractures Look Like? *JPT* **67** (05): 60-68.

Sagy, A. and Reches, Z.e. 2006. Joint Intensity in Layered Rocks: The Unsaturated, Saturated, Supersaturated, and Clustered Classes. *Israel Journal of Earth Sciences* **55** (1): 33-42. 23775806.

Saldungaray, P., Duenckel, R.J., and Palisch, T.T. 2014. Reducing Hydraulic Fracturing Hse Footprint through the Application of a Non-Radioactive Method for Proppant Placement and Propped Fracture Height Assessment. 2014/9/22/. http://dx.doi.org/10.2118/170333-MS.

Seth Busetti, W.J., and Ze'ev Reches. 2014. Geomechanics of Hydraulic Fracturing Microseismicity: Part 1. Shear, Hybrid, and Tensile Events. *AAPG Bulletin* **98** (11): 2439–2457. http://dx.doi.org/10.1306/05141413123.

Sharma, M.M. and Manchanda, R. 2015. The Role of Induced Un-Propped (Iu) Fractures in Unconventional Oil and Gas Wells. Paper presented at the SPE Annual Technical Conference and Exhibition, Houston, Texas, USA. 28-30 September, 2015. SPE-174946-MS. http://dx.doi.org/10.2118/174946-MS.

Shelby, P. 2008. The Fayetteville Shale Play of North-Central Arkansas – a Project Update. Paper presented at the AAPG Annual Convention, San Antonio, TX. April 20-23, 2008.

Shuck, T., Diller, D.E., Fish, B. et al. 2015. Surface Microseismic in an Extreme Environment. *The Leading Edge* **34** (8): 936-943. http://dx.doi.org/10.1190/tle34080936.1.

Simonson, E.R., Abou-Sayed, A.S., and Clifton, R.J. 1978. Containment of Massive Hydraulic Fractures. *Society of Petroleum Engineers Journal* **18** (01): 27-32. SPE-6089-PA. http://dx.doi.org/10.2118/6089-PA.

Smith, M.B., Bale, A.B., Britt, L.K. et al. 2001. Layered Modulus Effects on Fracture Propagation, Proppant Placement, and Fracture Modeling. Paper presented at the SPE Annual Technical Conference and Exhibition, New Orleans, Louisiana. 30 September-3 October, 2001. SPE-71654-MS. http://dx.doi.org/10.2118/71654-MS.

Tang, C.A., Liang, Z.Z., Zhang, Y.B. et al. 2008. Fracture Spacing in Layered Materials: A New Explanation Based on Two-Dimensional Failure Process Modeling. *American Journal of Science* **308** (1): 49-72. http://dx.doi.org/10.2475/01.2008.02.

Teufel, L.W. and Clark, J.A. 1984. Hydraulic Fracture Propagation in Layered Rock: Experimental Studies of Fracture Containment. *Society of Petroleum Engineers Journal* **24** (01): 19-32. SPE-9878-PA. http://dx.doi.org/10.2118/9878-PA.

Thiercelin, M., Jeffrey, R.G., and Naceur, K.B. 1989. Influence of Fracture Toughness on the Geometry of Hydraulic Fractures. *SPE Production Engineering* **4** (04): 435 - 442. http://dx.doi.org/10.2118/16431-PA.

Valko, P. and Economides, M.J. 1993. Fracture Height Containment with Continuum Damage Mechanics. Paper presented at the SPE Annual Technical Conference and Exhibition, Houston, Texas. 3-6 October, 1993. SPE-26598-MS. http://dx.doi.org/10.2118/26598-MS.

Valkó, P. and Economides, M.J. 1995. *Hydraulic Fracture Mechanics.* : Chichester : Wiley. Original edition. ISBN 0471956643 9780471956648.

van Eekelen, H.A.M. 1982. Hydraulic Fracture Geometry: Fracture Containment in Layered Formations. *SPE Journal* **22** (03): 341 - 349. SPE-9261-PA. http://dx.doi.org/10.2118/9261-PA.

Warpinski, N.R. 1991. Hydraulic Fracturing in Tight, Fissured Media. *Journal of Petroleum Technology* **43** (02): 146 - 209. http://dx.doi.org/10.2118/20154-PA.

Warpinski, N.R. 2009. Integrating Microseismic Monitoring with Well Completions, Reservoir Behavior, and Rock Mechanics. Paper presented at the SPE Tight Gas Completions Conference, San Antonio, Texas, USA. 15-17 June, 2009. SPE-125239-MS. http://dx.doi.org/10.2118/125239-MS.

Warpinski, N.R., Clark, J.A., Schmidt, R.A. et al. 1982. Laboratory Investigation on the -Effect of in-Situ Stresses on Hydraulic Fracture Containment. *SPE Journal* **22** (03): 333 - 340. SPE-9834-PA. http://dx.doi.org/10.2118/9834-PA.

Warpinski, N.R., Mayerhofer, M., Agarwal, K. et al. 2013. Hydraulic-Fracture Geomechanics and Microseismic-Source Mechanisms. *SPE Journal* **18** (04): 766 - 780. http://dx.doi.org/10.2118/158935-PA.

Warpinski, N.R., Moschovidis, Z.A., Parker, C.D. et al. 1994. Comparison Study of Hydraulic Fracturing Models—Test Case: Gri Staged Field Experiment No. 3 *SPE Production & Facilities* **9** (01): 7-16. http://dx.doi.org/10.2118/25890-PA.

Warpinski, N.R., Schmidt, R.A., and Northrop, D.A. 1982. In-Situ Stresses: The Predominant Influence on Hydraulic Fracture Containment. *Journal of Petroleum Technology* **34** (03): 653 - 664. SPE-8932-PA. http://dx.doi.org/10.2118/8932-PA.

Warpinski, N.R. and Teufel, L.W. 1987. Influence of Geologic Discontinuities on Hydraulic Fracture Propagation (Includes Associated Papers 17011 and 17074). *Journal of Petroleum Technology* **39** (02): 209 - 220. SPE-13224-PA. http://dx.doi.org/10.2118/13224-PA.

Warpinski, N.R., Wolhart, S.L., and Wright, C.A. 2004. Analysis and Prediction of Microseismicity Induced by Hydraulic Fracturing. *SPE Journal* **9** (01): 24 - 33. SPE-87673-PA. http://dx.doi.org/10.2118/87673-PA.

Weng, X., Kresse, O., Cohen, C.-E. et al. 2011. Modeling of Hydraulic-Fracture-Network Propagation in a Naturally Fractured Formation. *SPE Production & Operations* **26** (04): 368 - 380. SPE-140253-PA. http://dx.doi.org/10.2118/140253-PA.

Xiao, Y., Van Den Bosch, R.H., Liu, F. et al. 2011. Performance Evaluation in Data Rich Fayetteville Shale Gas Plays - Integrating Physics-Based Reservoir Simulations with Data Driven Approaches for Uncertainty Reduction. 2011/1/1/. http://dx.doi.org/10.2523/14940-MS.

Yang, M., Valko, P.P., and Economides, M.J. 2012a. Hydraulic Fracture Production Optimization with a Pseudo-3d Model in Low-Permeability, Multi-Layered Lithology. Paper presented at the SPE/EAGE European Unconventional Resources Conference and Exhibition, Vienna, Austria. 20-22 March, 2012. SPE-150002-MS. http://dx.doi.org/10.2118/150002-MS.

Yang, M., Valko, P.P., and Economides, M.J. 2012b. On the Fracture Height Migration under Unified Fracture Design Optimization. Paper presented at the SPE Canadian Unconventional Resources Conference, Calgary, Alberta, Canada. 30 October-1 November, 2012. SPE-161641-MS. http://dx.doi.org/10.2118/161641-MS.

Zhang, X., Jeffrey, R.G., Bunger, A.P. et al. 2010. Initiation and Growth of a Hydraulic Fracture from a Borehole under Toughness- or Viscosity- Dominated Conditions. 2010/1/1/.

Zuluaga, E., Schmidt, J.H., Dean, R. et al. 2010. Containment of a Vertical Tensile Region During Surfactant-Polymer Injection. *Journal of Canadian Petroleum Technology* **49** (07): 60 - 66. http://dx.doi.org/10.2118/139431-PA.

APPENDIX

	W_f				h_f				x_f			
	Entire	Closure	Drop	Drop %	Entire	Closure	Drop	Drop %	Entire	Closure	Drop	Drop %
Stg 1	597	494	**103**	17.3	225	198	27	12.0	525	525	0	0.0
Stg 2	702	463	**239**	34.0	230	207	23	10.0	819	718	101	12.3
Stg 3	868	604	**264**	30.4	237	175	62	26.2	978	894	84	8.6
Stg 4	1049	681	**368**	35.1	354	206	148	41.8	668	668	0	0.0
Stg 5	1070	894	**176**	16.4	490	302	188	38.4	693	670	23	3.3
Avg.	857.2	627.2	**230**	26.65	307.2	217.6	89.6	25.67	736.6	695	41.6	4.85

Table A-1—Effect of Closure Window on fracture geometry reduction, for Fayetteville Well 1 (W_f: fracture width of a stage, ft; h_f: fracture height of a stage, ft; x_f: fracture half-length of a stage, ft).

Complete results for Fayetteville Shale (Well 1) and Eagle Ford Shale (Wells 2-5) wells analyses (**Figs. A-1 through A-10**)**.** For example, Fayetteville Shale Well 1, Figs. A-1 and Fig. A-2, show many MS events in the Closure Window, which indicates valuable and unique information can be mined. Fig. A-1 shows plan view and side view of the entire window (all 3 windows included) (Figs. A-1 (a) (c)) and the Closure Window alone (Figs. A-1 (b) (d)) for all the stages. Fig. A-2 illustrates the plan and side views of three individual windows for each single stage.

A. Fayetteville Shale Well 1

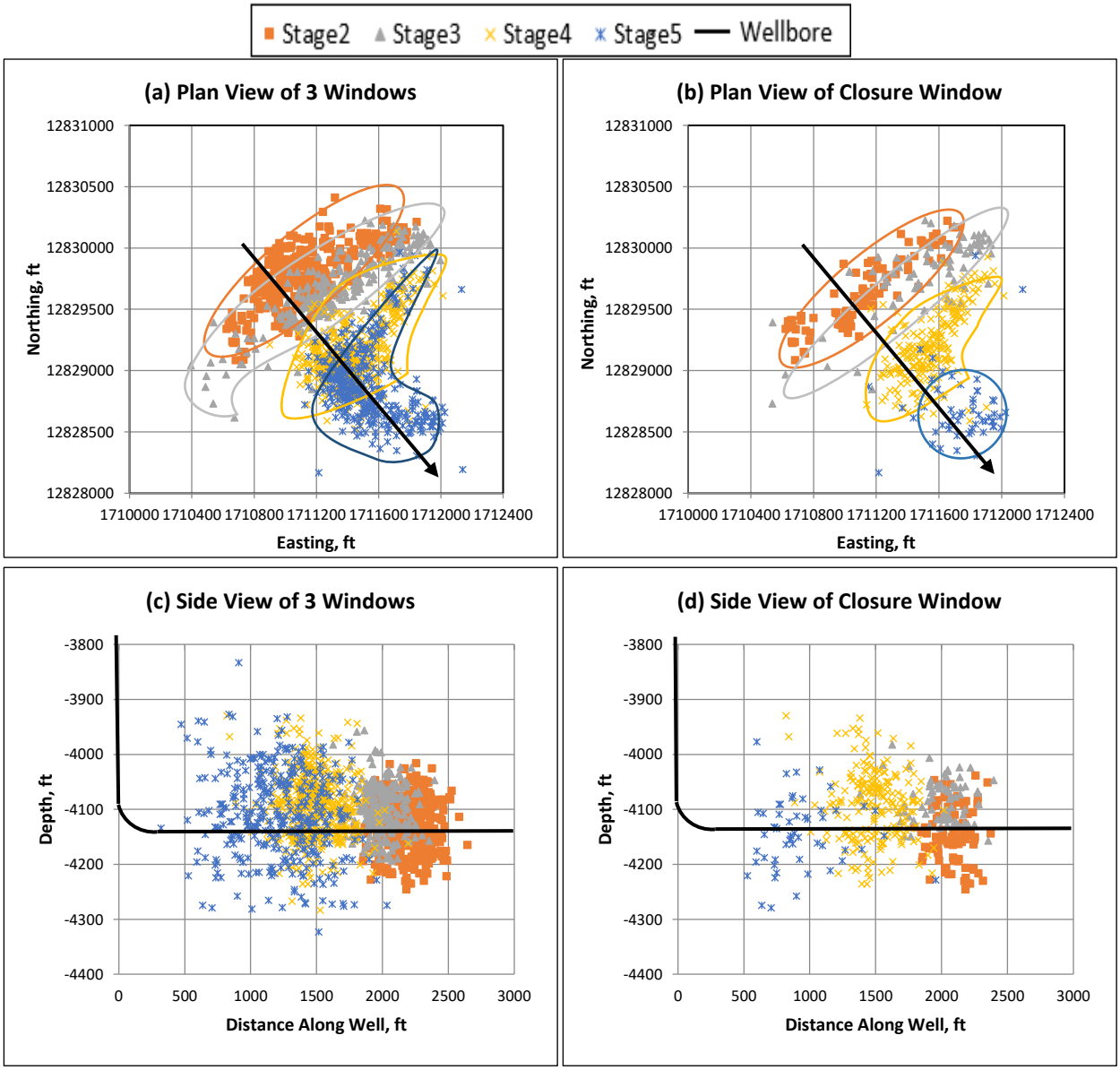

Fig. A-1— Plan view and side view of all 3 windows and closure window for stages 2-5 of Well 1.

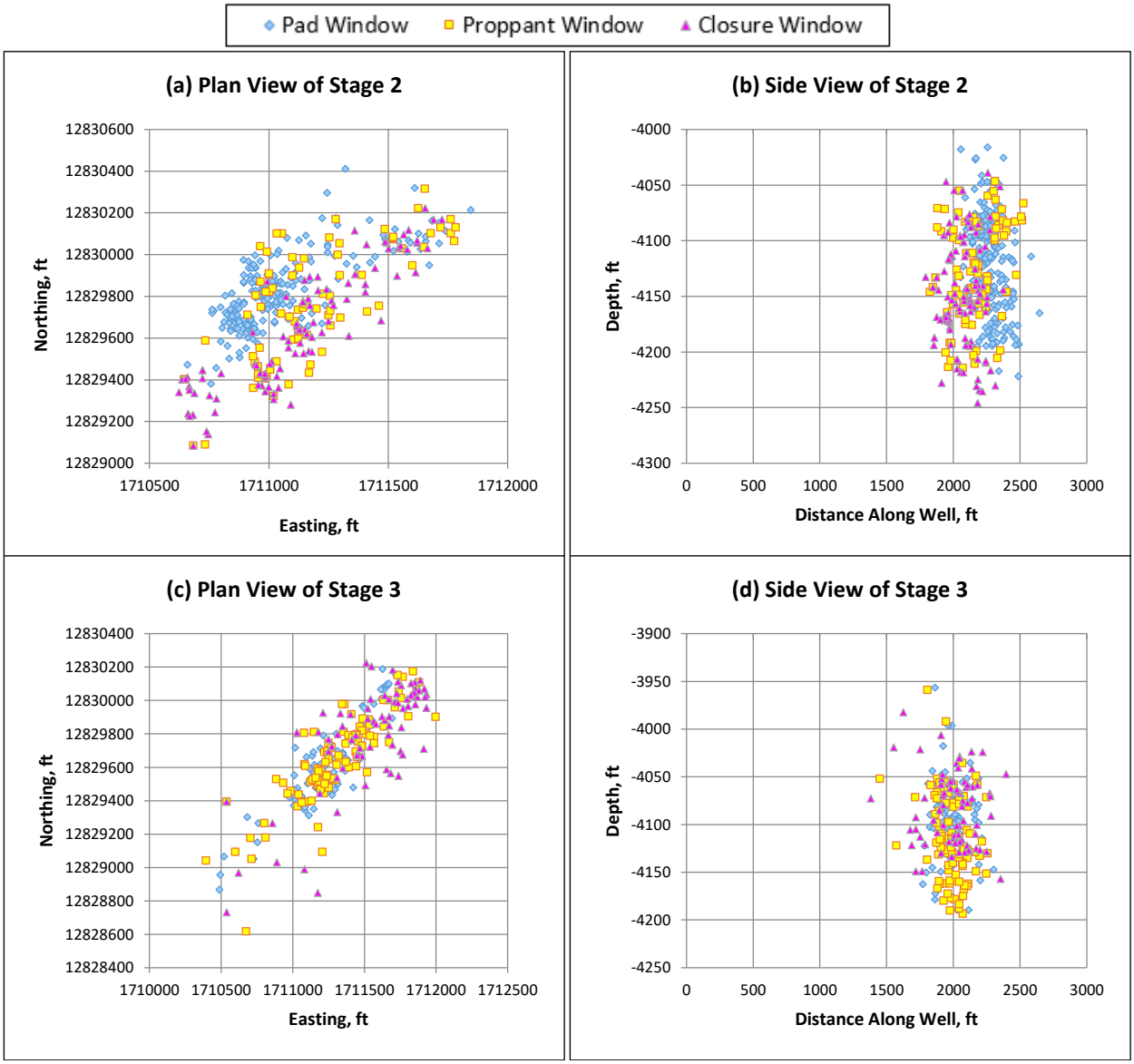

Fig. A-2— Plan view and side view of the 3 individual windows for each stage of Well 1

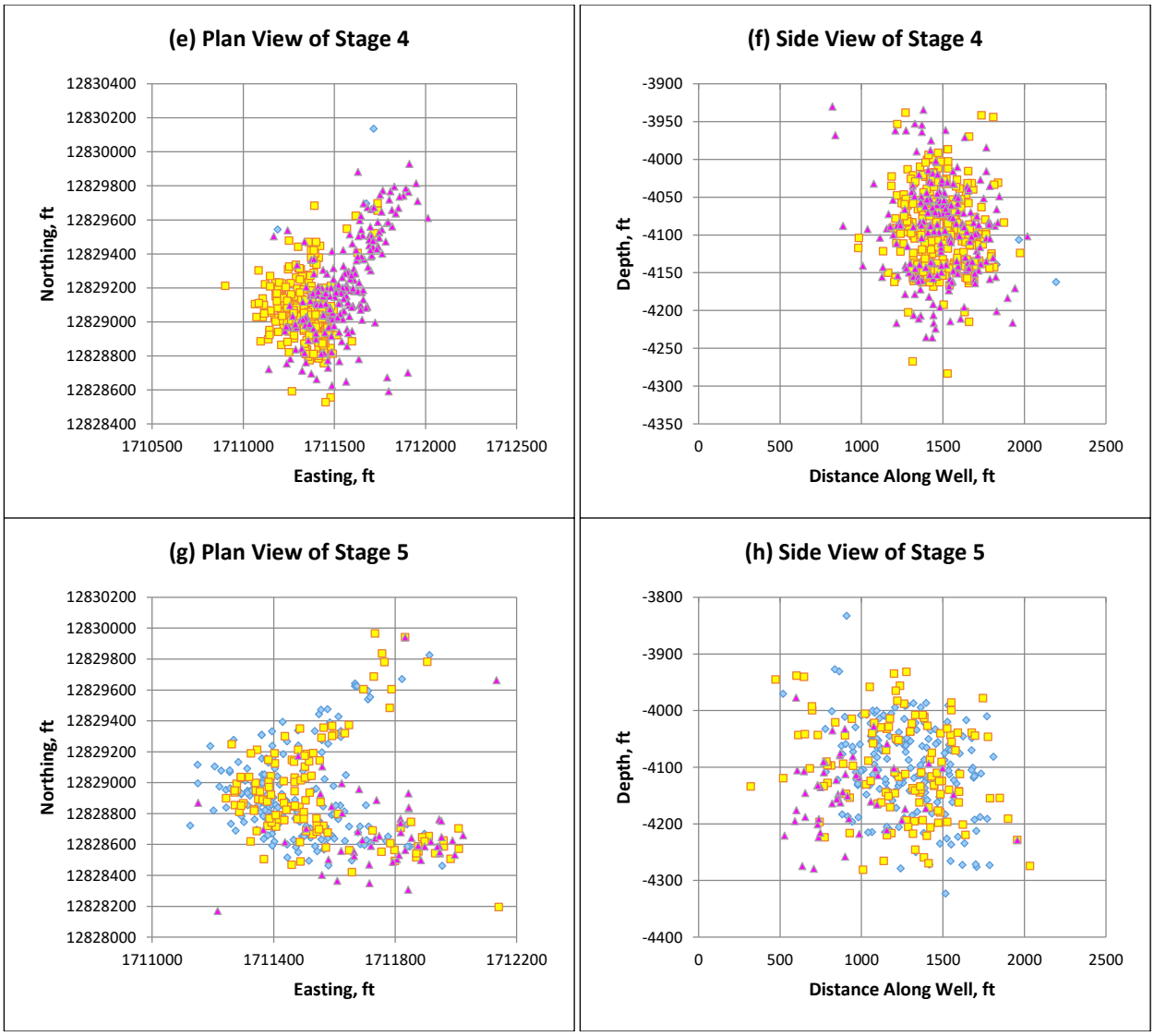

Fig. A-2—Continued.

B. Eagle Ford Shale Well 2

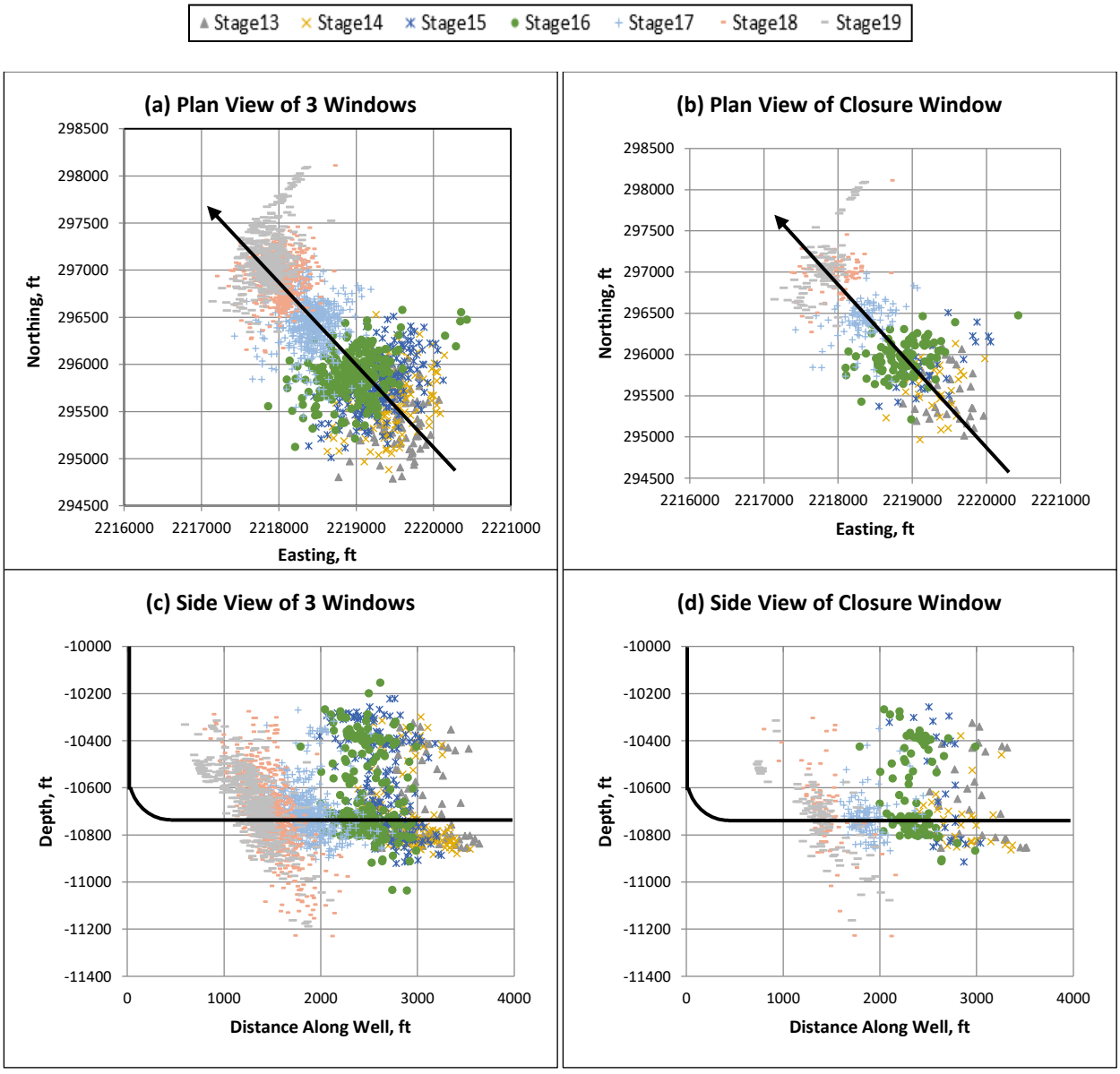

Fig. A-3— Plan view and side view of all 3 windows and closure window for stages 13-19 of Well 2

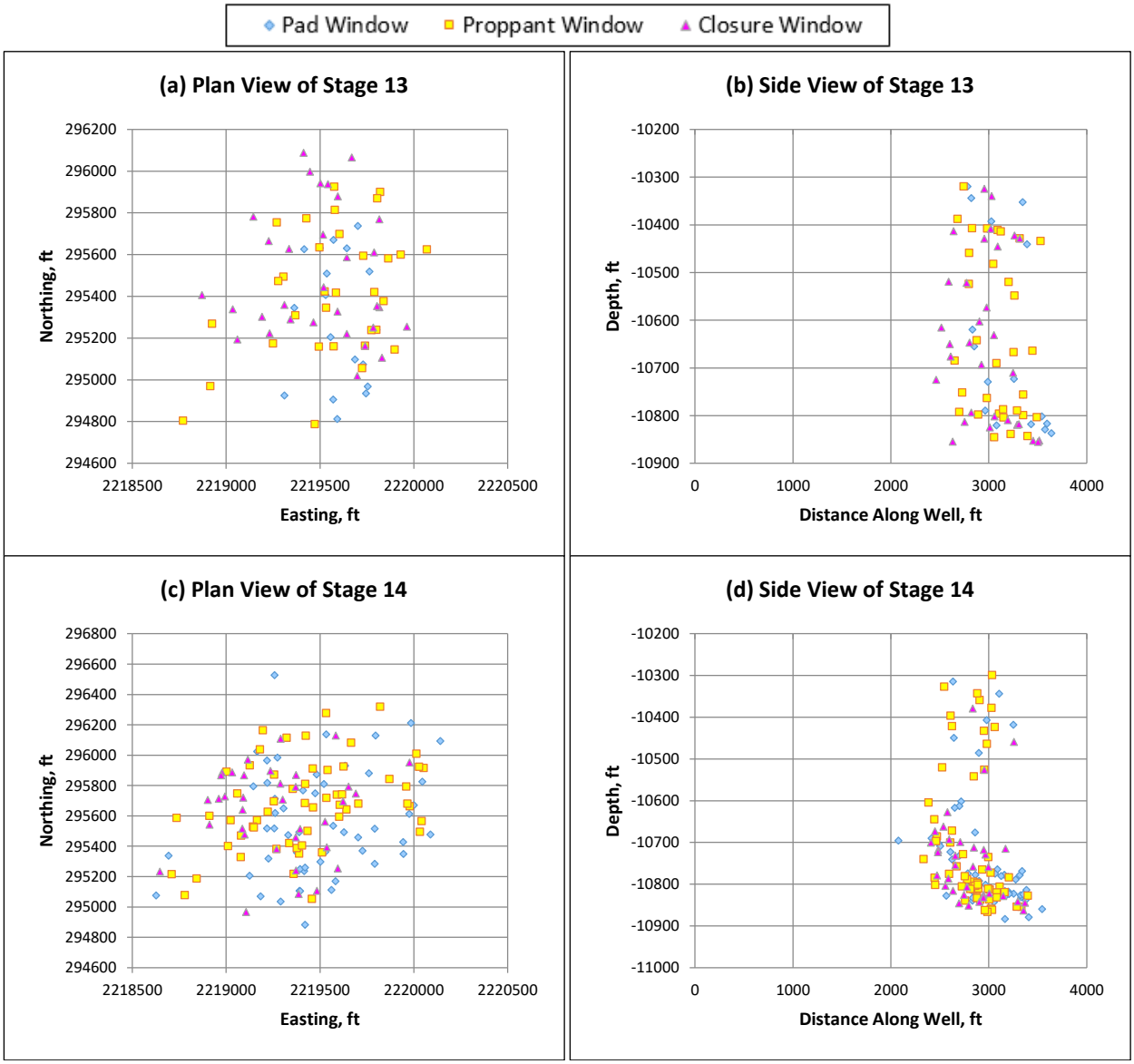

Fig. A-4— Plan view and side view of 3 individual windows for each stage of Well 2

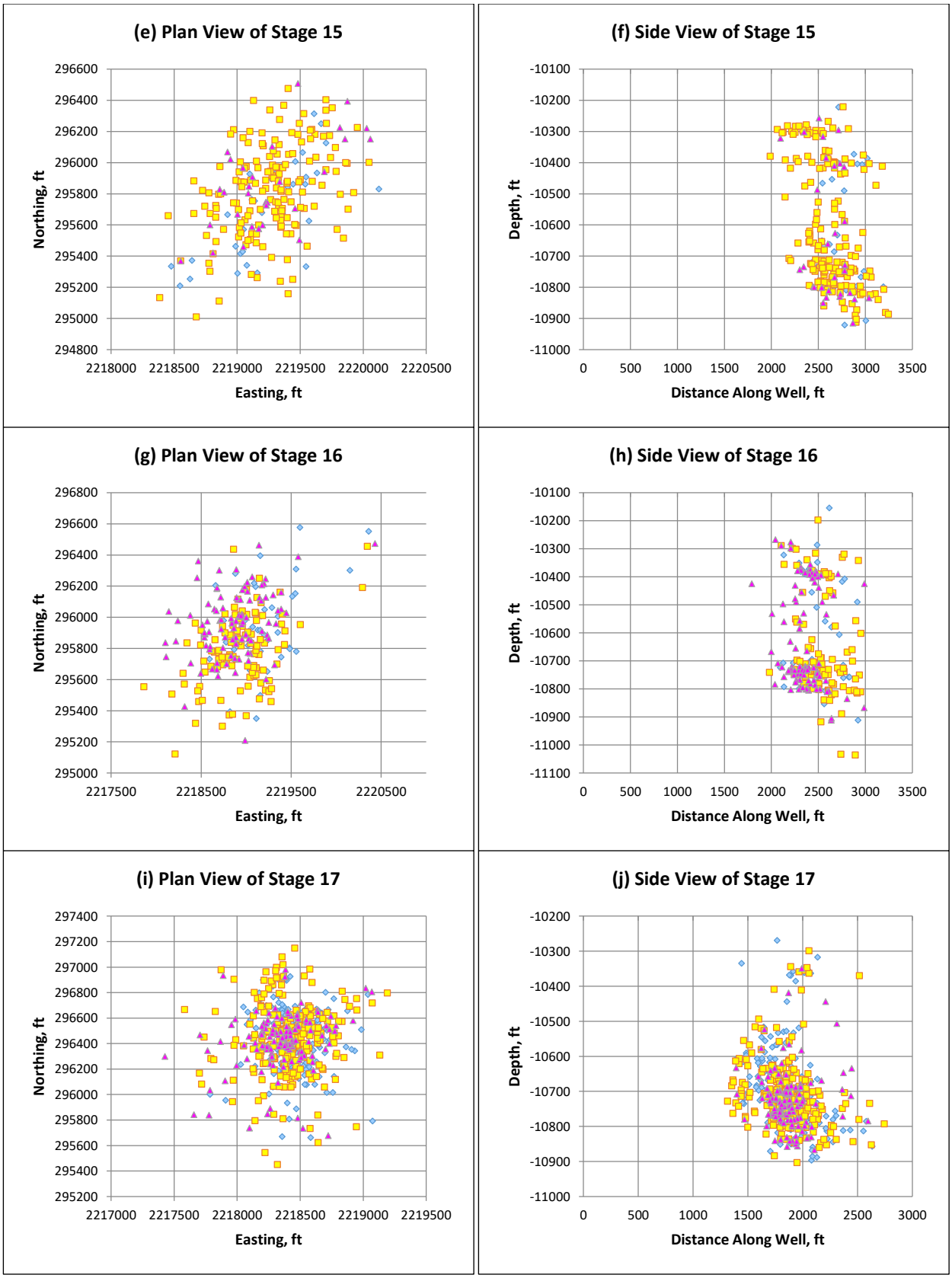

Fig. A-4— Continued.

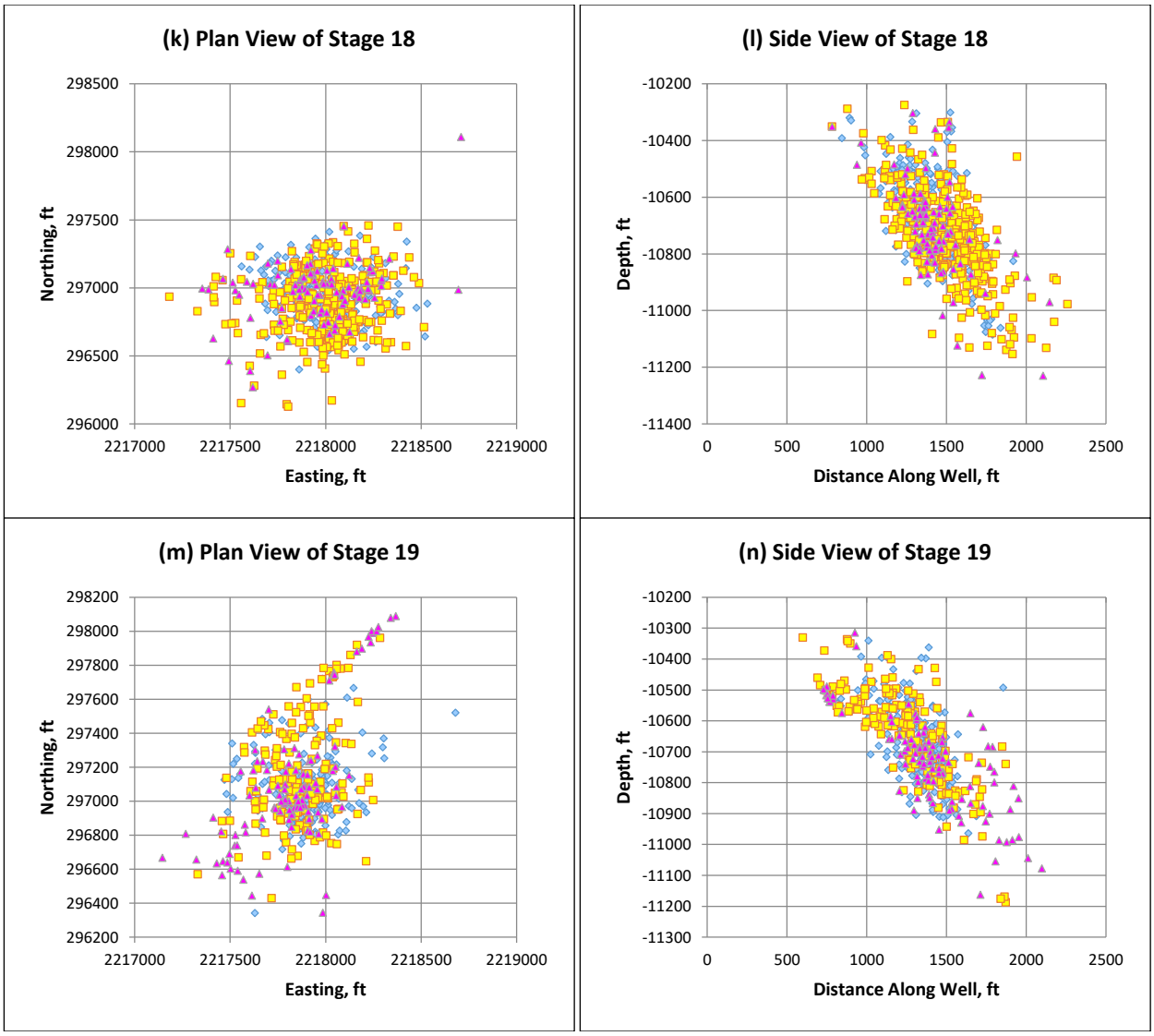

Fig. A-4— Continued.

C. Eagle Ford Shale Well 3

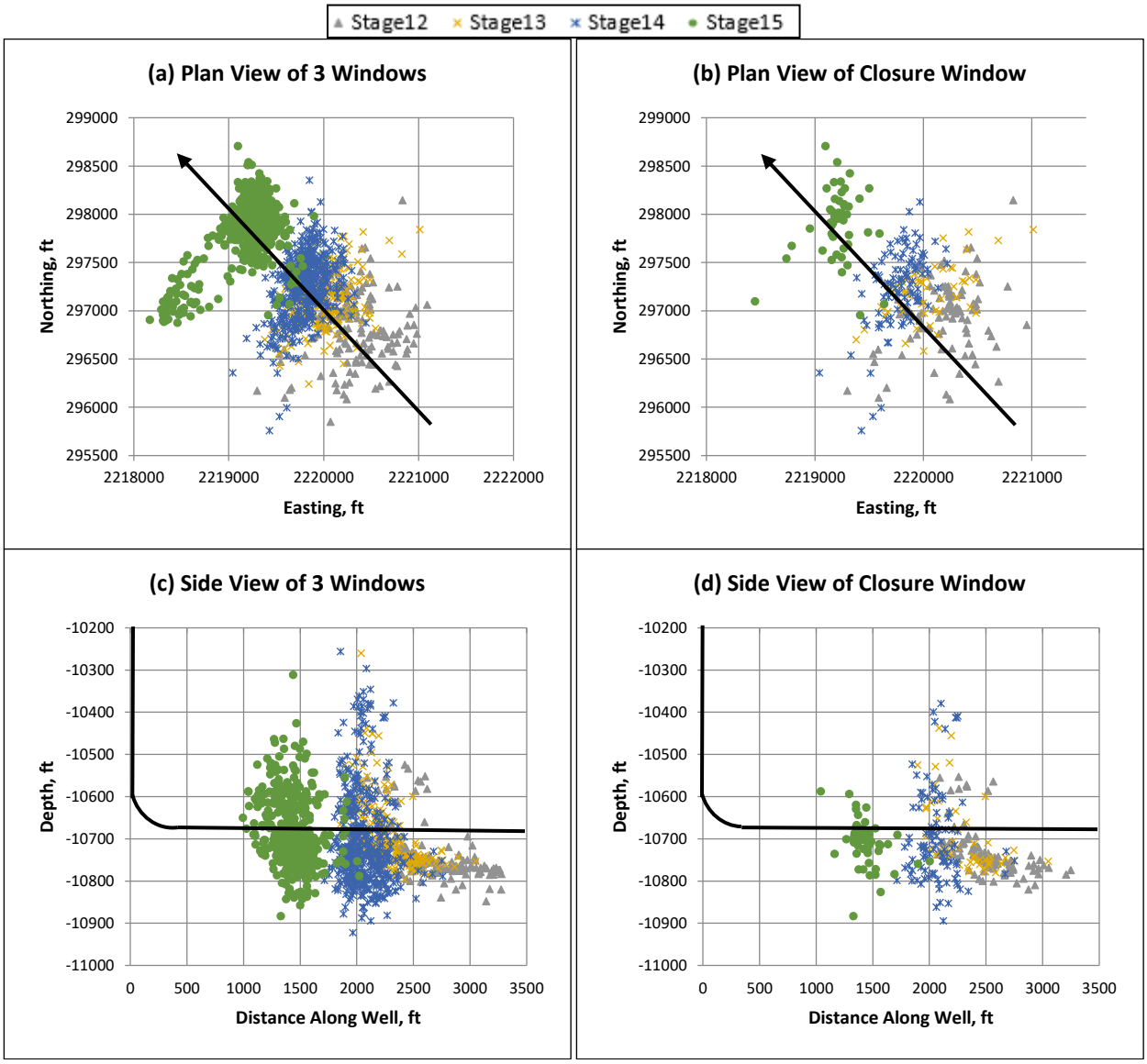

Fig. A-5— Plan view and side view of all 3 windows and closure window for stages 12-15 of Well 3.

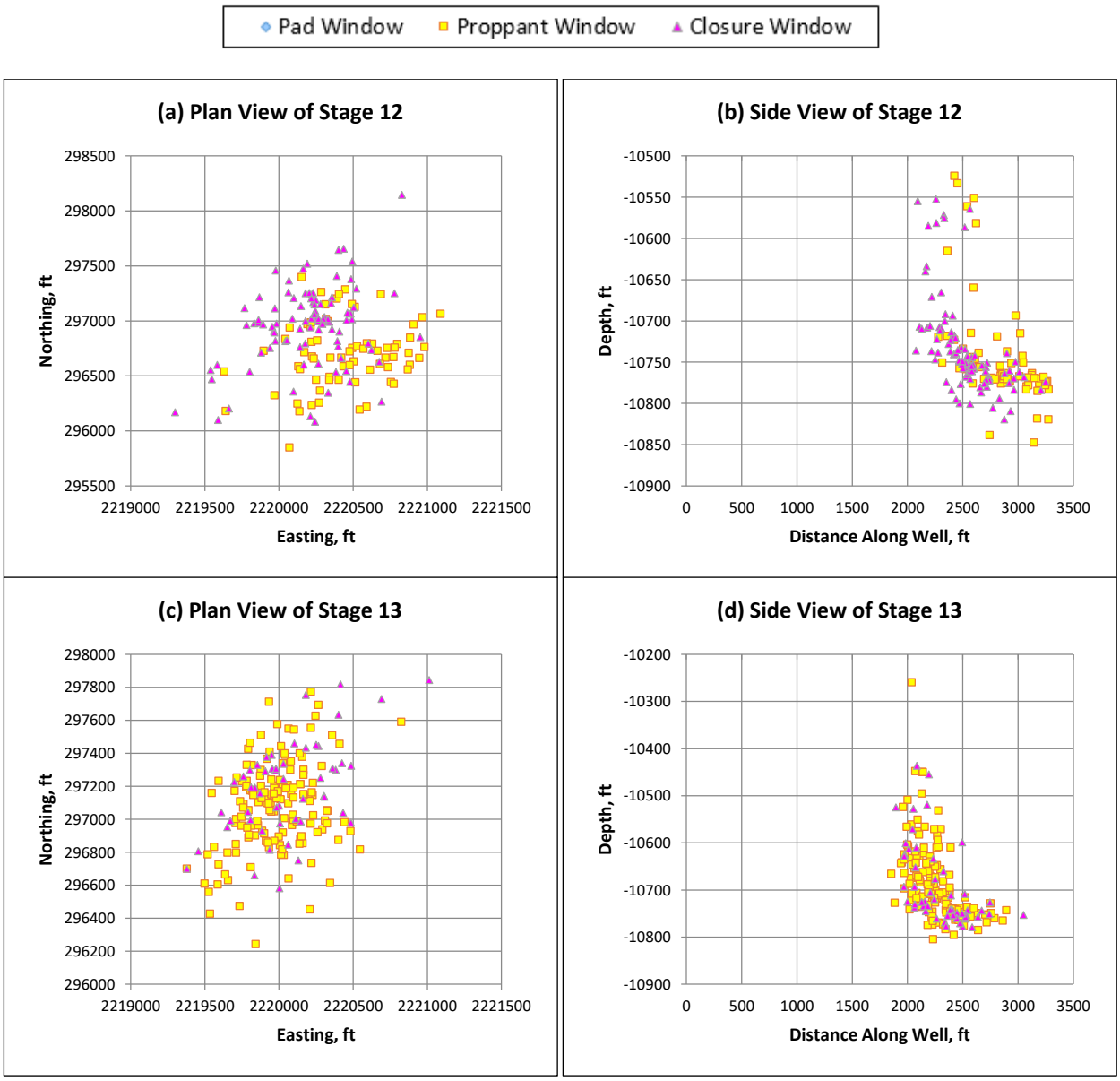

Fig. A-6— Plan view and side view of 3 individual windows for each stage of Well 3

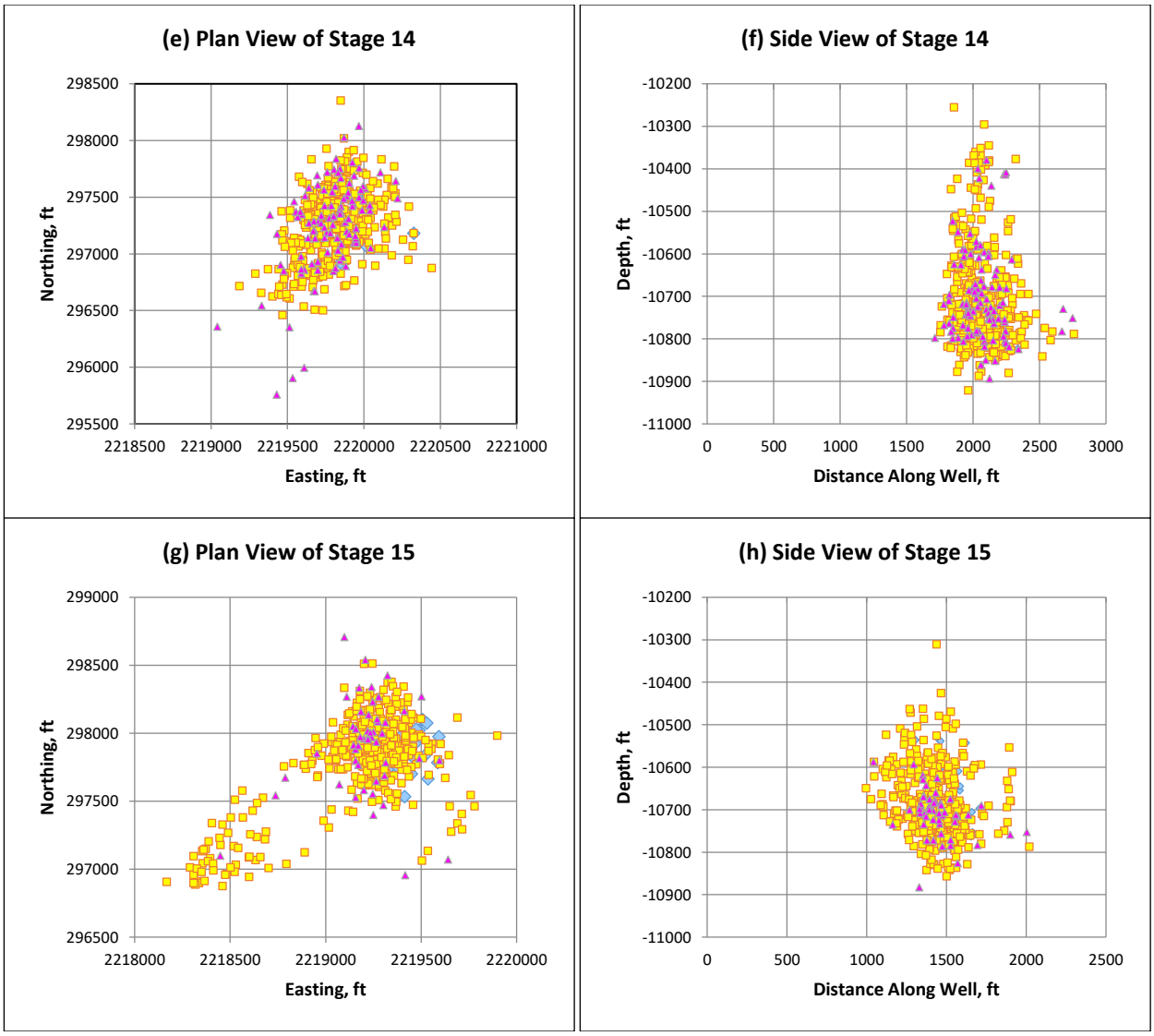

Fig. A-6— Continued.

D. Eagle Ford Shale Well 4

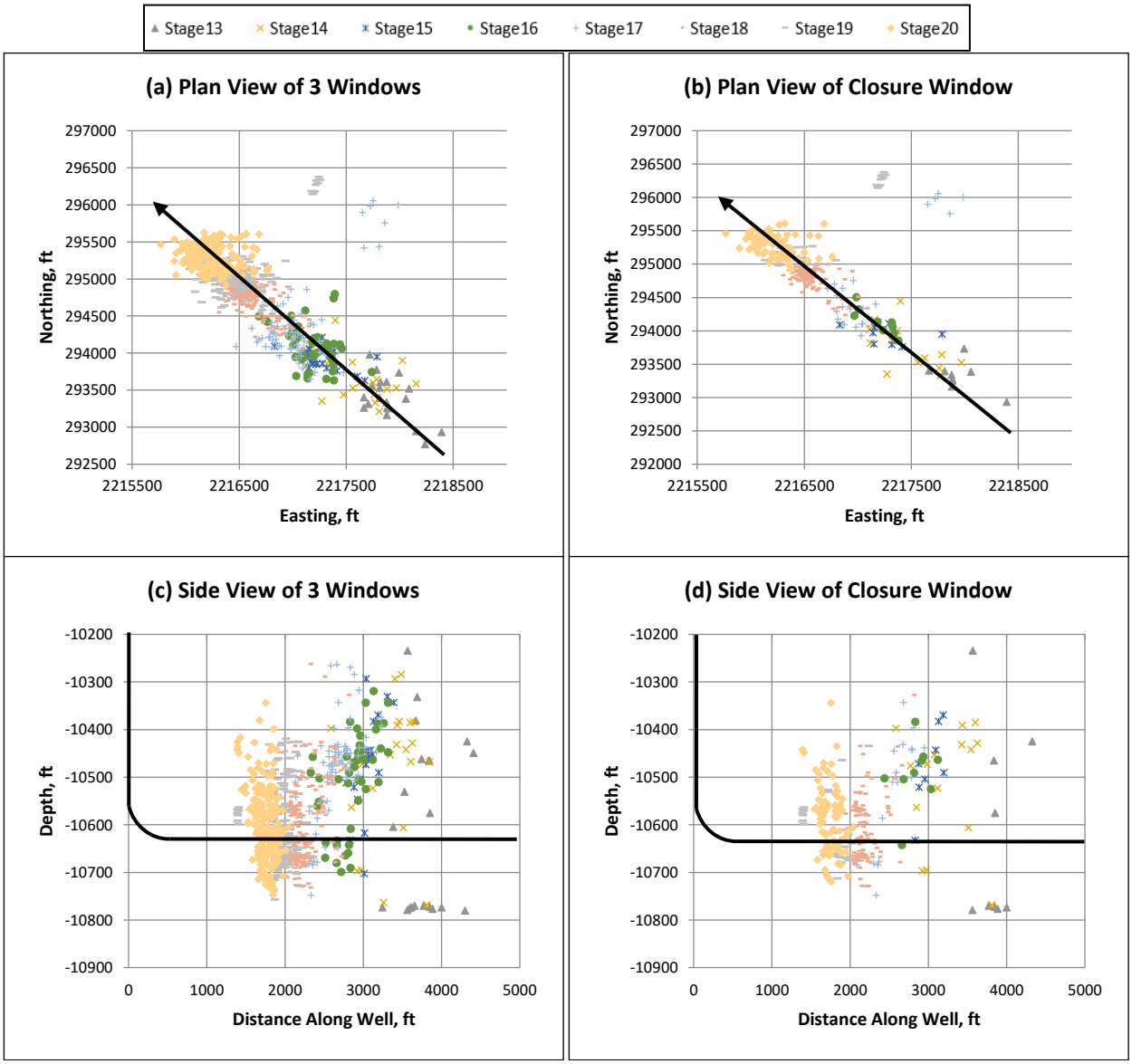

Fig. A-7— Plan view and side view of all 3 windows and closure window for stages 13-20 of Well 4.

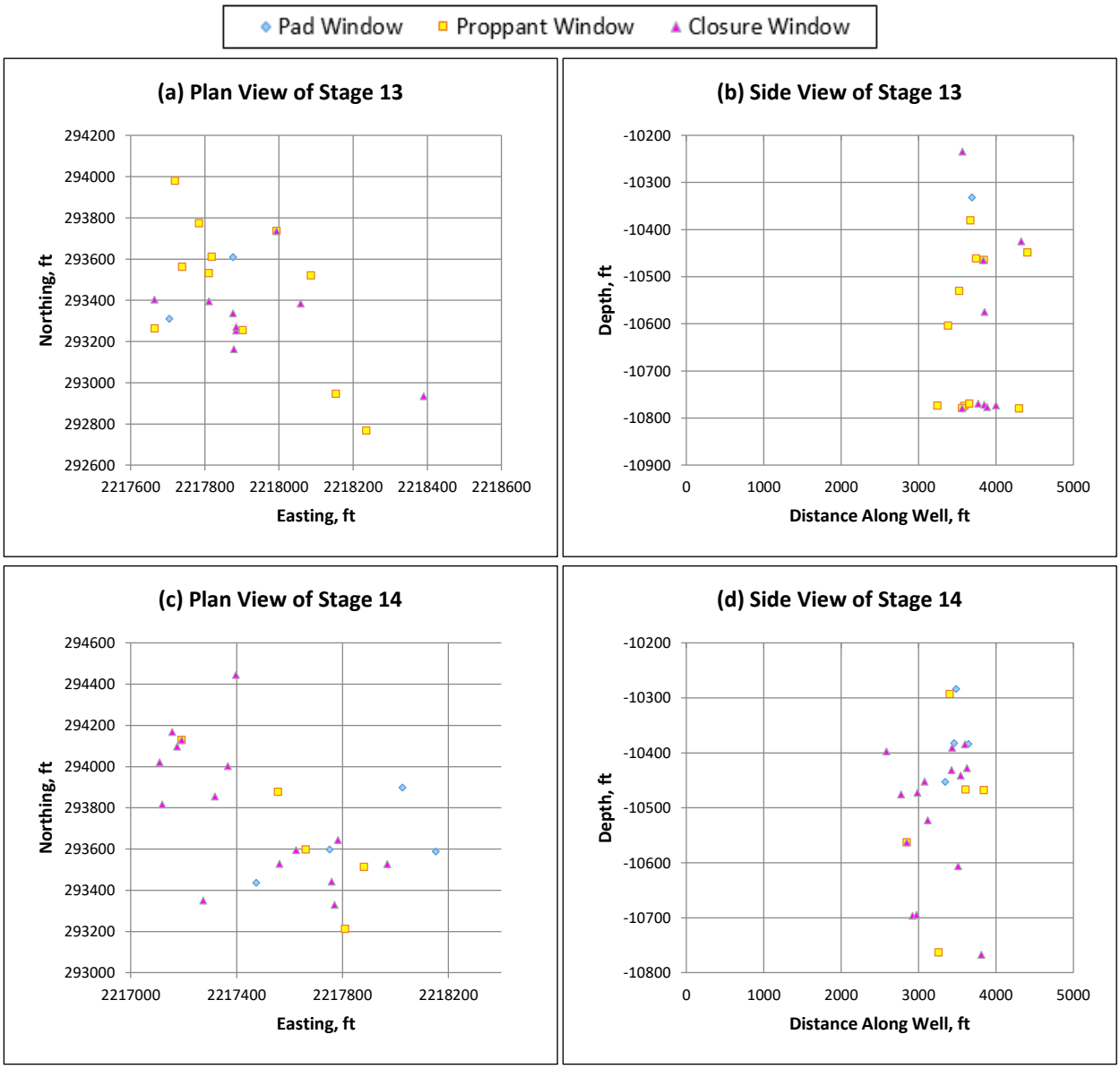

Fig. A-8— Plan view and side view of 3 individual windows for each stage of Well 4

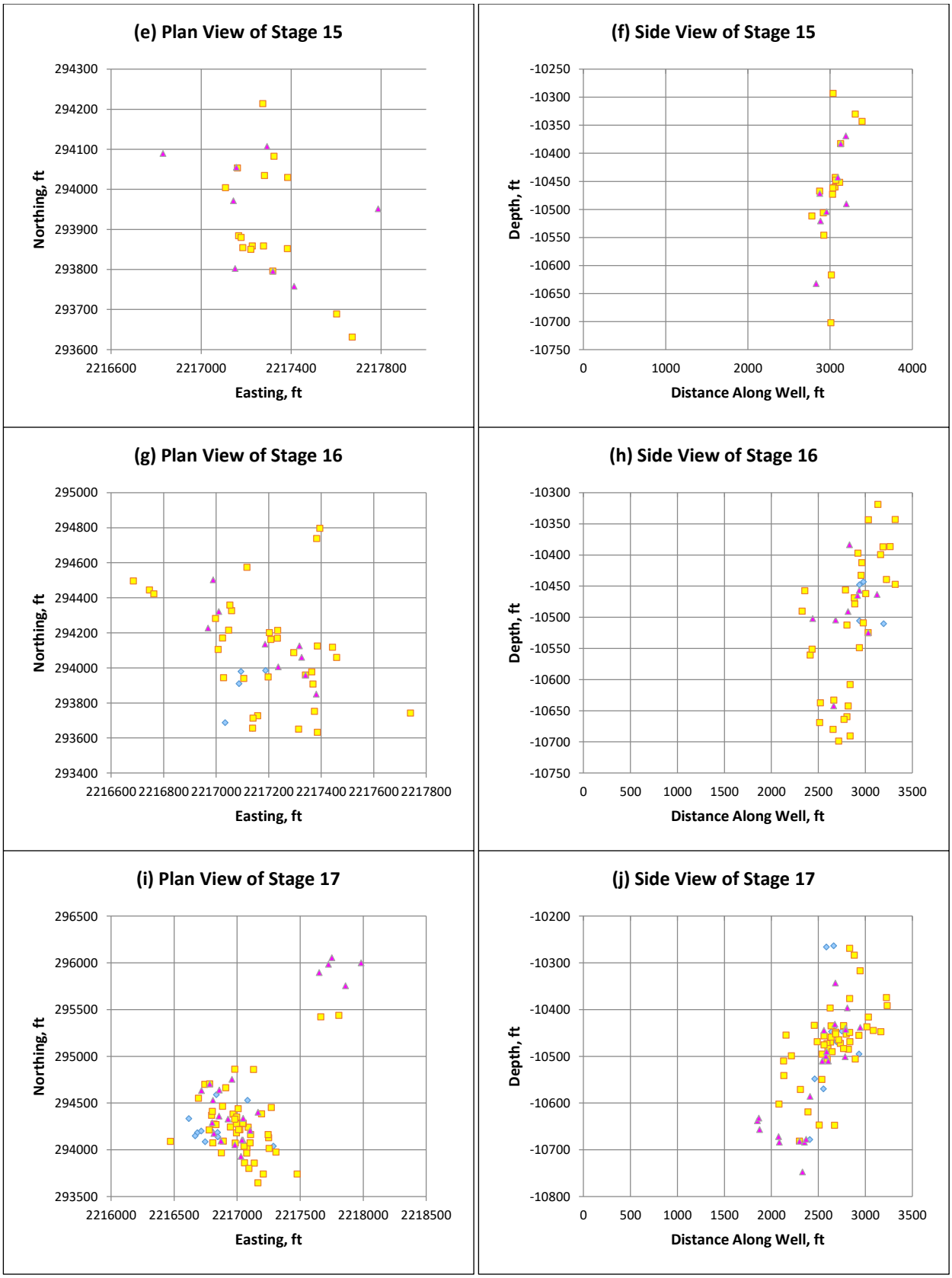

Fig. A-8—Continued.

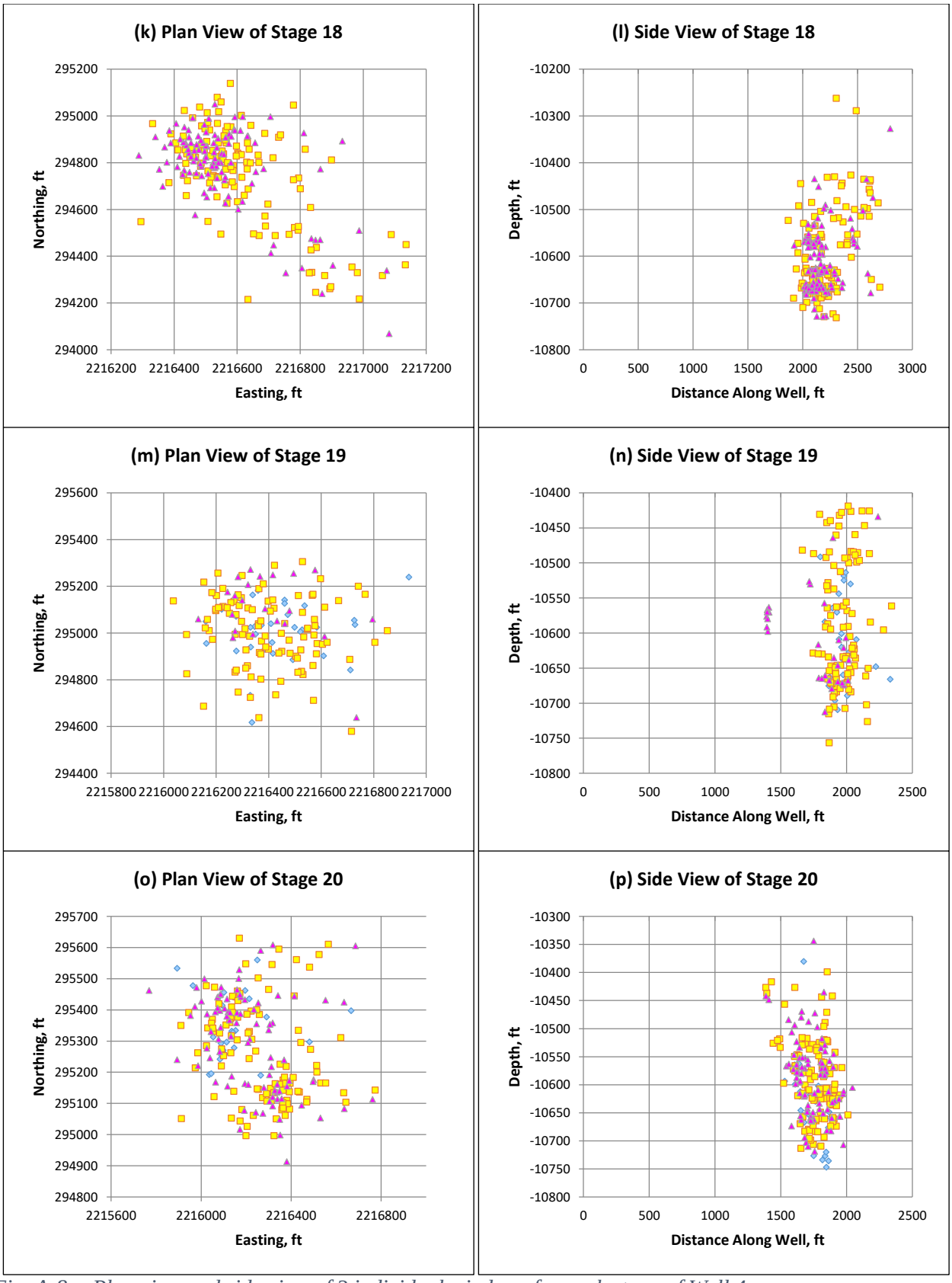

Fig. A-8— Plan view and side view of 3 individual windows for each stage of Well 4.

E. Eagle Ford Shale Well 5

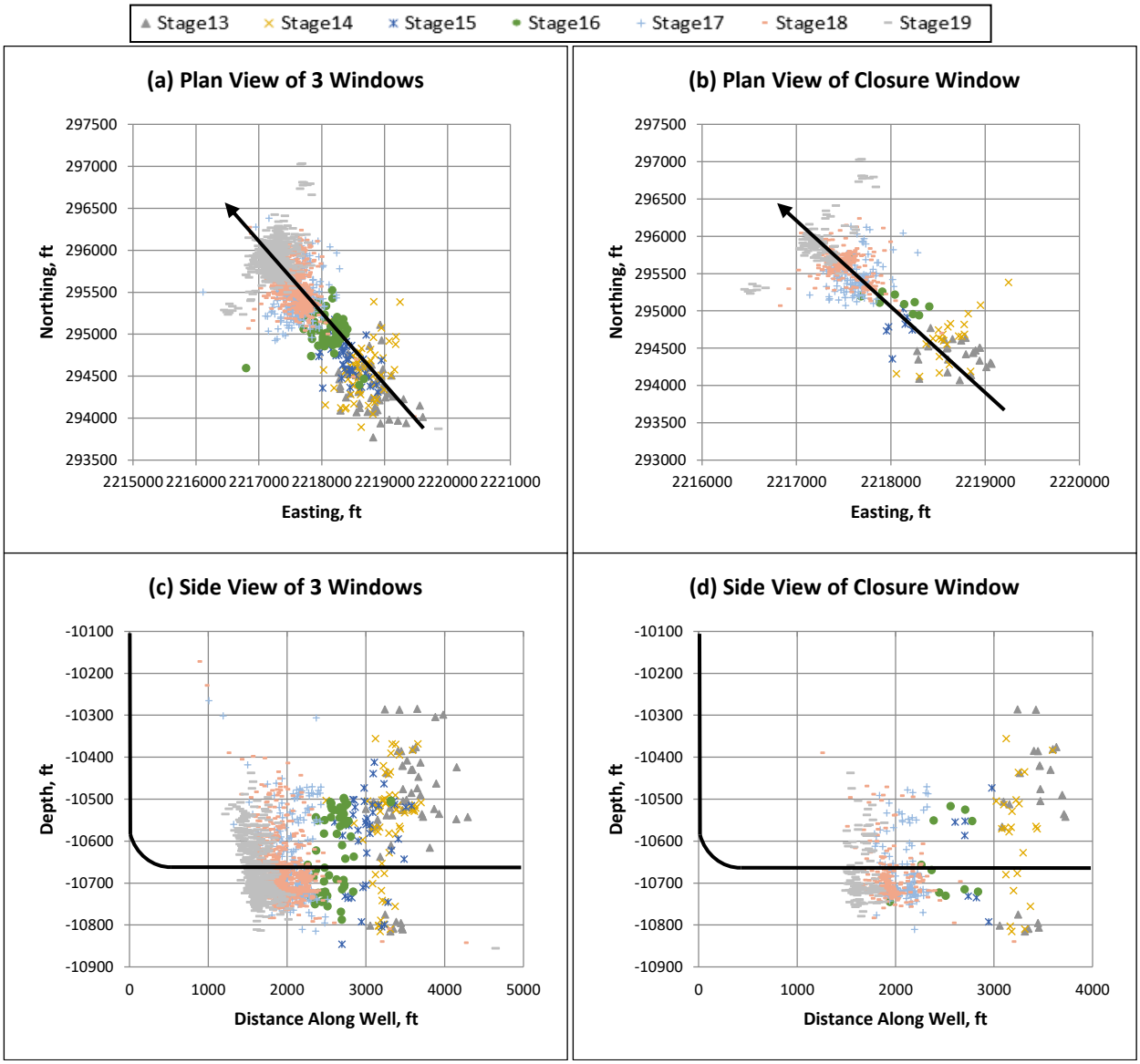

Fig. A-9— Plan view and side view of all 3 windows and closure window for stages 13-19 of Well 5.

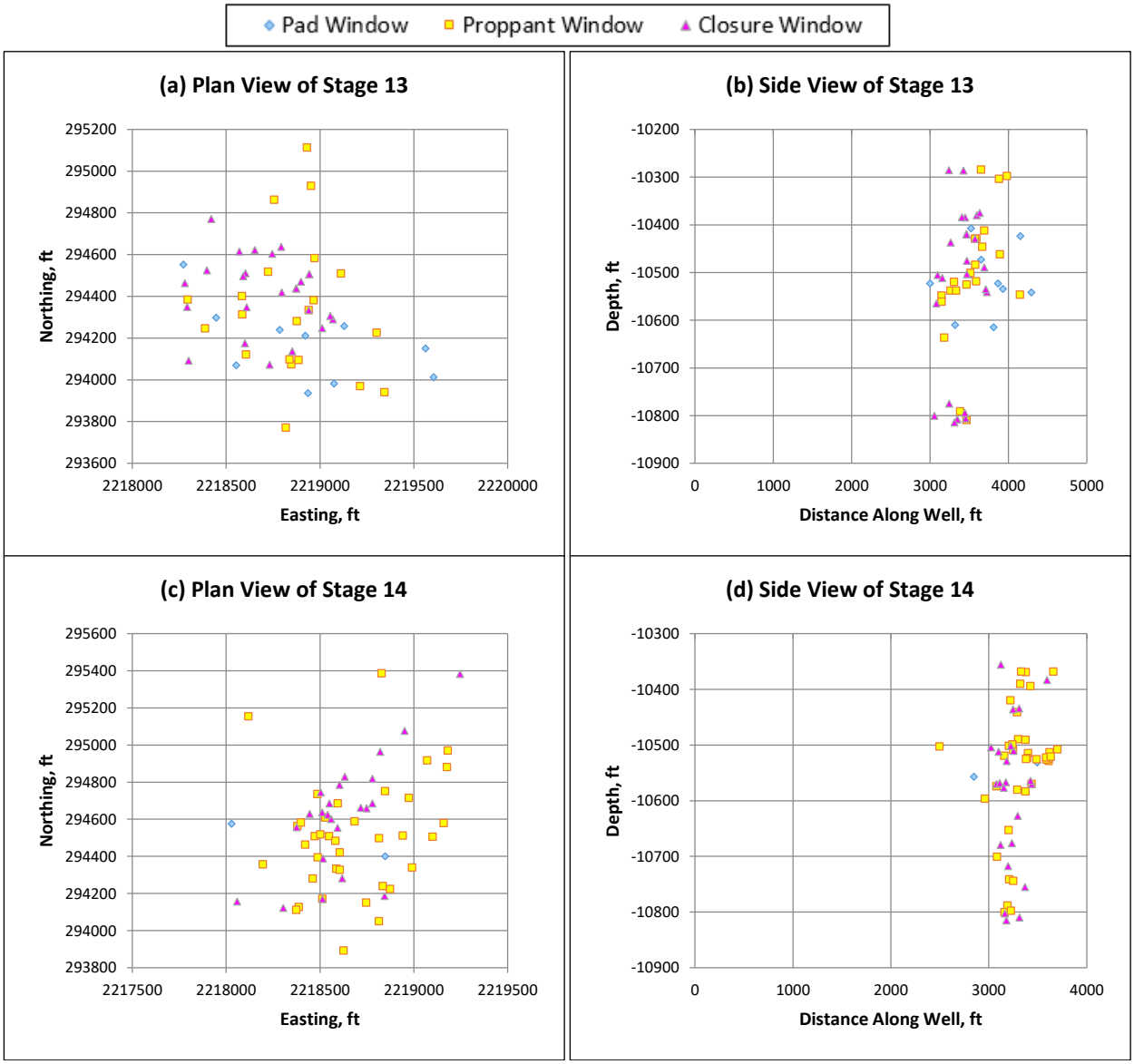

Fig. A-10— Plan view and side view of 3 individual windows for each stage of Well 5

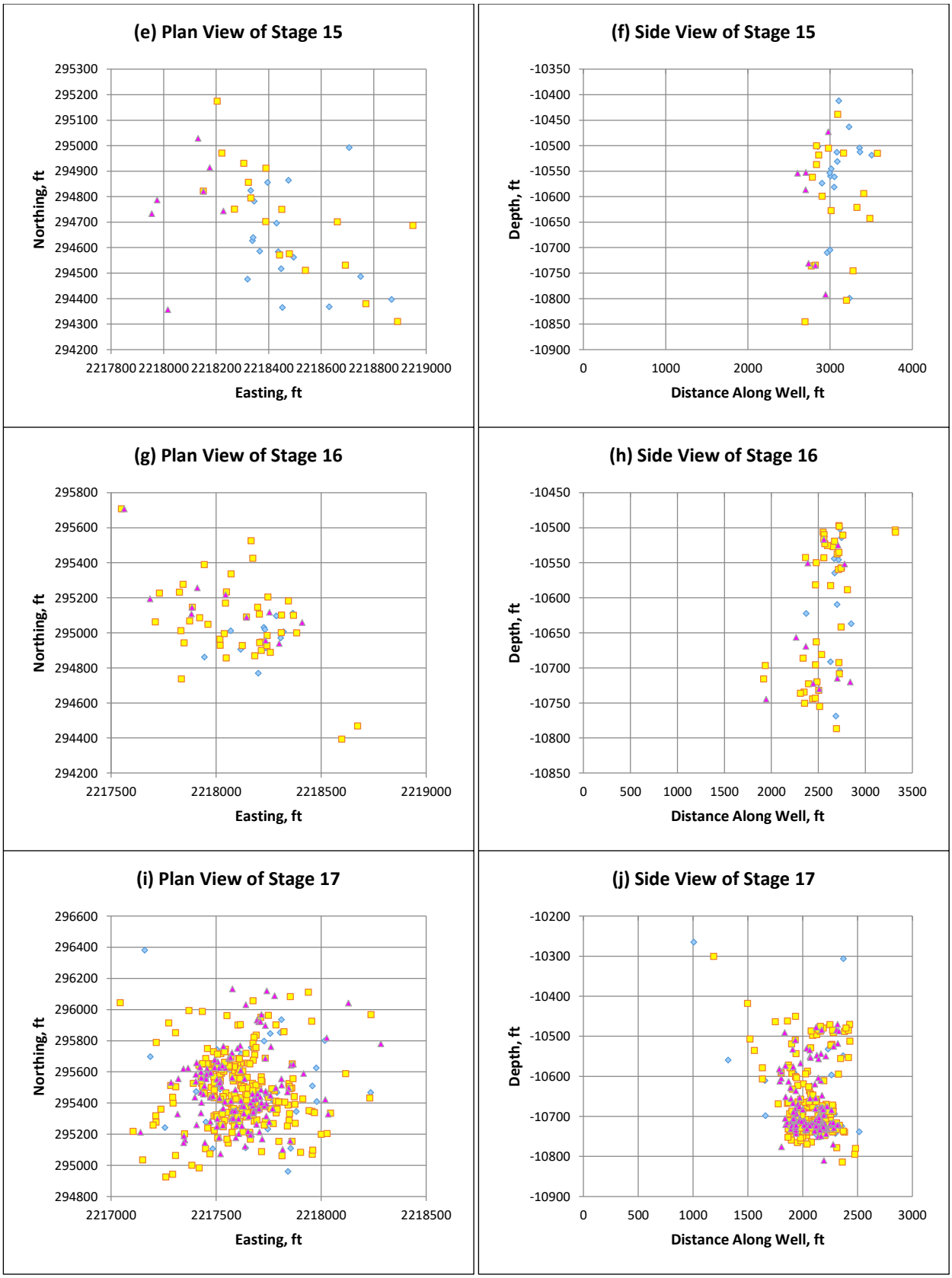

Fig. A-10— Continued.

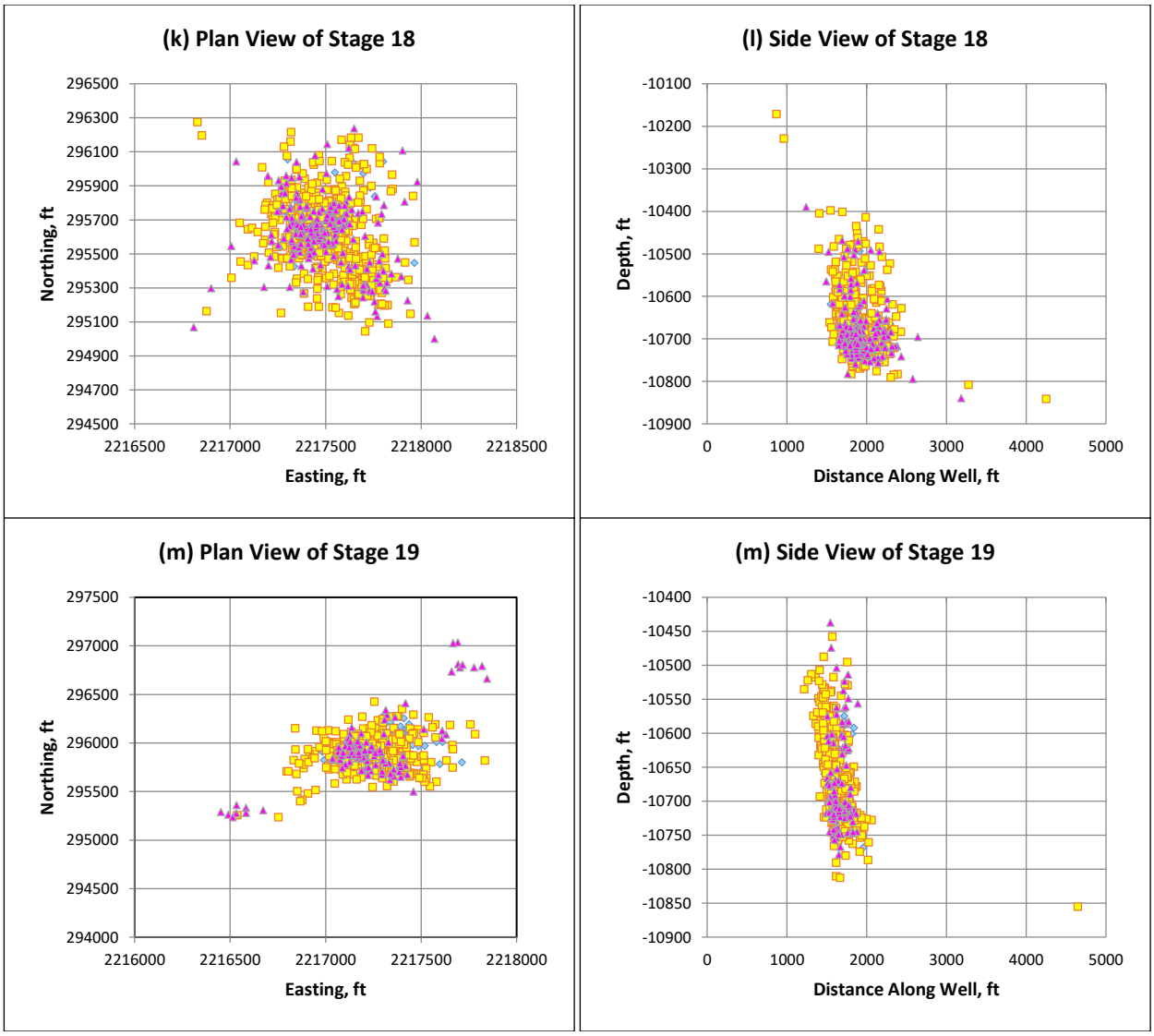

Fig. A-10— Continued.